CHALMERS
UNIVERSITY OF TECHNOLOGY

Investigation of interactions between nanobodies and their antigens using SPR detection methods

Master's thesis in Biotechnology

MICHELE MARIOTTI

Supervised by:

Professor Karen Martinez,
University of Copenhagen

Table of contents

Acknowledgements

I would like to thank my family for supporting me from abroad every time I needed. I thank my friends as well, from Italy, Sweden and Denmark, for the good time spent together and for being there when I needed them the most.
I also thank my supervisor Karen Martinez for giving me this amazing opportunity to carry out a project in the department of bionanotechnology of the university of Copenhagen. I am also thankful to all the people working in the research group of Karen Martinez, for all their advices and nice moments spent together. A special thanks to Eduardo della Pia, who spent so much time teaching me and helping me for all the duration of this project, I really learned a lot from you.

Abstract

Nanobodies, or single domain antibodies, have gained a lot of attention recently in nanoscience because of their attractive properties such as small size, high stability, high flexibility, hydophilicity and ease of manufacture, which make them ideal candidates for a lot of application areas, including biotechnology, therapeutics and diagnostics.
The aim of this Master Thesis is to evaluate the interactions between nanobodies and their binding partners by Surface Plasmon Resonance techniques.
The goal of the first part of the thesis is to overexpress, purify and characterize three different proteins: His-eGFP, GFP and nanobody. The results indicated a succesfull overexpression and purification of His-eGPP and GFP, with a high level of purity achieved for both proteins. Nanobody was overexpressed but its purification led to many challenges, as the final purified protein had a very low density.
The second part of the thesis investigates the experiments aimed at evaluating the interactions between a nanobody against GFP and a GFP protein, previously purified, on two biosensor surfaces: a Ni:NTA chip and an anti-his antibody immobilized on a CM5 chip. Furthermore, the interaction of a single nanobody on the two surfaces is compared with His-eGFP interaction on both surfaces. Results showed that the interaction between nanobodies and their binding partner can be investigated by SPR. In particular, nanobody showed a higher affinity for both biosensor surfaces compared to His-eGFP. Kinetics measurements indicated higher association rate constants and lower dissociation rate constants for nanobody binding to the anti-his-antibody surface compared to His-eGFP binding to same surface, confirming the high affinity of the nanobody for the anti-his-antibody surface.
Results of the experiments involving the interaction between GFP binding to nanobody immobilized on the two surfaces indicated a very similar affinity at equilibrium of GFP for the immobilized Nb on both surface. On the other hand, kinetics measurements showed that GFP had a higher affinity for nanobody immobilized on the anti-his surface, as slower dissociation rate constants and slightly higher association rate values were obtained.
In conclusion, the interaction between nanobody and its antigen was succesfully characterized and evaluated by SPR, but care must be taken while choosing the experimental parameters in order to minimize mass transport problems typical of SPR experiments.

Table of abbreviation

Name	Abbreviation
Nanobody	Nb; αGFP-Nb-His
Antibody	Ab
Surface Plasmon Resonance	SPR
His-enhanced Green Fluorescent Protein	His-eGFP
Green Fluorescent Protein	GFP
Fast protein liquid chromatography	FPLC
Immobilized Metal Ion Affinity chromatography	IMAC
Ion Exchange Chromatography	IEC
Bicinchoninic Acid	BCA
Isopropyl β-D-1-thiogalactopyranoside	IPTG
Phosphate buffer saline	PBS
Luria Bertani broth	LB
Terrific broth	TB
Molecular Weight	MW
Complementarity Determining Region	CDR
Sodium Dodecyl Sulphate - PolyAcrylamide Gel Electrophoresis	SDS-PAGE
Nitrilotriacetic Acid	NTA

Chapter 1.

Introduction

1.1 Aim and outline of the Master Thesis

The aim of this Master Thesis is to investigate the interaction between a single domain antibody (also known as nanobody ®, abbreviated as Nb) and its antigen by surface plasmon resonance technique (SPR). Nbs are novel and promising tools used in diagnostics, therapeutics and as research tools. The first part of my thesis will focus on an introduction about Nbs, their properties and different applications with a focus on their use and studies as research tools. The second chapter of my thesis will deal with the molecular biology techniques used to overexpress, purify and characterize different proteins used in the project, namely the His-enhanced Green Fluorescent Protein (His-eGFP), the GFP protein and the αGFP-Nb-His protein. The methods and results for the overexpression, purification and characterization of each protein will be presented and discussed. The last chapter of the thesis will focus on SPR. First the SPR method will be introduced and then the experiments involving Nbs and their interaction with GFP protein on different SPR chip surfaces will be described.

1.2 Nanobodies

1.2.1 Introduction

Single domain antibodies are defined as Nbs. They have been developed by Ablynx [1] and they consist of a single monomeric variable domain of an antibody. They are normally produced from heavy-chain only antibodies that are found in camelids, and they are called V_HH fragments. Nbs are characterized by flexible formatting, applicability to a wide spectrum of applications, facility of manufacture, as well as stability and robustness.[2]
Nbs have a molecular weight of only 12-15 kDa, which is significantly lower than common antibodies as it is about one tenth of the molecular weight of monoclonal antibodies. Nbs are devoid of light chains, but they are able to bind an antigen because of their single N-terminal domain.[2] Nbs possess several advantages and are used in several biotechnological and medical applications.
This chapter will present a short overview of Nbs, their structure, production, properties and applications.

1.2.2 Structure

A Nb consists of a chain of about 110 amino acids, including a variable domain of a heavy-chain antibody. Nbs comprise four framework regions and three complementarity-determining regions (CDRs), which are hypervariable loops responsible for antigen binding. [2]
Figure 1.1 shows the structures of a conventional antibody, a camel heavy-chain antibody and finally a V_HH (Nb) derived from the camel antibody. Conventional antibodies have larger size and possess heavy and light chains, while camel heavy-chain antibodies only have heavy chains and they are very stable.[3]
Figure 1.2 shows the ribbon diagram of a single-domain antibody, where the characteristic CDR3 region is shown in orange.[4]
By analyzing the crystal structure of Nbs, it was possible to show that the scaffolds consist of two α-sheeted structures, similarly to a VH immunoglobulin fold in a conventional antibody. By comparing the structures of a conventional heavy-chain antibody (VH) and that of a Nb it was possible to demonstrate that the CDR1 and CDR3 regions of a Nb are on average larger and

longer than those found in VH, and are connected by a disulfide bridge (figure 1.3).[5] The solubility of Nbs is enhanced by the hydrophilic amino acid substitutions present within the framework-2 region.[5]

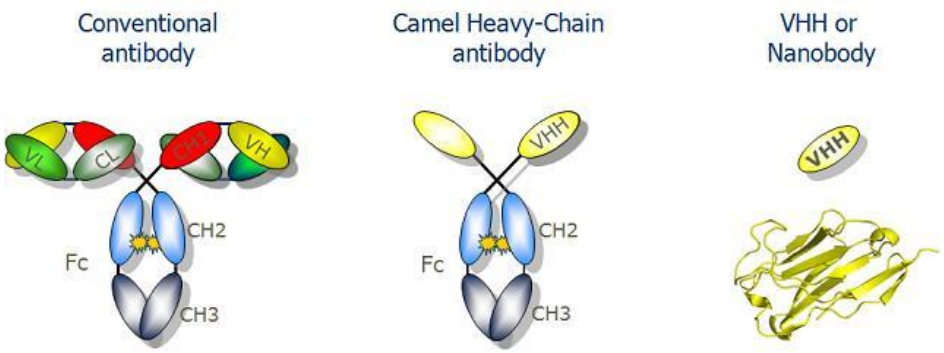

Figure 1.1. Structures of conventional antibody, camel heavy-chain antibody and Nb. [3]

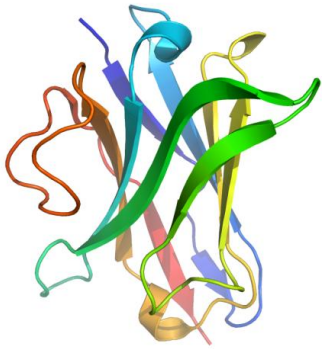

Figure 1.2. Ribbon structure of a Nb. The CD3 region is coloured in orange[4]

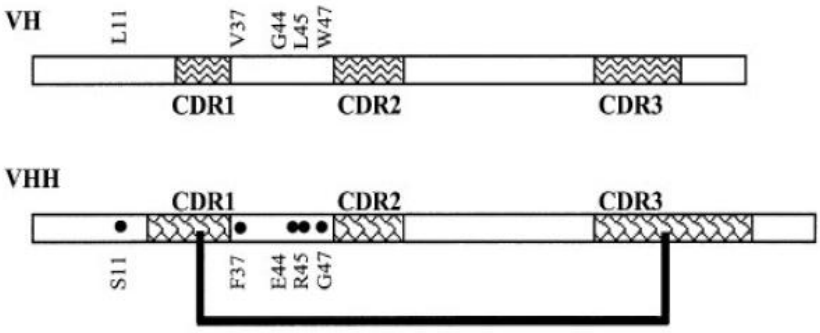

Figure 1.3. Scheme showing the differences between VH and V_HH (Nb) based on the sequence comparison of cDNA clones.[5]

1.2.3 Production

Nbs are normally produced from heavy chains antibodies lacking light chains of Camelidae. Production is obtained after immunizing dromedaries, camels, alpacas or sharks with the selected antigen. Subsequently, mRNA from peripheral blood lymphocytes is isolated and employed as template for synthesizing cDNA. VH and V_HH regions are then amplified by PCR. A gene library made up of million clones of single domain antibodies is generated by using polymerase chain and reverse transcription. Screening techniques such as ribosome display and phage display are then used to select the specific Nbs which are able to bind the antigen.[6]

As an alternative, Nbs can be produced from conventional antibodies, such as common murine or human IgG. In this case, similarly as before, gene libraries are produced from immunized donor and screening techniques are used to identify the Nbs binding the antigens. However, this approach presents a limit, since the binding domains of conventional antibodies show a tendency to dimerize or aggregate because they are hydrophilic.[7]

1.2.4 Properties and advantages

Nbs possess several biochemical properties that make them very promising tools in many application fields.
First of all, they are characterized by a small size and single domain nature, which make them more permeable in tissues and also capable to reach clefts, grooves or hidden epitopes which are not normally accessible to regular antibodies. This property is permitted by the extended CDR3 loop, which is able to reach some hidden antigens, such as the active site of enzymes.[8]
Secondly, as all antibody-derived fragments, Nbs can be easily expressed in bacteria as soluble and robust proteins. Another advantage is that Nbs can be easily generated, optimized and tailored since they are characterized by a single exon of 450 base pairs encoding for Nbs.[9]
Furthermore, an another advantage of Nbs resides in the fact that they can be tailored for a half life which can range from 30 minutes to 3 weeks[10], enhancing their flexibility and the number of therapeutic options (figure 1.4). They can also be engineered in different formats, for example multivalent (multiple V_HHs with the same binding sites for the same antigen), biparatopic (two V_HH binding two different epitopes), bispecific (V_HH binding two antigens), as illustrated in figure 1.4.[10]

Compared to conventional antibodies fragments, Nbs also offer other advantages, such a higher hydrophilicity, a more rapid tissue penetration due to their small size, an easier genetic manipulation and a high physicochemical stability[11]. The hydrophilicity of Nbs and their tendency to not aggregate depends on the substitution of hydrophobic by hydrophilic amino acids in the framework-2 region compared to conventional antibodies.
Nbs are also very homogeneous and do not show the tendency to spontaneously dimerize.[5]

Other studies have demonstrated that Nbs are more resistant to detergents and heat: in a previous research, Nbs survived a temperature of 90 °C preserving their capability to bind antigens[12].This resistance to heat is mainly due to their effective refolding after chemical denaturation, but also to a high resistance to denaturation. Nbs were also shown to resist against chaotropic agents, proteases and extremes pH values. [5] This ability to keep their activity

even in harsh conditions such as those found in the stomach makes Nbs ideal candidates for the treatment of gastrointestinal diseases.

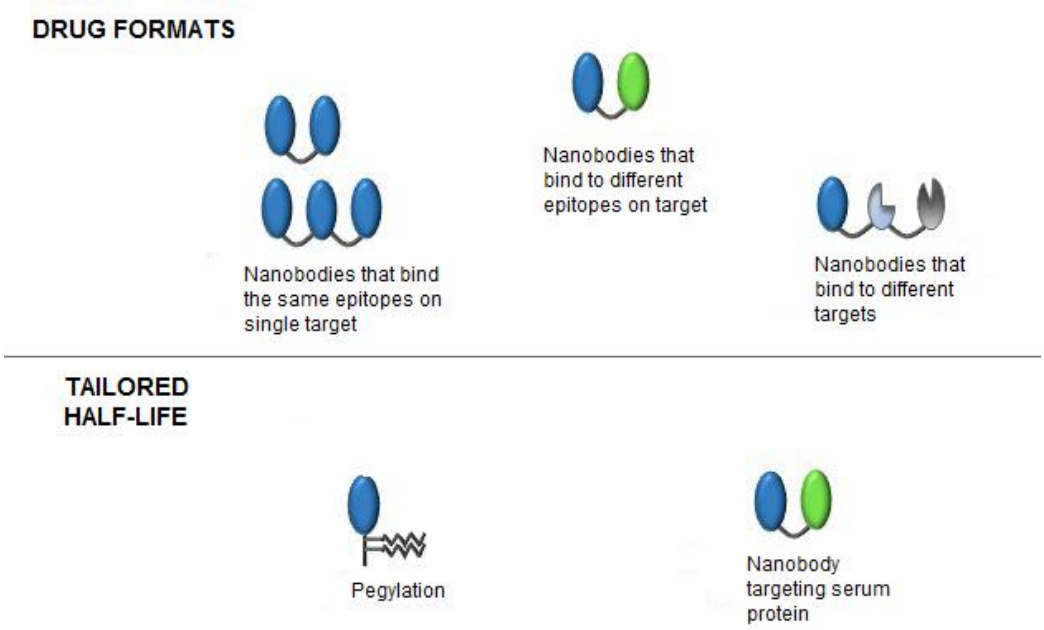

Figure 1.4. (Top), examples of different drug formats; (bottom), examples of tailored half-life.[10]

1.2.5 Applications

Owing to their many advantages compared to regular antibodies, Nbs are suited to a wide range of applications, from biotechnological applications to therapeutic and diagnostic applications.

1.2.5.1 Nanobodies as research tools

Nbs have been used in fusion with GFP proteins to create chromodies, which can be used to track down targets in different sections of living cells, therefore enhancing the possibility of live cell microscopy.[13]
Anti-GFP-Nbs have been coupled to a monovalent matrix, defined as GFP-nanotrap, in order to single out GFP-fusion proteins for biochemical analyses.[14]
Anti-GFP-Nbs have also been coupled to organic dyes to allow single-molecule localization with super-resolution imaging techniques; Nbs performed better than the whole antibodies since these ones can often lead to a misleading signal due to their large size, while the high affinity and small size of Nbs permits nanometer spatial resolution.[15]
Nbs can also be used as crystallization chaperones in order to bind to target molecules and increase the crystallization probability of it by reducing the conformational heterogeneity. Nbs were also used in the same study to mask surfaces hindering the crystallization.[16]

In a study of 2010[17], X-ray crystallography was used to investigate the structure of a GFP:-anti-GFP-Nb complex. The authors conducted experiments by using X-ray crystallography and isothermal titration calorimetry and explained in detail the basis of high affinity and high specificity of this protein binding, which depends on the structures of these molecules and the thermodynamics of their interaction. Figure 1.5 below shows the ribbon diagram of the GFP:-anti-GFP-Nb complex.

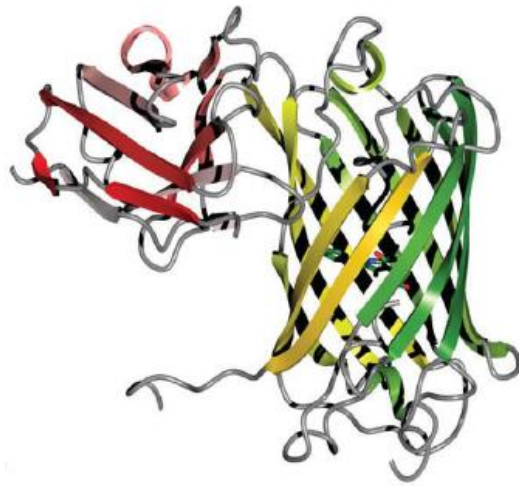

Figure 1.5. Ribbon diagram of the GFP:GFP-Nb complex: GFP is coloured in green to gold and Nb is shown in red to pink. [16]

1.2.5.2 Nanobodies as therapeutics

Nbs have been successfully tested used for oral immunotherapy, for example against *E. coli*-induced diarrhea; other targets include the inflammatory bowel disease, colon cancer and other diseases of the gastrointestinal tract.[18]
Nbs have also been used for the treatment of neurological diseases, targeting drugs across the blood brain barrier into the brain[19]; Nbs could penetrate into solid tumors more easily than normal antibodies.
Another promising therapeutical application of Nbs is photothermal therapy for the treatment of breast cancer: Nbs have been coupled to gold nanoparticles, exploiting the ability of Nbs to bind tumor antigens such as HER2.[20]
In another research, Nbs have been tested in mice for the treatment of Influenza A virus subtype H5N1, and proved to successfully prevent the replication of the virus in vivo and to significantly reduce the morbidity and mortality caused by this virus.[21]
Several Nb-therapeutics are in clinical trials, for example anti-IL6R or anti-TNFα for the treatment of inflammatory diseases or anti-von Willebrand factor to prevent thrombosis in patients affected by thrombotic thrombocytopenic purpura .[22]
Nbs for theurapeutic applications are also often produced in multivalent and multispecific constructs in order to optimize their functionality by increasing their antigen binding ability.[23]

1.2.5.3 Nanobodies as diagnostics tools

Nbs are very promising tools in biosensing applications because of their small size, which allows them to attach more densily onto biosensors surfaces. Nbs can be readily modified to avoid reactive groups, therefore by immobilizing them on sensor surfaces they are able to maximize the binding capacity of the antigen[9]. Another property that makes Nbs perfect tools for diagnostics is their high intrinsic domain stability that has been documented in many sources.[2] Their stability at high temperatures is an asset for *in vivo* imaging. Nbs are also very attractive in diagnostics because of their facility of production, engineering and optimization. Their high solubility and presence of hydrophilic mutations make them less susceptible to aggregation, which is very relevant in nanoconjugates and biosensor development.[9]
The ability of Nbs to bind to their target antigens with nanomolar affinity is also a very attractive property in diagnostics applications.[9]
In several researches[24], Nbs were covalently coupled to solid, magnetic or inert surfaces to create affinity adsorbents, as it was shown by the generation of nanotraps. Nanotraps consist of Nbs immobilized to a monovalent matrix and that are able to recognize GFP proteins as targets.[13] Nbs can also be directed against different immunoglobulin isotypes.
A Dutch company produced a Nb that specifically recognizes the tetra-aminoacids Glu-Pro-Glu-Ala that can be cloned as a tag behind every protein[25]. Since Nbs have a small size, only few proteins in a complex mixture will be able to recognize the Nbs, therefore reducing the non specific adsorption of other molecules.[25]
Nbs have also been employed as binding proteins in affinity chromatography applications[9] as they allowed fast and efficient purifications of fusion and native proteins.
Furthermore, Nbs have been successfully used as detection probes for diagnostic ELISA assays (enzyme-linked immunosorbent assays*),* as an alternative to monoclonal antibodies because of their differential epitope recognition.[9]
Nbs have also been used to develop an *S.aureus* detection assay with Nb-based nanoconjugates, which are antibody-nanoparticle conjugates. [26] In this assay it took only 10 minutes to detect *S. aureus*; this is because nanoconjugate particles showed multiples Nbs on their surface. Therefore, Nbs have proven to be very efficient in nanobiotechnology to act as the recognition moiety inside nanowires and nanoparticles, performing better than other antibody fragments.

A research in 2005[27] investigated the use of Nbs in biosensor applications by testing their potential in sensing human prostate-specific antigen (hPSA) using SPR technology.
The aim of the study was to investigate and compare the performance of Nbs in detecting clinical significant concentration of hPSA compared to the antibodies. Nbs were immobilized on different chip surfaces. The capturing performance of Nbs and antibodies was first compared using ELISA assay, then using SPR assays. After testing the capturing binding level with SPR on the different chips, Nbs showed a higher analyte detection sensitivity compared to regular antibodies. In addition, Nbs demonstrated a higher protein intrinsic stability, as they indicated a higher resistance to harsh regeneration conditions.
In another research conducted in 2011[28], SPR experiments have been performed on Nbs binding to an immobilized HER2-Fc protein. The aim was to assess the kinetics parameters of different anti-HER2 Nbs for molecular imaging of breast cancer, where HER2 is tumor human epidermal growth factor receptor 2.

In a recent study conducted in 2013[29], llama nanobodies have been used against the phage TP901-1 baseplate in order to examine and identify the molecular determinants of phage infection. The authors were able to identify the baseplate binders and to determine their affinity. SPR has been used to investigate the affinity of different Nbs on the baseplate components. Finally, a study conducted in 2012[30] involved the selection of Nbs targeting human neonatal Fc receptors (FcRn). SPR was used here to detect the binding affinity of an anti-FcRn Nb.

Chapter 2.

Molecular Biology

2.1 Introduction

2.1.1 Aim

The aim of the experiments described in this chapter is to overexpress, purify and characterize three different proteins: His-eGFP, GFP and Nb. The purified proteins were then used in the SPR experiments described in the third chapter of the thesis.

2.1.2 His-eGFP, GFP and Nb

Three different proteins have been used in the experiments described in this chapter: His-eGFP, GFP and Nb. In this section an overview of each one of these proteins will be given.
GFP protein is also known as eGFP (enhanced GFP). GFP was first isolated from the Jellyfish Aequorea Victoria and it was discovered by Osamu Shimonura.[31] Its molecular weight is 26.9 kDa and it is able to emit a green fluorescent light upon excitation with ultraviolet or blue light.[32] [33]

Wild-type GFP (wtGFP), when exposed to blue light, emits a relatively low emission and excitation spectra. Spectral characteristics of GFP have significantly improved with the work of R. Tsien[34], followed by Thastrup, Falkow and Cormack.[35] Their work led to the production of eGFP: a double mutant protein was created, with mutations Ser65→Thr and Phe64→Leu. This new protein had an increased photostability, fluorescence and a significantly higher excitation peak.
eGFP has an extinction coefficient (denoted ε) of 55.000 $M^{-1}cm^{-1}$. It has a beta barrel structure, which consists of 11 β-sheets with six alpha helices containing the inserted chromophore.[36]
eGFP shows three major absorbance peaks in the absorbance spectrum: two at 400 nm and 489 nm and one peak at 280 corresponding to the absorption of aromatic amino acids.[37]
The GFP gene is an efficient reporter of expression and many biosensors have been developed using GFP.[38] The GFP gene has been inserted in many organisms, such as bacteria, yeast, fish, plants and mammalian cells. GFP application areas include fluorescence microscopy, for example for the creation of automated fluorescence microcopy complexes, where cells expressing proteins tagged with GFP proteins are constantly monitored. [39]
Two eGFP proteins have been used in the experiments described in this thesis: a His-eGFP protein, which contains a (histidine)6-tag on the N terminus, and a GFP protein, which lacks this His-tag.
Nb is the other protein that has been used in the experiments described in this thesis. Chapter 1.2 contains a review of Nb, its structure, properties and applications.
The Nb protein used in the experiments contains a (histidine)6-tag on the N terminus and it is developed to specifically recognize GFP.

2.1.3 Fast protein liquid chromatography (FPLC) techniques

This subsection contains a brief theoretical introduction short overview of the three types of FPLC purification techniques used in the experiments for protein purification.

2.1.3.1 Immobilized-metal affinity chromatography (IMAC)

IMAC is a separation technique that is based on the affinity between proteins and metal ions. This most used IMAC column is the His-Trap column. The purpose of this column is to purify proteins which contain a His-tag, taking advantage of the capacity of histidine to bind a chelated metal ion (Nickel). The column is made of a matrix composed of cross-linked agarose beads where a chelating group is attached to them. The metal ion Nickel is immobilized onto this chelating matrix.[41]
The function of this matrix is to selectively bind proteins only if their surface exposes compatible amino acids. His-tagged proteins are the strongest binders, while other proteins that do not contain histidine residues pass through the matrix without attaching to the column.[40 41]
Imidazole is an organic compound used as a competitive agent. It is used, at low concentrations, to increase the column selectivity for His-tagged proteins (binding step): imidazole reduces non-specific binding by competing with proteins exposing histidine residues for available binding sites on the Nickel . Afterwards, imidazole at high concentrations is used to elute the His-tagged proteins. Binding of non-tagged proteins is prevented with imidazole, but if imidazole concentration is too high, this will also prevent binding of His-tagged proteins.[42]

2.1.3.2 Size Exclusion Chromatography (SEC)

Size exclusion chromatography is based on the separation of molecules based on their size, as they pass through a gel filtration medium contained in a column[43]. During SEC, molecules do not bind to the chromatography medium, differently from IMAC.
Superdex gel filtration media consists of dextran covalently bound to cross-linked agarose. Cross-linked dextran is responsible for the gel filtration properties of the column while cross-linked agarose provides a high chemical and physical stability[41].
In order to separate a mixture of proteins, the sample proteins are applied at the top of the SEC column. As the molecules in the sample progress through the column, large molecules move faster than small ones. This is due to the fact that the beads surface is characterized by holes of different sizes; as the mobile phase moves the molecules down past the beads, the smallest molecules can freely penetrate all the holes and this process significantly slows down their movement. On the other hand, the biggest molecules cannot penetrate all the holes, therefore they move very fast. As the molecules move down the column, they slowly separate. As the different molecules finally arrive at the bottom of the column, the biggest molecules will be the first ones to elute, followed by medium-size molecules and finally the smallest ones will elute at the end.[44]

2.1.3.3 Ion Exchange Chromatography (IEC)

Ion exchange chromatography is a technique based on the separation of polar molecules depending on their affinity to the column. Cation exchange chromatography is responsible for retaining cations using negatively charged functional groups, while anion exchange chromatography is able to retain anions. These ion exchangers promote the binding of ions of higher charge and increased polarizability. There are three kinds of ion exchanger: gels, resins and inorganic exchangers.[45] Gels are used to separate proteins.
Charged molecules attach to the separation medium when ionic strength is low and the elution process occurs through a pH gradient or a salt: pH variation is important for changing selectivity in the ion exchange separation, while salts are used to provide a stronger or weaker retention.

A constant gradient elution is often used in the ion exchange chromatography.
The IEC column consists of cross-linked agarose beads and this matrix is responsible for excellent chemical and physical stability. The particles are small and stiff, therefore permitting fast adsorption and desorption, even if sample loadings and flow rates are large. The Q functional group is a quaternary amino group which is bound to the matrix through stable ether bonds. [41 46]

2.2 Materials and methods

2.2.1 Materials

This section lists all the instruments, columns, solutions and other materials used in this chapter.
Plasmids used were: pUCBB-ntH6-eGFP plasmid (for His-eGFP expression), pKEN GFP mut2 plasmid (for GFP expression) and pKEN GFP mut2 plasmid for Nb expression.
Luria Broth (LB) was prepared from Sigma powder microbial growth medium (Lennox). Terrific Broth (TB) was prepared from Sigma EZMix™ powder microbial growth medium. Minitron ® incubator shaker has been used for plate incubation. Eppendorf® BioPhotometer was used for measuring absorbance. For cell lysing, Sonicator Microson XL200 has been used; different compounds used for lysing include lysozyme (from chicken egg white), phenylmethanesulfonylfluoride (prepared stock from Thermo Scientific PMSF), anti-protease cocktail (tablets from ThermoScientific).
Centrifuges used were: Eppendorf 5702 centrifuge and Eppendorf 5810R centrifuge.The analytic balance was XS105 DeltaRange Analytical Balance from METTLER TOLEDO.
Filter used was Amicon Ultra-15 Centrifugal filter. Microplate reader used was BioTek Synergy 4.
Column used for IMAC purification was Nickel Sepharose High Performance His-Trap column (GE Healthcare), prepacked with 5 ml of the matrix Nickel Sepharose High Performance.
Column used for SEC purification was Superdex 200 10/300GL. Column used for IEC purification is Q-Sepharose HP column. All these columns were used on a FPLC system (Äkta purifier, Amersham Biosciences).
Buffers used for IMAC purification were: binding buffer (20 mM sodium phosphate, 0.5 M NaCl, 20 mM imidazole, pH = 7.4) and elution buffer (20 mM sodium phosphate, 0.5 M NaCl, 500 mM imidazole, pH = 7.4). Buffer used for SEC purification was 10 mM potassium phosphate (0.138 M NaCl, 0.0027 M KCl, pH =7.4). Buffers used for IEC purification were: binding buffer (10 mM Tris Buffer, pH = 8.0) and elution buffer (10 mM Tris Buffer + 1M NaCl, pH = 8.0).
Eppendorf Thermomixer Comfort was used for BCA assay; 96-well UV-transparent microplates and Thermo Scientific Pierce BCA Protein Assay Kit were also used for BCA. For SDS-PAGE gel assay NuPAGE® Bis-Tris precast gels from Life Technologies™, NuPAGE® LDS Sample Buffer and 0.1 M reducing agent (DTT) were used. NuPAGE® MES SDS running buffer was used as medium and SimplyBlue™ SafeStain (Life Technologies™) was used for staining.

2.2.2 Methods

2.2.2.1 His-eGFP protein

2.2.2.1.1 His-eGFP protein overexpression

Expression of His-eGFP was carried out by using pUCBB-ntH6-eGFP plasmid. This plasmid vector was introduced and expressed in *E.coli* strain BL21 (DE3). Figure 2.1 below shows the plasmid used. This plasmid contains a his-tag with thrombin cleavage site on the N terminal; the vector backbone is pUCBB.

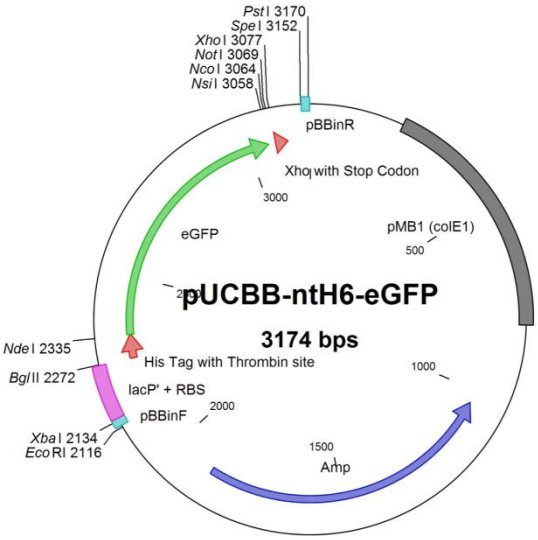

Figure 2.1. pUCBB-ntH6-eGFP plasmid, introduced into *E. coli.* [47]

The plates were set up for His-eGFP expression and an agar solution was poured onto them. The LB agar plates were then incubated for 30 minutes with shaking (250 rpm). After that, bacteria were streaked from the culture stab on the LB agar plates and these were then incubated overnight at 37 °C and 250 rpm. The bacteria cells transformed with pUCBB-ntH6-eGFP were then inoculated in a small volume (15 ml) of Luria-Bertani (LB) medium, containing 100 μg ml^{-1} ampicillin and kept at 37 °C and 250 rpm overnight. A new large scale expression of bacteria culture was then prepared: a large flask containing 600 ml of LB was prepared, containing 100 μg ml^{-1} ampicillin. A new culture was then prepared with absorbance 0.1 at 600 nm (where OD_{600} was measured using an Eppendorf® BioPhotometer) and it was grown at 37 °C and 250 rpm. When the measured absorbance at 600 nm was ~ 0.8, protein expression was then induced by adding Isopropyl β-D-1-thiogalactopyranoside (IPTG) up to a final concentration of 0.5 mM. After inducing the expression, incubation temperature was lowered from 37 °C to 30 °C and cells were grown at 250 rpm for 3 hours. Samples were collected after 0 hours, 1 hour, 2 hours and 3 hours from the time of IPTG induction.
After that, cells were harvested by centrifuging at 3000 g for 15 minutes at 4°C using Eppendorf® centrifuge 5810 R. The pellet was kept frozen at -20°C until further use.
In order to lyse the cells, they were resuspended in phosphate buffer saline (PBS) (0.138 M NaCl, 0.0027 M KCl, pH 7.4) (Sigma). Then, phenylmethanesulfonylfluoride (PMSF) and Lysozyme were added to a final concentration of 1 mM and 1 mg ml^{-1}, respectively, in order to inhibit the protease. Cells were then incubated for 30 minutes on ice and kept in the darkness. Anti-protease cocktail (Thermo Scientific) was then also added to the solution (diluted according

to the manufacturer's protocol). The lysate obtained was then sonicated for 2 minutes (with 10 seconds bursts and 10 seconds cooling between bursts). The lysate was then centrifuged at 14000 rpm for 45 minutes at 4°C by using Eppendorf® centrifuge 5810 R and supernatant was collected after centrifugation. The final sample obtained was stored at -20°C.

2.2.2.1.2 His-eGFP protein purification

His-eGFP protein was purified from the supernatant by first using IMAC. A His-Trap column (GE Healthcare) was used for this purpose on a FPLC system (Äkta purifier, Amersham Biosciences). The column was first washed for 5 column volumes (CV) of ethanol, then 5 CV of deionized water (18 MΩ cm). The column was also equilibrated with 5 CV of binding buffer (20 mM sodium phosphate, 0.5 M NaCl, 20 mM imidazole, pH = 7.4). The protein supernatant sample was then injected into the column and the system was then washed with binding buffer in order to wash away any unbound proteins, until the absorbance level in the monitored chromatogram reached a steady baseline. Elution buffer (20 mM sodium phosphate, 0.5 M NaCl, 500 mM imidazole, pH = 7.4) was then used to elute the remaining protein. Fractions of 1.5 ml were collected for all the duration of the elution process. The fractions corresponding to the elution peak of the protein were collected and stored for further analysis. The elution peak is an absorbance peak at 490 nm observed on the chromatogram corresponding to the protein elution. At the end of the experiment the FPLC system was washed with MQ water and ethanol. The samples collected from the His-Trap purification and corresponding to the elution peak were concentrated using Amicon Ultra-15 Centrifugal filter obtaining a final sample of 1500 µl. A second purification process was carried out using SEC. The column used was Superdex 200 10/300 GL. Superdex column has first been washed for 5 CV of MQ and then with 10 mM potassium phosphate buffer (0.138 M NaCl, 0.0027 M KCl, pH 7.4). 500 µl of concentrated sample were then injected into the system. After sample injection fractions of 1.5 ml were collected. Purified fractions corresponding to the protein elution have been collected and kept for further analysis.

2.2.2.2 GFP protein

2.2.2.2.1 GFP protein overexpression

Expression of GFP was carried out by using pKEN GFP mut2 plasmid. This plasmid vector was introduced and expressed in *E.coli* strain BL21 (DE3). Figure 2.2 below shows the plasmid used. This figure shows that the protein was expressed in pKEN vector. An Xbal site was inserted at the beginning of GFP.

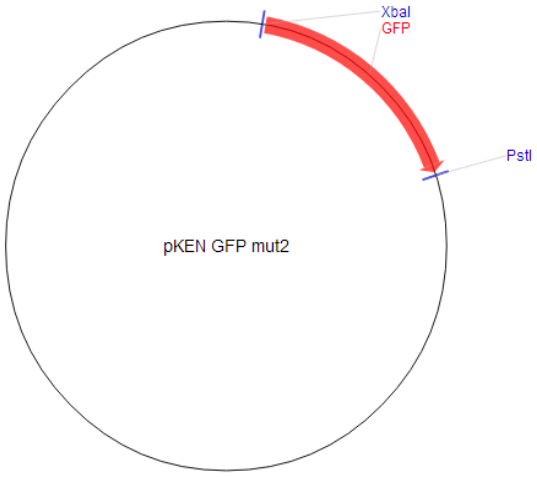

Figure 2.2: pKEN GFP mut2 plasmid. [47]

Different plates were set up for His-eGFP expression and an agar solution was poured onto them. The LB agar plates were then incubated for 30 minutes with shaking (250 rpm). After that, bacteria were streaked from the culture stab on the LB agar plates and these were then incubated overnight at 37 °C and 250 rpm. Figure 2.3 shows the agar plates streaked with bacteria from the culture stab. The bacteria cells transformed with pUCBB-ntH6-eGFP were then inoculated in a small volume (15 ml) of Luria-Bertani (LB) medium, containing 100 μg ml^{-1} ampicillin and kept at 37 °C and 250 rpm overnight. A new large scale expression of bacteria culture was then prepared: a large flask containing 600 ml of LB was prepared, containing 100 μg ml^{-1} ampicillin. A new culture was then prepared with absorbance 0.1 at 600 nm (where OD_{600} was measured using an Eppendorf® BioPhotometer) and it was grown at 37 °C and 250 rpm. When the measured absorbance at 600 nm was ~ 0.7, protein expression was then induced by adding Isopropyl β-D-1-thiogalactopyranoside (IPTG) up to a final concentration of 0.5 mM. After inducing the expression, incubation temperature was lowered from 37 °C to 30 °C and cells were grown at 250 rpm for 3 hours. Samples were collected after 0 hours, 1 hour, 2 hours and 3 hours from the time of IPTG induction.
After that, cells were harvested by centrifuging at 3000 g for 15 minutes at 4°C using Eppendorf® centrifuge 5810 R. The pellet was kept frozen at -20°C until further use.
In order to perform the cell lysing, cells were resuspended in phosphate buffer saline (PBS)(0.138 M NaCl, 0.0027 M KCl, pH 7.4) (Sigma). Then, phenylmethanesulfonylfluoride (PMSF) and Lysozyme were added to a final concentration of 1 mM and 1 mg ml^{-1}, respectively, in order to inhibit the protease. Cells were then incubated for 30 minutes on ice and kept in the darkness. Anti-protease cocktail (Thermo Scientific) was then also added to the solution (diluted according to the manufacturer's protocol). The lysate obtained was then sonicated for 2 minutes (with 10 seconds bursts and 10 seconds cooling between bursts). The lysate was then centrifuged at 14000 rpm for 45 minutes at 4°C by using Eppendorf® centrifuge 5810 R and supernatant was collected after centrifugation. The final sample obtained was stored at -20°C.

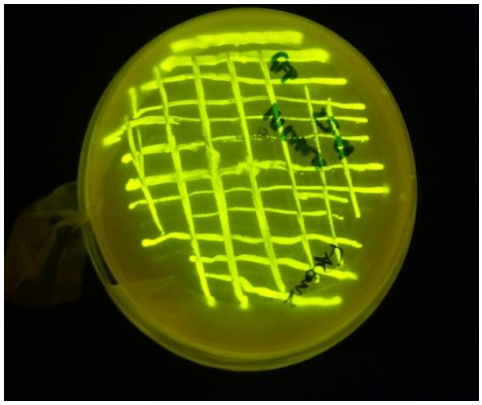

Figure 2.3 Agar plate streaked with bacteria from pKEN GFP mut2 plasmid.

2.2.2.2.2 GFP protein purification

IEC was first used to purify the GFP protein. In order to do so, a Q-Sepharose HP column on a FPLC system was used.
Two different buffers were used for this purification: Buffer A was 10 mM Tris Buffer, pH = 8.0. Buffer B was 10 mM Tris Buffer, pH = 8.0 and 1M NaCl.
The Q-sepharose column was equilibrated with 5 CV of deionized water (18 MΩ cm) and then 5 CV of Buffer A. Afterwards, the GFP sample obtained from lysing was injected into the system. After injection, the column was washed with buffer A for 5 CV, and then a gradient was run, starting from 0% buffer A to 50% buffer B, for 100 ml. All the fractions corresponding to the protein elution have been collected, for a total of around 15 ml sample volume.

A SEC purification was then performed. The samples collected from the previous purification were concentrated by using Amicon Ultra-15 Centrifugal filter obtaining a final sample of 500 µl. SEC column (Superdex 200 10/300 GL)was washed for 5 CV with MQ water, then for other 5 CV with buffer (10 mM potassium phosphate). The concentrated sample (500 µl) was then injected into the system and fractions corresponding to the major protein elution peak were collected.
Another round of SEC purification was performed by injecting 500 µl of the fraction corresponding to the protein peak obtained in the first SEC purification. Finally, fractions were collected and kept for further analysis.

2.2.2.3 Nanobody protein

2.2.2.3.1 Nb protein overexpression

Expression of Nb was carried out by using pOPINE GFP nanobody plasmid. This plasmid vector was introduced and expressed in *E.coli* strain BL21 (DE3). Figure 2.4 below shows the plasmid used. This plasmid shows that the amino acids sequence of the Nb was cloned into pOPINE vector using PmeI nucleases. The Nb sequence contains a his-tag on the C terminal and a GFP sequence inserted in the pOPINE backbone.

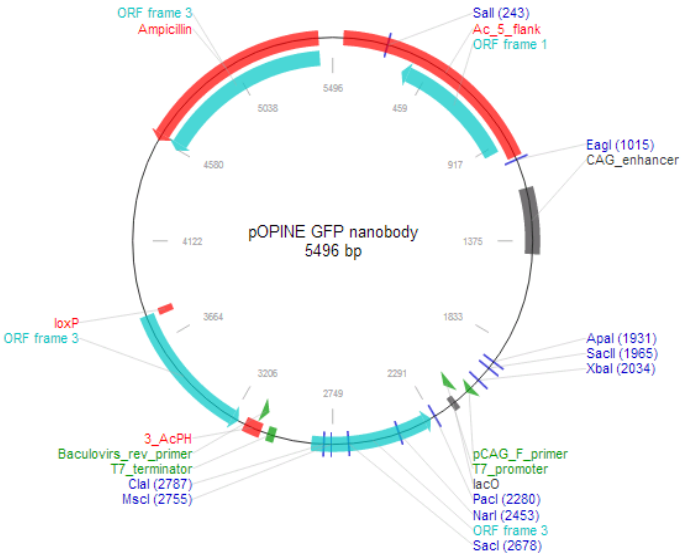

Figure 2.4 pOPINE GFP nanobody plasmid. [47]

The protocol used for Nb overexpression presents some significant differences compared to the protocol used for expressing GFP.
The plates were set up for His-eGFP expression and an agar solution was poured onto them. The LB agar plates were then incubated for 30 minutes with shaking (250 rpm). After that, bacteria were streaked from the culture stab on the LB agar plates and these were then incubated overnight at 37 °C and 250 rpm. The bacteria cells transformed with pUCBB-ntH6-eGFP were then inoculated in a small volume (15 ml) of Terrific Broth (TB) medium, containing 100 μg ml^{-1} ampicillin and kept at 37 °C and 250 rpm overnight. A new large scale expression of bacteria culture was then prepared: a large flask containing 600 ml of TB was prepared, containing 100 μg ml^{-1} ampicillin. A new culture was then prepared with absorbance 0.1 at 600 nm (where OD_{600} was measured using an Eppendorf® BioPhotometer) and it was grown at 37 °C and 250 rpm. When the measured absorbance at 600 nm was ~ 0.6, protein expression was then induced by adding Isopropyl β-D-1-thiogalactopyranoside (IPTG) up to a final concentration of 0.5 mM. After inducing the expression, incubation temperature was lowered from 37 °C to 20 °C and cells were grown for 20 hours.
After that, the bacteria cells were harvested by centrifuging at 3000 g for 15 minutes at 4°C using Eppendorf® centrifuge 5810 R. The pellet was kept frozen at -20°C until further use.
In order to perform the cell lysing, cells were resuspended in phosphate buffer saline (PBS)(0.138 M NaCl, 0.0027 M KCl, pH 7.4) (Sigma). Then, phenylmethanesulfonylfluoride (PMSF) and Lysozyme were added to a final concentration of 1 mM and 1 mg ml^{-1}, respectively, in order to inhibit the protease. Cells were then incubated for 30 minutes on ice and kept in the darkness. Anti-protease cocktail (Thermo Scientific) was then also added to the solution (diluted according to the manufacturer's protocol). The lysate obtained was then sonicated for 2 minutes (with 10 seconds bursts and 10 seconds cooling between bursts). The lysate was then centrifuged at 14000 rpm for 45 minutes at 4°C by using Eppendorf® centrifuge 5810 R and supernatant was collected after centrifugation. The final sample obtained was stored at -20°C.

2.2.2.3.2 Nb protein purification

Nb protein was purified from the supernatant by first using IMAC. A His-Trap column (GE Healthcare) was used for this purpose on a FPLC system (Äkta purifier, Amersham Biosciences). The column was first washed for 5 column volumes (CV) of ethanol, then 5 CV of deionized water (18 MΩ cm). The column was also equilibrated with 5 CV of binding buffer (20 mM sodium phosphate, 0.5 M NaCl, 20 mM imidazole, pH = 7.4). The protein supernatant sample was then injected into the column and the system was washed with binding buffer in order to wash away any unbound proteins, until the absorbance level in the monitored chromatogram reached a steady baseline. Two elution buffers have been used to elute the Nb protein: first, an elution buffer with 60 mM sodium phosphate, 0.5 M NaCl and 500 mM imidazole (pH=7.4), then an elution buffer with the same composition but 300 mM sodium phosphate. The goal was to start cleaning the sample by eluting with the first elution buffer at 60 mM imidazole; afterwards a gradient from 0% 60 mM imidazole buffer to 100% 300 mM imidazole buffer over 100 ml has been used in order to elute the protein. Fractions corresponding to the elution peak and also the ones corresponding to the binding step were collected for further analysis.
A SEC purification was then performed with the following protocol.
SEC column (Superdex 200 10/300 GL) was washed for 5 CV with deionized water (18 MΩ cm), then for other 5 CV with buffer (10 mM potassium phosphate). 500 µl of protein from previous IMAC purification was injected into the system with the Hamilton Syringe. Fractions during elution were collected for further analysis.

2.2.2.4 His-eGFP, GFP and Nb characterization

2.2.2.4.1 SDS-PAGE gels

The samples purity was analyzed using a sodium dodecyl sulfate-polyacrylamide gel electrophoresis (SDS-PAGE). For this purpose, NuPAGE® Bis-Tris precast gels from Life Technologies™ were used. The samples were prepared by mixing protein sample to a ratio of 6.5:10 (volume of protein : final volume), 4x NuPAGE® LDS Sample Buffer with a ratio 1:4 (NuPAGE®LDS Sample Buffer : final volume) and 0.1 M reducing agent (DTT). The samples were then heated at 70°C for 15 min and they were loaded onto the gels.
The gels were run at 150 V for 50 min and NuPAGE® MES SDS running buffer was used as a medium. After that, they were stained with SimplyBlue™ SafeStain (Life Technologies™) according to the manufacturer's protocol. Gels were heated in the microwave, washed with water and shaken according to this protocol. Afterwards they have been destained and a scanned image was saved for further analysis.
Analysis of the scanned gel image was performed using ImageJ®.

2.2.2.4.2 Fluorescence spectra

For analysis of the fluorescence spectra, microplate reader BioTek Synergy™ H4 was used. Absorbance, emission and excitation measurements have been recorded in a 96-well UV-transparent microplate (Corning).

Absorbance spectra were monitored between 230 nm and 800 nm.
Emission spectra of His-eGFP were collected by exciting the sample at 400 nm and monitoring the emission between 500 nm and 800 nm, while excitation spectra were monitored between 250 and 510 nm.
Emission spectra of GFP were collected by exciting the sample at 430 nm and monitoring the emission between 500 nm and 800 nm, while excitation spectra were monitored between 250 and 510 nm.

2.2.2.4.3 BCA assay

Bicinchoninic acid (BCA) assay has been used to determine the total protein concentration. This assay was carried out using a Thermo Scientific Pierce BCA Protein Assay Kit according to the manufacturer's protocol.
Diluted albumin standards (BSA) at different concentrations and different protein samples were allowed to react with BCA working reagents in a 96-well UV-transparent microplate (Corning) at 37 °C for 30 minutes. Afterwards, Synergy H4 microplate reader has been used to read absorbance at 562 nm. A standard curve was then prepared by plotting the average Blank-corrected 562 nm measurement for each BSA standard versus its concentration in µg/ml. Finally, the standard curve was used to determine the protein concentration of each sample.

2.3 Results and discussion

2.3.1 His-eGFP protein

The SDS-PAGE gel in figure 2.5 shows the purity of the sample obtained from the same His-eGFP protein supernatant sample at the end of the overexpression process, after lysing. This gel clearly indicates in both columns B and C the presence of a His-eGFP protein at around 28 kDa, as two dark bands are clearly visible around that MW.

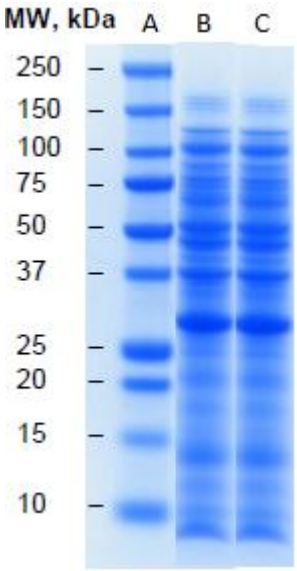

Figure 2.5. SDS-PAGE gel of supernatant samples from His-eGFP overexpression (A=marker; B, C= supernatant)

Figure 2.6 and 2.7 shows the binding and elution steps of the His-Trap purification. Absorbance was monitored at 280 nm (blue curves), which corresponds to the wavelength where aromatic amino acids absorb light; therefore this wavelength is used to detect any proteins. Absorbance was also monitored at 490 nm (red curves), which corresponds to the wavelength of the absorbance peak of the GFP protein.

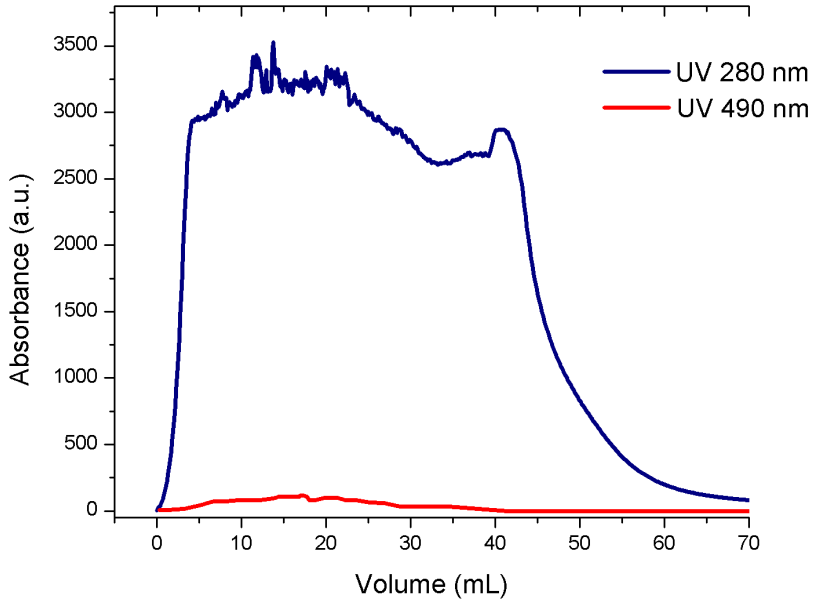

Figure 2.6 Chromatogram corresponding to the binding step of the His-Trap protein purification of His-eGFP. Absorbance was monitored at 490 nm and 280 nm.

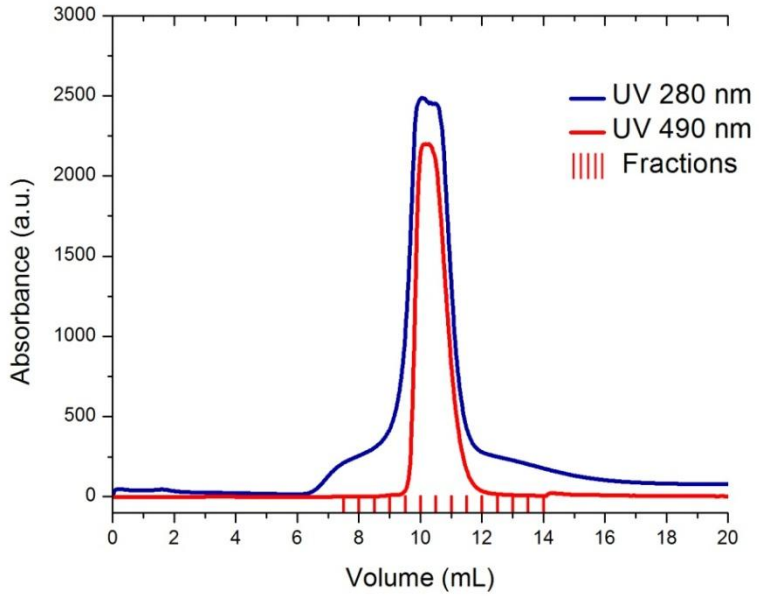

Figure 2.7 Chromatogram corresponding to the elution step of the His-Trap protein purification of His-eGFP. Absorbance was monitored at 490 nm and 280 nm. Fractions collected are shown as red vertical lines.

During binding step, the his-tagged proteins are binding to the column. Here, as expected, absorbance at 280 nm reached high absorbance values, around 3000 a.u. for about 50 ml, indicating the successful selectivity of the column for His-tagged proteins binding onto it. Figure 2.7 shows the elution process, where imidazole at a high concentration was used to elute His-eGFP protein. Fractions collected are shown as vertical lines in figure 2.7. The absorbance peak of His-eGFP (red curve in figure 2.7) corresponded to fractions between 9 and 12 ml. Since the absorbance curve at 280 nm (blue curve in figure 2.7) clearly indicates the presence of some impurities, it is possible to infer that the eluted protein will not be pure enough. This is confirmed by the SDS-PAGE gel in figure 2.8: column J of this gel indicates the purity of the IMAC sample, revealing that the protein is still not pure enough.

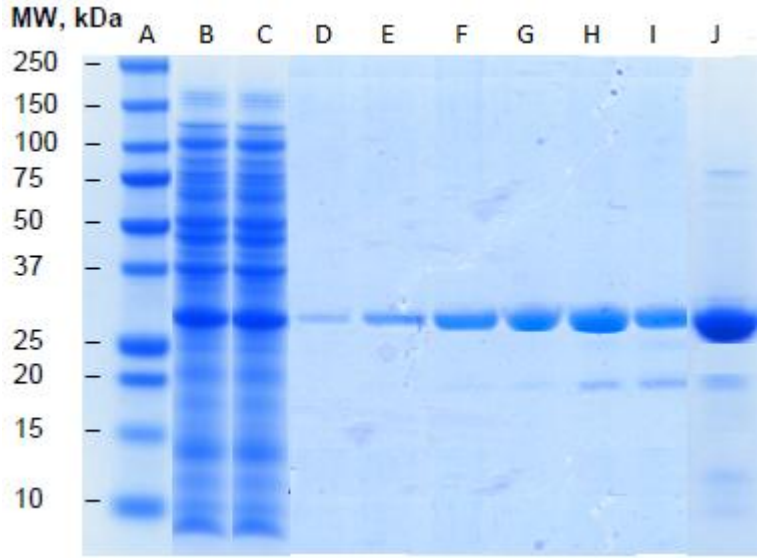

Figure 2.8 SDS-PAGE gel of different samples from previous IMAC and SEC His-eGFP purifications (A=marker; B, C=supernatant; D, E, F, G, H, I=samples from SEC purification corresponding to fractions from 8 to 13 ml; J=sample from IMAC purification).

Figure 2.9 shows the chromatogram of the SEC purification performed with Superdex 200 column. As illustrated by this chromatogram, the peak corresponding to the His-eGFP protein elution is between 14 and 18 ml from the time of injection. Calibration of the column indicated that samples eluted around 16 ml corresponds to proteins of size of ~30 kDa. Collected fractions are indicated by vertical lines in the chromatogram; these fractions corresponded to the major absorption peak.

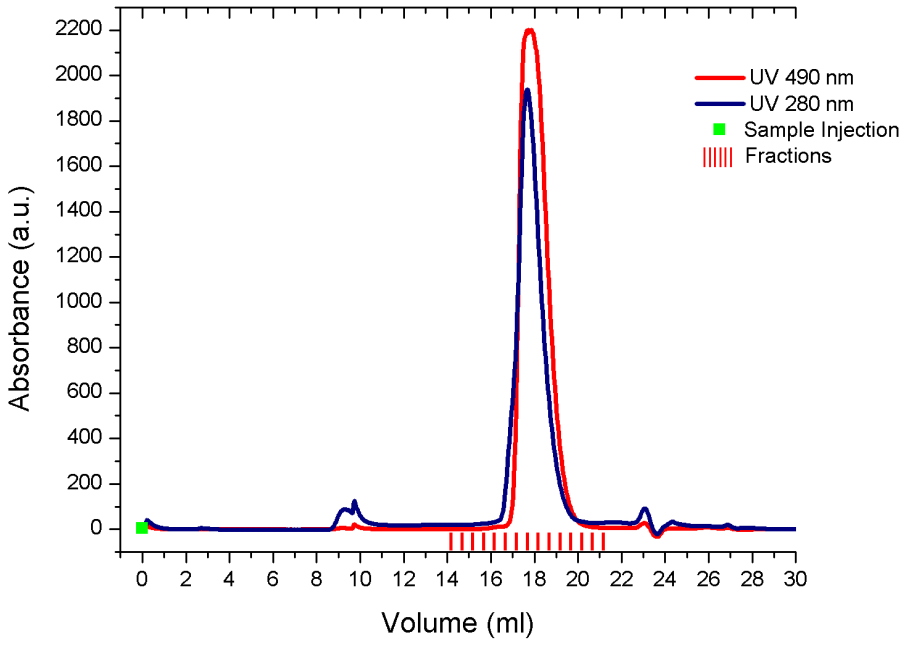

Figure 2.9 Chromatogram corresponding to the SEC purification of the His-eGFP protein. Absorbance was monitored at 490 and 280 nm. Collected fractions as shown as vertical red lines.

SDS-PAGE gel in figure 2.8 shows different samples corresponding to the His-eGFP protein supernatant, His-Trap purification and SEC purification. Each sample used from the SEC purification corresponds to a different fraction collected from the FPLC.
From this SDS-PAGE gel it is possible to observe a band that is constantly present around 30 kDa in all the different fractions from SEC. As it is known that the size of GFP is 28 kDa, then it is possible to infer that the purified protein is the His-eGFP.
Column J of this gel shows that the protein after His-Trap purification still presents some impurities.
Regarding the purity of the protein after SEC purification, it is clear that, out of the six SEC samples used, the first four samples (D, E, F, G) from the left show a higher purity compared to the other two (H, I) suggesting a difference in purity among the SEC samples. Samples shown in columns H and I correspond to the fractions collected at the end of the protein absorbance peak shown in chromatogram of figure 2.9, around 18 ml: as indicated by the gel, these fractions are slightly less pure, despite the curve in the chromatogram looks very symmetrical. Columns D and E of the gel correspond to the fractions collected at the beginning of this absorbance peak, they are very pure but they also have less protein density compared to the other samples used.
Analysis of the gels with ImageJ indicated indicated a purity of the samples of ~ 90 %.
In conclusion, His-eGFP protein was successfully purified. Purification with SEC showed an increased purity of the samples compared to the previous His-Trap purification.

Figure 2.10 shows the absorbance spectrum of the His-eGFP sample corresponding to the fraction collected at 16 ml after SEC purification (figure 2.8) and analyzed in column F of gel in figure 2.9. The same sample has been used for analysis of emission and excitation spectra illustrated in figure 2.11.
In the absorbance spectrum in figure 2.10 there are two significant peaks, as expected, at 280 nm and 488 nm. This spectrum shows that the ratio between absorbance at 488 nm and 280 nm is around 2.2 : 1, which is similar to the ratio found in the literature[32] (2.5 : 1). This confirms the good purity of the sample.

The excitation and emission spectra (figure 2.11) also match those found in the literature[32], proving that His-eGFP protein retains its functionality after expression and purification.

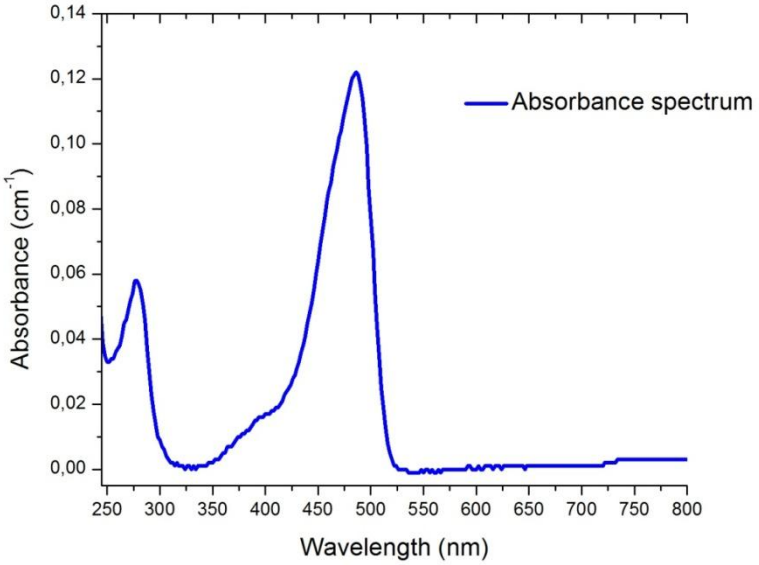

Figure 2.10 Absorbance spectrum of His-eGFP sample after purification through IMAC and SEC. The absorbance was corrected to a pathlength of 1 cm.

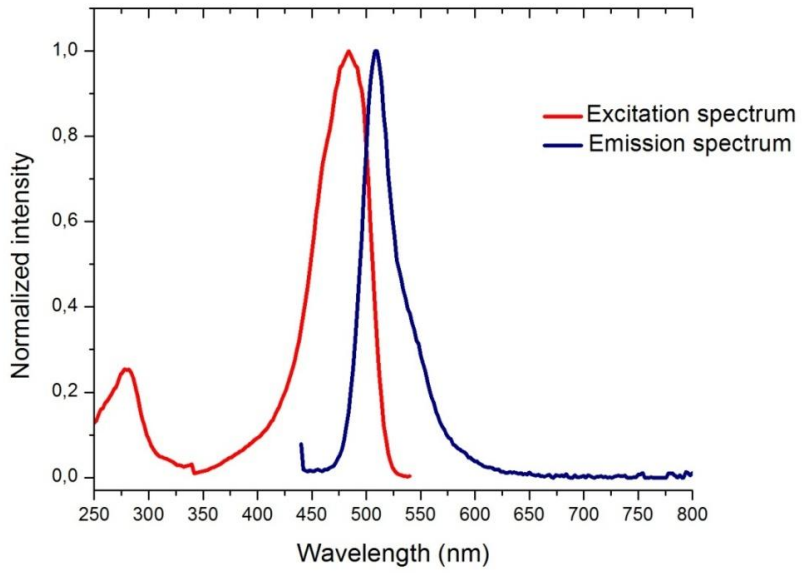

Figure 2.11 Emission ($\lambda_{excitation}$=430 nm) and excitation ($\lambda_{emission}$=530 nm) spectra of His-eGFP protein sample (diluted 1:15) after purification through IMAC and SEC.

Lambert-Beer law was used with the results obtained from the absorbance spectra of the protein samples. For each sample, the corrected absorbance (which is obtained by subtracting the blank absorbance from the real absorbance value) was calculated. The obtained result indicated a protein yield of 1.14 mg/ml, which will be confirmed by BCA.
The average concentration determined by BCA gave a yield of 1.32 mg/ml.

2.3.2 GFP protein

The SDS-PAGE gel in figure 2.12 illustrates two samples obtained from the same GFP protein supernatant sample at the end of the overexpression process. This gel clearly indicates the presence of a protein of MW of around 30 kDa, (where two darker bands are clearly noticeable) that corresponds to the size of GFP.

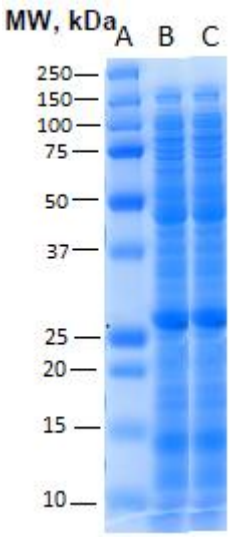

Figure 2.12 SDS-PAGE gel of supernatant samples from GFP overexpression (A=marker; B, C= supernatant).

Figure 2.13 shows the chromatogram of the IEC purification of GFP protein. Absorbance was monitored at 280 nm (blue curve), which corresponds to the wavelength where aromatic amino acids absorb light; therefore this wavelength is used to detect any proteins. Absorbance was also monitored at 490 nm (red curve) which corresponds to the wavelength of the absorbance peak of the GFP protein.

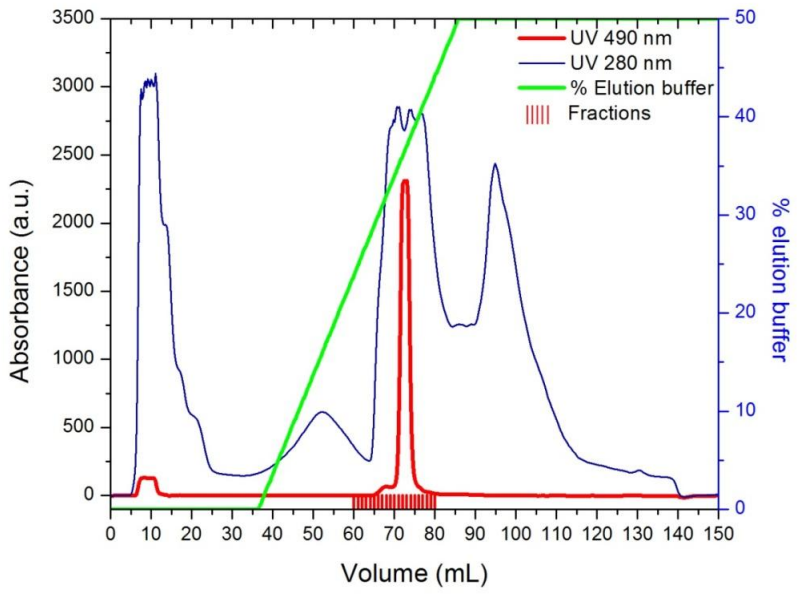

Figure 2.13 Chromatogram corresponding to the purification of GFP protein using Q-Sepharose column. % elution buffer corresponds to fraction of elution buffer used. Absorbance was monitored at 490 and 280 nm. Collected fractions are shown as vertical lines.

In chromatogram of figure 2.13, it is possible to observe that some material with absorbance at 280 and 490 nm elutes at 70 mL, corresponding to around 30 % elution buffer (10 mM Tris Buffer + 1M NaCl). Fractions were collected between 60 and 80 ml. As already indicated by the absorbance curve monitored at 280 nm, several bands are visible in the corresponding SDS PAGE gel (figure 2.14).
SDS-PAGE gel in figure 2.14 shows the different fractions obtained from Q-sepharose purification, corresponding to gel columns D, E and F. From this gel it is possible to observe that the samples corresponding to the fractions collected after Q-sepharose purification (see figure 2.13) are still not pure, as little difference can be detected between the purity of these samples (column D, E, F of figure 2.14) and the supernatant (columns B and C). A band is clearly noticeable in this gel at 30 kDa, corresponding to the GFP protein.

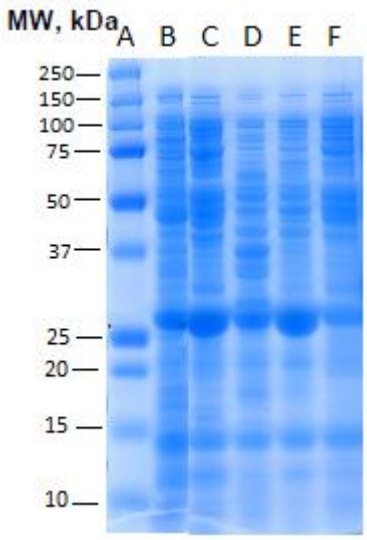

Figure 2.14 SDS-PAGE gel of different fractions collected after IEC purification (A=marker; B, C=supernatant; D, E, F = fractions after Q-sepharose purification from 72 to 75 ml).

Figure 2.15 shows the chromatogram obtained after the first SEC purification. This purification did not give good results since the injected sample was too concentrated. This chromatogram shows that the protein is still not well purified, and this is clearly visible as the curves are not symmetrical at all. Fractions shown as vertical lines in the figure were collected, and some of these fractions were chosen and examined on a SDS-PAGE gel, shown in figure 2.16.

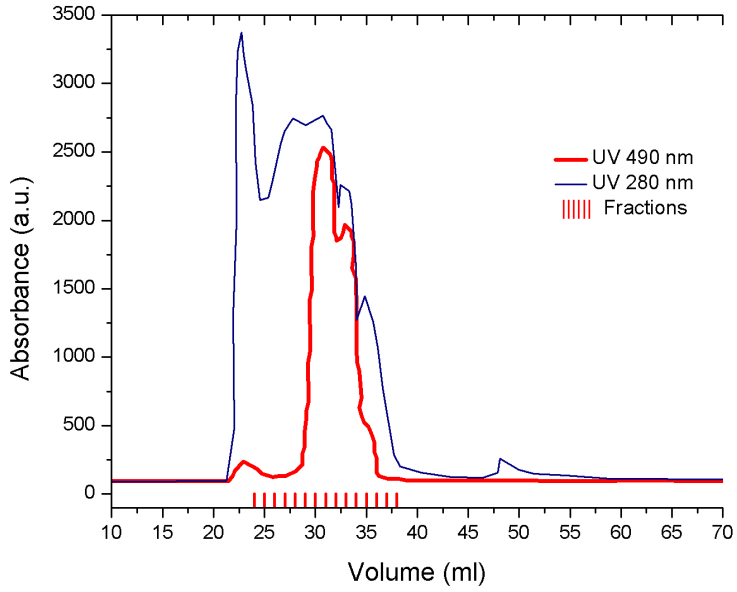

Figure 2.15 Chromatogram corresponding to the first SEC purification of GFP protein. Absorbance was monitored at 490 and 280 nm. Collected fractions are shown as vertical lines.

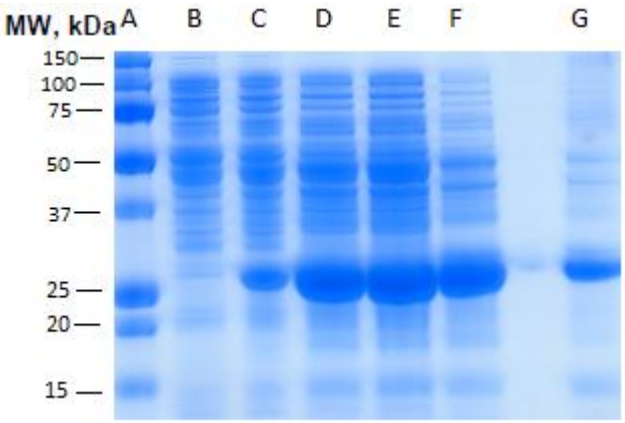

Figure 2.16 SDS-PAGE gel of different fractions collected after the first SEC purification (A=marker; C, D, E, F, G=samples from the first SEC purification, from 31 to 35 ml).

The SDS-PAGE gel shown in figure 2.16 illustrates the purity of different fractions collected after the first SEC purification (figure 2.15). Some fractions corresponding to the SEC purification are slightly more pure than those corresponding to the IEC purification, such as the fraction corresponding to column G in figure 2.16, although this fraction contains less protein. Nevertheless, the protein is still not pure, as indicated by all the other fractions on the gel, which present several bands. Therefore, another SEC purification was needed to further purify GFP. Fractions from this SEC purification were collected and injected again into the system, obtaining the chromatogram shown in figure 2.17.

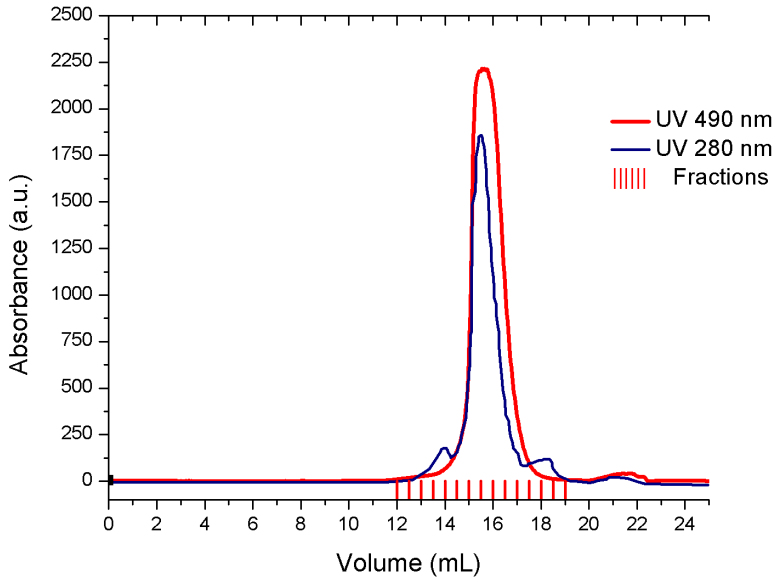

Figure 2.17 Chromatogram corresponding to the final SEC purification of GFP protein. Absorbance was monitored at 490 and 280 nm. Collected fractions are shown as vertical lines.

Chromatogram in figure 2.17 shows the final SEC purification of GFP protein. This chromatogram is comparable to the SEC purification of His-eGFP protein, shown previously in figure 2.9. Calibration of the column indicated that samples eluted around 15 ml corresponds to proteins of size of ~30 kDa, which is the MW of GFP. Fractions corresponding to this elution peak between 14 and 19 ml (shown as vertical lines in figure 2.17) were collected and kept for further analysis.

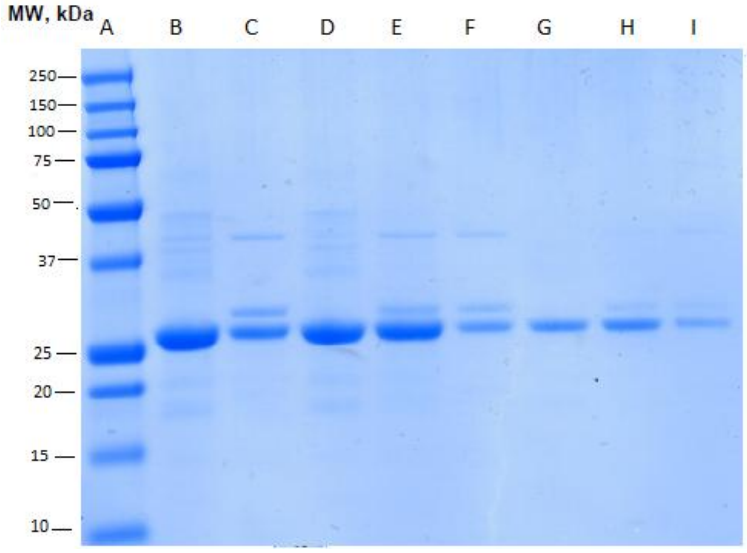

Figure 2.18 SDS-PAGE gel of different fractions collected after the final SEC purification (A=marker; B, C, D, E, F, G, H, I =samples from the final SEC purification, from 14 to 19 ml).

Figure 2.18 shows different fractions corresponding to the elution peak of the final SEC purification, visible in chromatogram of figure 2.17.
Fractions in columns B and D appear to be the purest among the different samples analyzed. Fractions in columns G and H are also very pure but show little protein concentration, as they correspond to the end of the GFP elution peak. Fractions in columns C and E show a lower purity compared to the other ones.
Overall, it is possible to affirm that the purification was successful and the different samples appear to be pure enough, especially fractions in columns B and D. It is interesting to notice that at a MW slightly above 30 kDa a light band is still visible, especially in columns C, E and F of the gel, indicating some level of impurity.

ImageJ was used to evaluate with more precision the percentage of purity of the samples. Analysis of fractions corresponding to columns B and D of the gel in figure 2.18 indicated a purity of around 85%.
The average concentration determined by BCA gave a yield of 1.63 mg/ml.

Figure 2.19 shows the absorbance spectrum of the GFP sample corresponding to the fraction collected at 15 ml after the final SEC purification (figure 2.17) and analyzed in column B of gel in figure 2.18. The same sample has been used for analysis of emission and excitation spectra illustrated in figure 2.20.
In the absorbance spectrum shown in figure 2.19 there are two significant peaks, at 280 nm and 488 nm. These peaks match those reported in the literature. The spectrum shows also that the ratio between absorbance at 488 nm and 280 nm is around 1.5 : 1, which is quite different from the ratio of 2.2 : 1 corresponding to the spectrum previously calculated for His-eGFP protein (figure 2.10).

The excitation and emission spectra (figure 2.20) are very similar to those obtained after the His-eGFP protein purification, shown in figure 2.11, indicating that this purified GFP protein also retains its functionality after expression and purification.

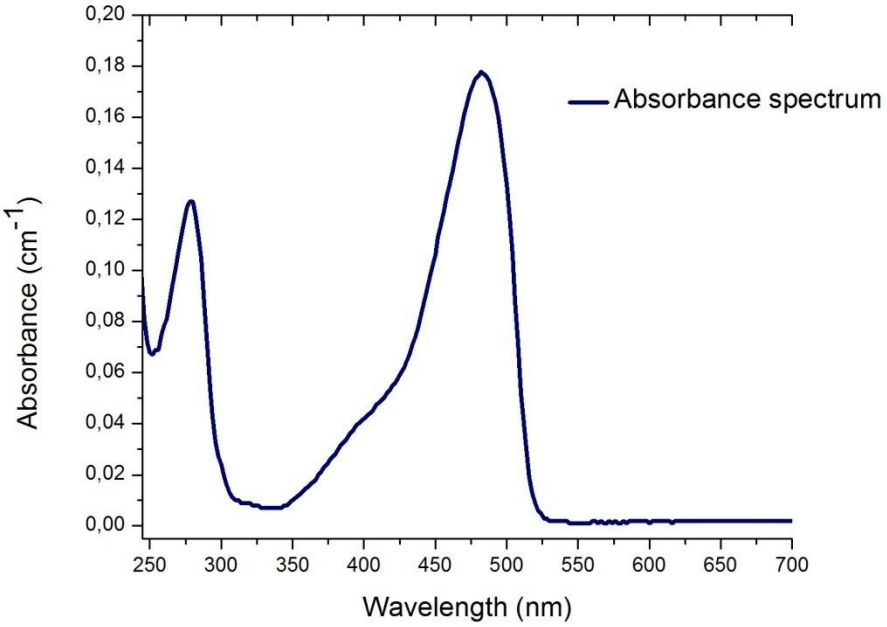

Figure 2.19 Absorbance spectrum of a GFP sample (diluted 1:10) after purification through IEC and SEC. The absorbance was corrected to a pathlength of 1 cm.

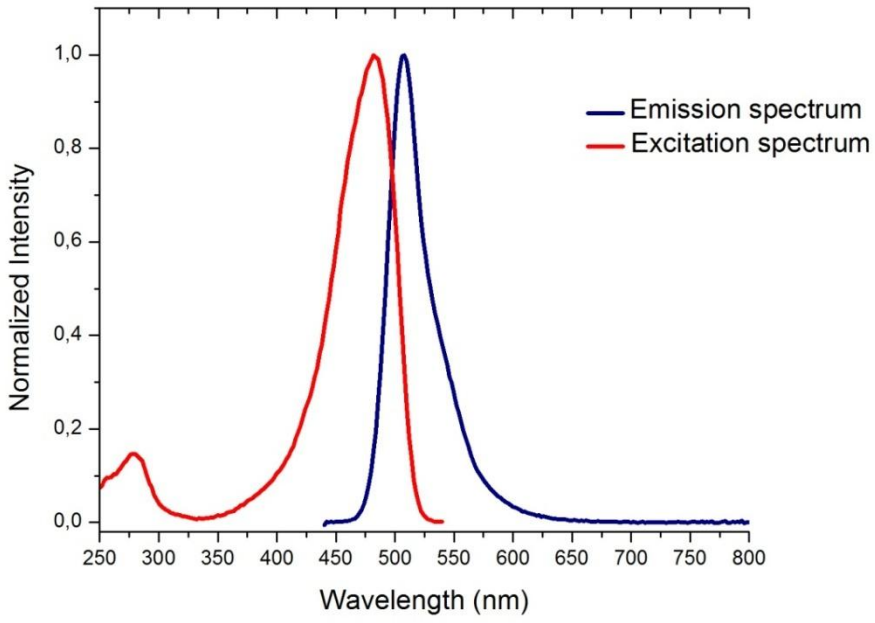

Figure 2.20 Emission ($\lambda_{excitation}$=430 nm) and excitation ($\lambda_{emission}$=530 nm) spectra of GFP protein sample (diluted 1:25) after purification through IEC and SEC.

2.3.3 Nb protein

The SDS-PAGE gel in figure 2.21 shows a sample obtained from the supernatant of the Nb protein at the end of the second cycle of overexpression and lysing . A dark band is visible around 15 kDa, which corresponds to the MW of the Nb protein.

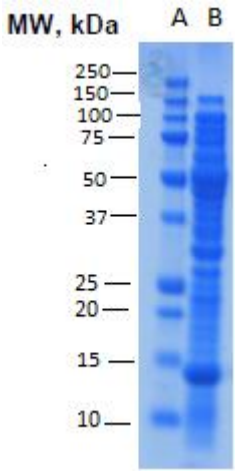

Figure 2.21 SDS-PAGE gel of supernatant samples from Nb overexpression (A=marker; B= Nb supernatant).

Nb overexpression and purification was repeated twice. In the first cycle, Nb protein was purified first with a His-Trap column. As a result of this purification, a protein elution peak was observable when the concentration of the elution buffer (500 mM imidazole) was around 30%; therefore the fractions corresponding to this peak were collected. Analysis on a SDS-PAGE gel of these fractions indicated that the protein was not pure, as shown in figure 2.22. Therefore, purification with SEC was also performed. Purification with SEC also did not give satisfying results, as no isolated single peak corresponding to the Nb protein was identified.

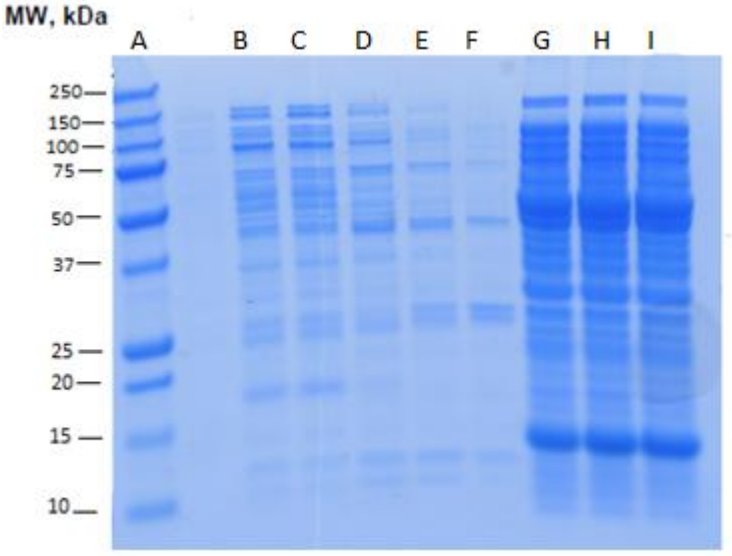

Figure 2.22 SDS-PAGE gel showing different fractions corresponding to the first His-Trap purification of Nb. (A=marker; B, C, D, E, F= fractions corresponding to the binding step of the protein; G, H, I = fractions corresponding to the elution peak of the protein).

After the second cycle of Nb overexpression, purification was repeated with His-Trap column. This time small amounts of diluted Nb sample were injected, corresponding to 500 µL. The purification was performed several times. Figure 2.23 below illustrates a chromatogram obtained from this purification. Absorbance was monitored at 280 nm, corresponding to the absorption of aromatic amino acids.

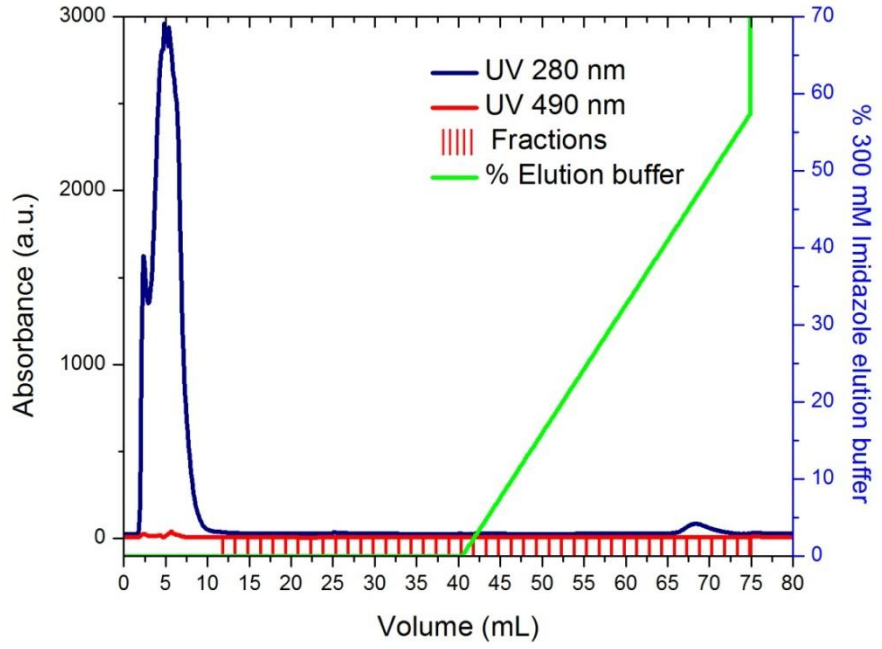

Figure 2.23 Chromatogram corresponding to the purification of Nb protein using His-Trap column. Absorbance was monitored at 490 and 280 nm. Collected fractions are shown as vertical lines. % elution buffer corresponds to fraction of 300 mM imidazole elution buffer used.

As shown by the chromatogram in figure 2.23, a small elution peak was obtained at around 65 ml, corresponding to around 40% 300 mM elution buffer. A small elution peak was expected as the injected protein volume was quite small (500 µl).

However, the Nb purification did not give satisfactory results. SDS-PAGE gel in figure 2.24 below shows the concentrated sample of the fractions corresponding to the elution peaks obtained from the several His-Trap purifications, such as the one shown in chromatogram of figure 2.23. From this gel one can observe that the Nb protein is barely visible and there is still not enough quantity, even after concentrating the different fractions available.

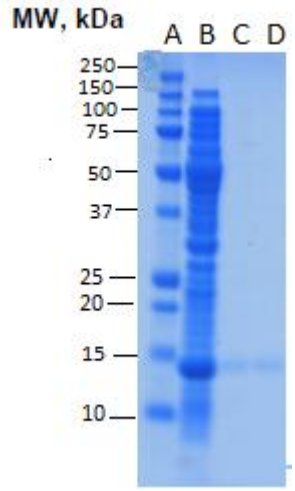

Figure 2.24 SDS-PAGE gel of the concentrated fractions from the IMAC purification (A=marker; B=supernatant; C,D= concentrated Nb).

2.4 Conclusion

In conclusion, both GFP and His-eGFP proteins were successfully overexpressed, purified and characterized. Both proteins indicated a high level of purity of ~90%, which is very satisfactory, and their absorbance, emission and excitation spectra match those found in the literature. Furthermore, the final yield of the proteins was ~1.3 mg/ml for His-eGFP and ~1.6 mg/ml for GFP.

The purification of Nb on the other hand presented many challenges. The overexpression of Nb was successful, but the Nb purification led to many difficulties and an unclear result, as the final obtained purified Nb protein had a very low density, even after repeating the experiments three times.

A reason for that might be that there is only a single protocol available in the literature for the Nb overexpression and purification, as Nb is relatively novel tool in nanoscience. Therefore, many conditions in the experiments probably need to be optimized in order to achieve a more satisfactory result.

Chapter 3.

Surface Plasmon Resonance

3.1 Introduction:

3.1.1 Aims

The major goal of this chapter is to introduce the SPR technique and report the experiments performed to characterize and evaluate the interaction between αGFP-Nb-His (Nb against GFP tagged with a histidine tag) and an antigen, namely GFP, using Biacore X100 sensor. This interaction will be assessed by the association and dissociation rate constants, as well as by the equilibrium dissociation constant. This interaction will be performed using two types of protein immobilization techniques, which will be analyzed and compared.
Other goals include the characterization of the interaction between the αGFP-Nb-His protein to two sensor surfaces, and the comparison of the interaction with that of a model protein, His-eGFP, to the same surfaces.

3.1.2 Theoretical background

Figure 3.1 shows the principle of Surface Plasmon Resonance in the so-called Kretschmann configuration. A surface plasmon is a longitudinal wave which is present at the interface of two media, where one is metallic and the other one is dielectric. Surface Plasmon Resonance is defined as the oscillation of electrons in a liquid or solid material; SPR is caused by a polarized light hitting the surface at the interface between the two media.[48] Once the light hits a half circular prism, it is directed towards the plane of interface, changing from a thicker medium to a less dense one. This will change the incident angle, and consequently the incident light, until a critical angle has been reached. The light will be totally reflected at the interface and will then penetrate into the higher refractive index medium and bounce into a detector. Total Internal Reflection (TIR) is the situation where all the light is reflected in the half circular prism.[49] [50]

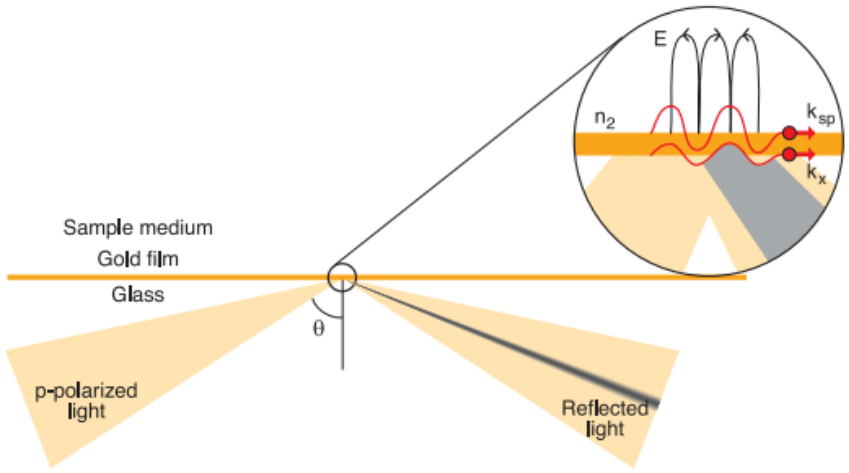

Figure 3.1 Principle of Surface Plasmon Resonance. A polarized light hits SPR; this light is reflected internally at a glass/metal interface. In Biacore systems this interface is a gold-coated glass side. For a single wavelength of p-polarized light, SPR is defined as a dip in the amplitude of reflected light at a selected SPR incidence angle.[51]

Since the surface plasmon resonance angle is dependent on the properties of the metal film, the metal coating the surface needs to possess conduction band electrons able to resonate with the received light at an appropriate wavelength; also, the metal has to be devoid of oxides and sulphides. Metals that fulfill these requirements are gold, aluminium, sodium and indium, but gold is the only one which is completely resistant to oxidation and therefore it is the most practical one used in SPR.[52]
By coating the prism with a noble metal thin film such as gold, SPR signal will be characterized by an optimal reflectance angle and wavelength; also, gold is inert to many solutions that are used in different biochemical settings. Furthermore, gold, unlike other metals, has a great resistance to oxidation and many other atmospheric pollutants.

In TIR, the fully reflected light will yield an electric field which will diffuse into the lower refractive index medium, called evanescent field wave. This evanescent wave is absorbed by electron clouds that are present in the gold layer, thus producing electron charge density waves (plasmons) and inducing a decrease in the intensity of the reflected light. As shown in Figure 3.2, the intensity of this evanescent field wave declines exponentially as the distance from the solid interface expands. The depth of penetration of the evanescent field wave is equivalent to the distance at which the intensity of this wave decreases to 1/e of its total highest amplitude.[53]
The penetration depth of the evanescent wave which can give significant results for SPR measurements is less than 300 nm of the sensor surface. The wavelength of the evanescent field coincides with that of the incident light (445 nm).[53]

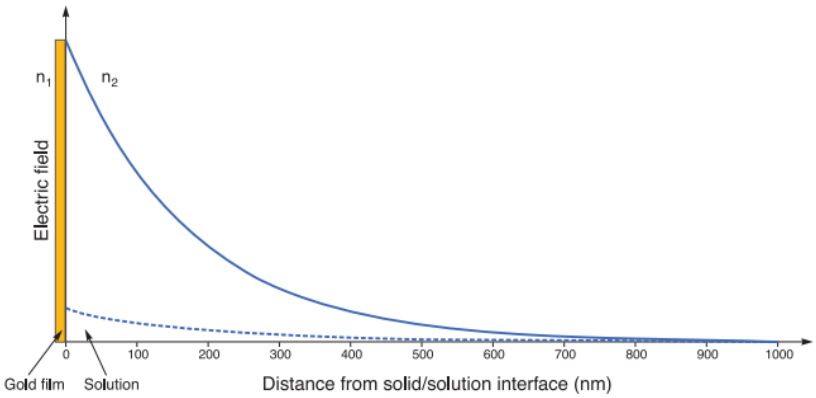

Figure 3.2 Amplitude of the evanescent field wave (electric field on the Y axis) versus distance from the solid or solution interface.[51]

By binding biomolecules of an injected sample on the sensor surface, a change in the refractive index on the surface is observed; this change is measured as a change in resonance angle or wavelength and it is proportional to the change in mass concentration[50]. Data detected from these changes is presented in a sensorgram, as it will be explained in the next paragraph.
Biacore X100 is able to monitor in real time interactions between two molecules using a label free detection method which depends on the principle of Surface Plasmon Resonance, described before.
This molecular interaction involves an immobilized molecule that has been coupled to the surface of a sensor chip and another molecule that has been injected into the system and that can freely move in solution over the sensor surface.[54] A change in refractive index is observed when molecules from the injected sample start to bind to the immobilized molecules. This change in refractive index is monitored in real time and it also corresponds to a change in the mass concentration. As shown in the lower left diagram of figure 3.3, the SPR angle changes as biomolecules are coupling to the surface therefore causing a change in mass concentration.[50] This angle change can be detected monitored in real time in a non-invasive manner.

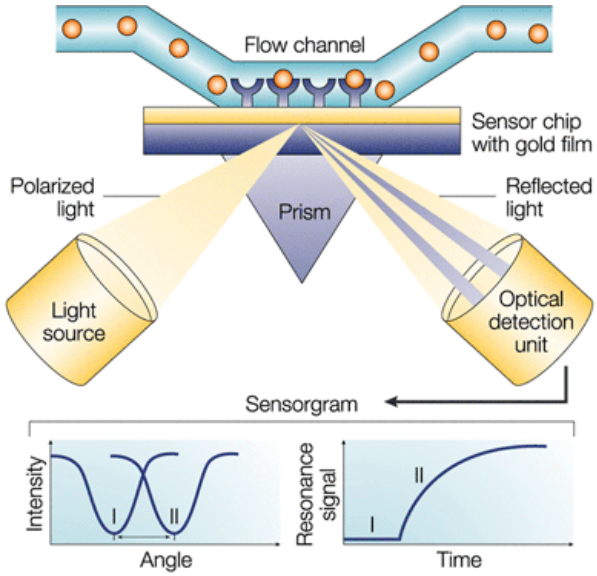

Figure 3.3 Typical set-up for a SPR biosensor. SPR monitors changes in the refractive index near the surface of a sensor chip. SPR can be observed as a shadow or dip in the reflected light at an angle which depends on the mass of biomolecules bound to the surface. [50]

3.1.3 Terminology and experimental set-up

A ligand is defined as the interaction partner bound to the sensor surface. A ligand can be bound to the surface by covalent immobilization or by capturing through an immobilizing capturing molecule.
An analyte is defined as the interaction partner which is free to move in solution over the immobilized ligand, as illustrated in figure 3.4.[55]

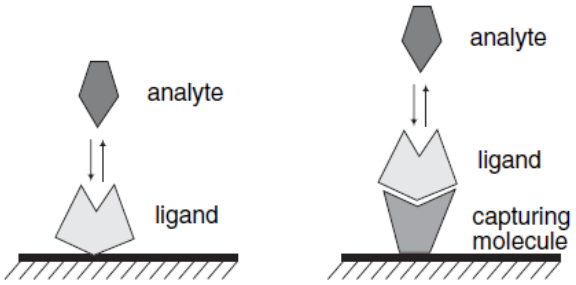

Figure 3.4 (left) analyte interacting with ligand immobilized to a surface; (right) analyte interacting with ligand captured by a capturing molecule.

An experiment starts by injecting a sample into the system in a controlled fashion. The sample will be transported through a running buffer, which is a constant flow of buffer. The analyte will bind to a ligand immobilized to a sensor surface or to a capturing molecule.
Afterwards, the regeneration will occur, which consists in dissociating the bound analyte from the surface after a cycle, in order to prepare a new cycle. The regeneration conditions do not have to be too harsh as the activity of the biomolecules bound to the surface needs to stay unaltered, but they have to efficiently eliminate any trace of analyte from the surface at the same time.
The response from the analysis is measured in resonance units (RU), converted from the actual angle change in reflected light, where 1000 RU correspond to an angle shift of 0.1. [56]This response is directly proportional to the quantity of molecules coupled to the surface. In most cases, 1000 RU is equivalent to a binding of ~1 ng per square mm of protein immobilized on the surface. The maximal response is based on the assumption that the binding is 1:1 and that the bound ligand is active and attainable. The following formula defines the maximal response:
$Rmax = \frac{analyte MW}{ligand MW} \times Rl \times Sm$, where Rl is the immobilized ligand level, MW is the molecular weight and Sm is the stoichiometric ratio.
A sensorgram is a curve plotting the response units as a function of time and it shows the development over time of the analyte-ligand interaction on the sensor surface (figure 3.5).

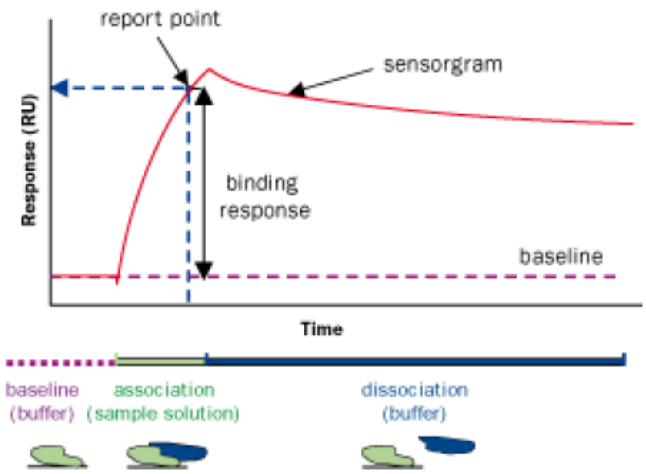

Figure 3.5 Example of a sensorgram, showing the response units progress as a function of time.[57]

3.1.4 Advantages of using SPR

SPR sensor has many advantages. First of all, it is based on a label-free detection and a real-time monitoring process. The sensor chips can be reusable, it is a rapid investigation tool and it allows performing a high-throughput analysis with wide experimental design and reproducible measurements. [58]
SPR is mainly powerful technique for analyzing interactions between two proteins: compared to other techniques, SPR provides an efficient way to investigate low affinity interactions and small amounts of proteins are needed to study an interaction. Another advantage of using SPR is that its binding analysis is an effective way for assessing the structure of recombinant molecules. Furthermore, SPR can be successfully used for studying and analyzing affinity, enthalpy, kinetics, stoichiometry of a protein-protein interaction. [61]

3.1.5 Protein Immobilization techniques

The starting point of an SPR experiment is the correct surface preparation, which involves the choice of the right protein immobilization technique. This section present the theory behind two immobilization techniques.
An immobilization technique is the binding of a capture molecule or ligand onto the sensor surface. There are different immobilization techniques, divided in two categories: direct immobilization and capturing. Direct immobilization techniques are characterized by a covalent binding, a strong binding capacity and a heterogeneous orientation, and they include amine coupling, ligand thiol, surface thiol and others. On the other hand, capturing techniques are orientation-specific, they are characterized by a selective ligand capture from raw samples and an inferior binding ability; examples of capturing techniques include Ni:NTA-His-tag and Ab-antigen interactions.
Three protein immobilization techniques have been used in my experiments: capturing of a His-Tagged protein via metal chelation on a Ni-NTA chip surface, amine coupling of a penta-His-Ab on a CM5 chip and capturing of his-tagged protein on an anti-histidine Ab.

3.1.5.1 Ni-NTA capturing via metal chelation

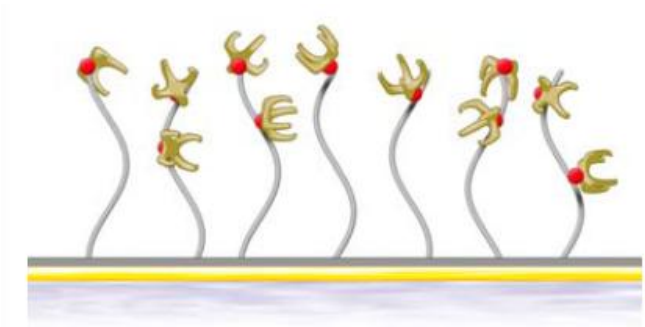

Figure 3.6. Sensor chip NTA, which is made of a carboxymethylated dextran matrix functionalized with NTA. This chip can bind to his-tagged biomolecules.[59]

A sensor Chip NTA is composed of a carboxymethylated dextran matrix functionalized with NTA (figure 3.6). Its purpose is to bind his-tagged biomolecules for interaction analysis in SPR Biacore systems. Capture of His-tagged ligands on the chip occurs via metal chelation of Ni^{2+} by the NTA chip on the surface and the histidine amino acids residues present in the ligand tag.

3.1.5.2 Immobilization via amine coupling on a CM5 chip

Figure 3.7 shows the chemistry behind the immobilization on a CM5 chip. CM5 is a very versatile chip surface and it is characterized by a high biochemical stability. It is composed by a carboxymethylated dextran covalently attached to a gold surface. Sensor chip CM5 is the favourite choice of immobilization for covalently attaching biomolecules through amine, thiol or carboxyl groups. This is why it was the preferred choice for immobilizing an anti-his-Ab via amine coupling in my project.

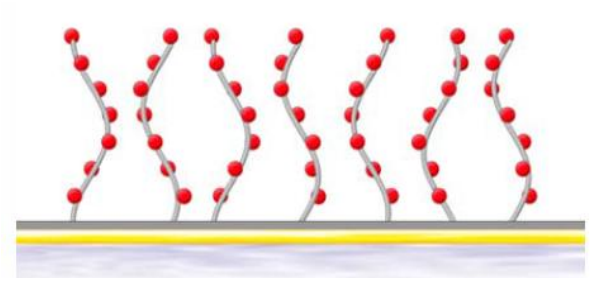

Figure 3.7 Immobilization of a molecule on a CM5 chip, which is made of a carboxymethylated dextran matrix surface.[60]

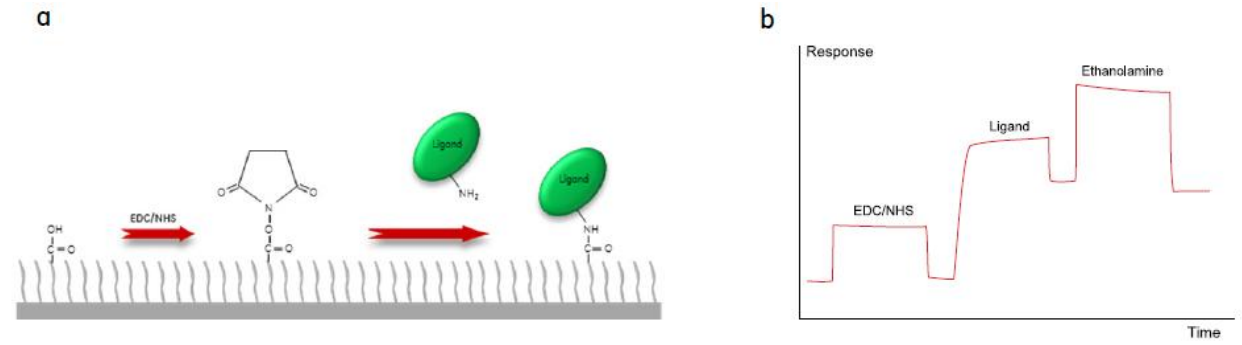

Figure 3.8 (left) Chemistry of amine coupling; (right) Sensorgram indicating the three major steps in amine coupling.

In this project, an anti-his-Ab will be immobilized via amine coupling on the CM5 chip.

Figure 3.8 on the left shows the chemical reactions behind the ligand immobilization via amine coupling, where the surface is first activated by coupling to EDC/NHS, therefore converting 30% of the carboxylates on the matrix into succinamide esters, which are highly reactive with primary amine. Covalents bond are then formed with the amino groups of lysine residues of the ligand; ethanolamine is used to deactivate the free esters. Figure 3.8 on the right illustrates a sensorgram indicating the major three steps of this immobilization technique: surface activation via EDC/NHS, ligand contact and ethanolamines blocking. There is a RU increase after ligand contact since this event leads to electrostatic attraction and ligand binding to the surface.[60]
Amine coupling requires different solutions that are listed in table 3.1.

Table 3.1. Solutions required for amine coupling.

Solution	Composition
EDC	0.4 M 1-ethyl-3-(3-dimethylaminopropyl)-carbodiimide in distilled water.
NHS	0.1 M N-hydroxysuccinimide in distilled water.
Ethanolamine	1 M ethanolamine-HCl, pH 8.5

In general, the first step for amine coupling is the activation of the surface by injecting a mixture of EDC/NHS (1:1) for about 10 minutes. Ligand is then immobilized by injecting it for 5-10 minutes. Finally, ethanolamine is injected for 7 minutes in order to inactivate reactive groups. Figure 3.7-a shows the chemistry behind the immobilization of ligand.

3.1.5.3 Anti-tagged antibodies used for capturing of tagged proteins

A tagged protein can be bound to an anti-tagged-Ab through its affinity to the tag.
As described above, an anti-tag-Ab can be covalently coupled via amine coupling to a CM5 sensor chip. The most commonly used affinity tags are the polyhistidine (His) and glutathione S-transferase (GST) tags.

3.1.6 Steady-state affinity and fit kinetics analysis tools

SPR is an efficient tool for kinetics and steady-state affinity analysis measurements.
Steady-state affinity analysis is based on a model calculating the equilibrium dissociation constant K_D for a 1:1 interaction obtained from a plot of steady state binding levels (R_{eq}) against analyte concentration (C). The equation used by the software to calculate K_D is $Req = \frac{CRmax}{KD+C} + RI$, where R_{eq} is the equilibrium response level, K_D is the equilibrium dissociation constant (M), R_{max} is the analyte binding capacity of the surface in Response Units, RI is the bulk refractive index contribution and C is the analyte concentration. Steady-state affinity analysis is time-independent and it quantifies the amount of ligand-analyte complex created at equilibrium in a condition where association equals dissociation.
Fit kinetics analysis is time-dependent and it gives information on how quickly the biomolecules bind to a surface and how fast they dissociate. Therefore, this analysis provides two important parameters: K_{on} (association rate constant, measured in $M^{-1}s^{-1}$) and K_{off} (dissociation rate constant, measured in s^{-1}). In order to determine these two constants, the fitting can be performed using different models. In this thesis, the fitting is based on a simple 1:1 Langmuir interaction model between analyte A and ligand B, as followed: $A + B \leftrightarrows AB$.

3.2 Materials and methods

All experiments have been performed using Biacore® X100 instrument and the results were analyzed by the program Biacore X100 Evaluation Software. All data were recorded at 25°C. Proteins used in my experiments are listed in table 3.2 below:

Table 3.2 List of proteins used in the experiments with their molecular weights

Protein	MW
αGFP-Nanobody-His	12 kDa
Anti-his Ab	~150 kDa
GFP	27 kDa
His-GFP	27 kDa
Bovine serum albumin (BSA)	66.4 kDa
Lysozyme (Lys)	14.3 kDa
Streptavidin (SA)	52.8 kDa

GFP and His-GFP proteins were overexpressed and purified as described in Chapter 2, and the αGFP-Nb-His protein was purchased from Ablynx.

3.2.1 Experiments on NTA chip surface

NTA chip (GE healthcare) was used for capturing of his-tagged proteins. Following activation of the chip with an activation buffer, His-GFP or αGFP-Nb-His proteins were immobilized on the chips. The surface was then regenerated with a re generation buffer. The buffers used in these experiments are listed in table 3.3 below:

Table 3.3 Buffers used in Ni-NTA experiments

Buffer	Composition and pH
Running buffer	10 mM potassium phosphate buffer pH 7.2.
Activation buffer	10 mM potassium phosphate buffer pH 7.2, 500 µM $NiCl_{2.}$
Regeneration buffer	0.01 M HEPES pH 7.4, 0.15 M NaCl, 0.35 M EDTA, 0.005% P20.

Two flow cells have been used in these experiments: Flow Cell 1 and Flow Cell 2. Flow Cell 2 is the active surface, as the nickel solution is only injected in this specific flow cell. Flow Cell 1, on the other hand, is the reference surface as no Nickel solution is injected on it. His-tagged proteins were injected on both surfaces.
The nickel chloride solution was injected for a contact time of 60 seconds at a flow rate of 10 µl/min and with a stabilization period of 120 seconds. After injecting the Nickel chloride solution on the sensor surface, it was possible to assess that the nickel bound to the NTA chip yields a response of around 85 RU. Figure 3.9 shows the average Nickel binding response achieved in the experiments: after the stabilization period, the $NiCl_2$ level recorded was around 80 RU. As it will be

shown later, $NiCl_2$ binding level may vary in different experiments, and this has to be taken into account.

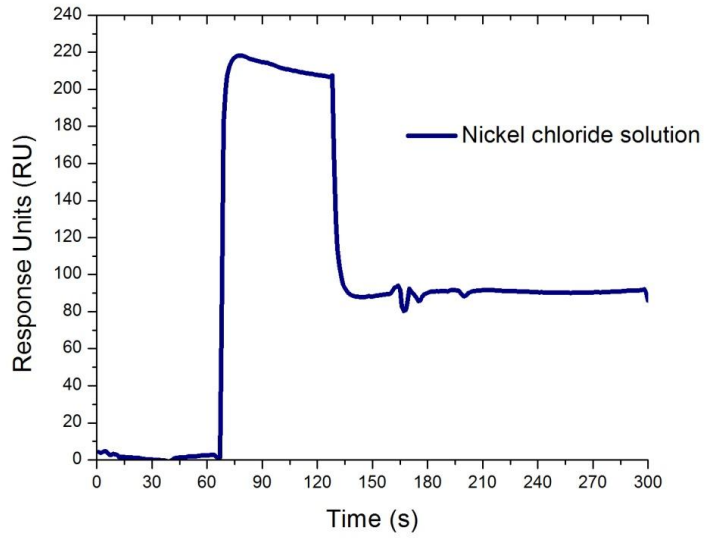

Figure 3.9 Chromatogram showing the $NiCl_2$ solution response measured in RU, after binding to the NTA surface. The final response is around 85 RU.

Another way of activating a NTA chip surface would be to functionalize it by injecting Copper, Zinc or Cobalt solutions instead of Nickel, but none of these three solutions proved to efficiently bind to the chip in the experiments, therefore Nickel remained the preferred choice throughout all NTA experiments.

3.2.1.1 His-eGFP binding to Ni-NTA:

His-eGFP were used to test the binding of his-tagged proteins to the Ni-NTA surface.
After equilibrating sensor chip NTA for a few minutes, the Biacore X100 instrument was prepared with filtered (0.22 µm) and degassed running buffer (0.01 M HEPES pH 7.4, 0.15 M NaCl, 0.35 M EDTA, 0.005% P20 (HBS-P 20)). The chip was washed with running buffer for 60 seconds with a 10µl/min flow rate. Nickel activation buffer (10 mM potassium phosphate buffer pH 7.2, 500 µM $NiCl_2$) was then injected for 60 seconds with a flow rate of 10 µl min^{-1}. Afterwards, running buffer was injected again for 120 seconds with a flow rate of 10 µl/min. At this point, the ligand solution was injected, in this case the His-eGFP protein.
The final optimized conditions used for ligand injection were: ligand contact time of 120 seconds (as longer contact time gave an unwanted early protein dissociation), flow rate of 30 µl/min (in order to minimize mass transport) and ligand dissociation time of 300 seconds (at flow rate of 30 µl/min). The regeneration buffer was then injected for 60 seconds with a flow rate of 10 µl/min. Finally, running buffer was injected again for 300 seconds with flow rate 10 µl/min.
A multi-cycle kinetics analysis was performed using the following concentrations of His-eGFP: 5 nM, 10 nM, 35 nM, 50 nM, 100 nM, 250 nM, 500 nM, 1000 nM and 1500 nM, all prepared in a dilution series and injected in a random order. The same concentrations were also used to immobilize the nanobody protein and for the other experiments. Each cycle comprises of Nickel binding, ligand binding and dissociation, and surface regeneration. In addition to this multi-cycle analysis an experiment where GFP (without Histidine tag) was bound to the surface was performed, in order to assess if there was any unspecific binding.

3.2.1.2 αGFP-Nb-His binding to Ni-NTA

The optimized conditions described above for the His-eGFP interaction with the Ni-NTA surface were used, in order to obtain comparable results.
Therefore, in an analogous manner, a multi-cycle kinetics analysis was run, with αGFP-Nb-His concentrations of 5 nM, 10 nM, 35 nM, 50 nM, 100 nM, 250 nM, 500 nM, 1000 nM and 1500 nM were injected on the surface in a random order.

3.2.1.3 GFP- αGFP-Nb-His interaction on Ni-NTA

This set of experiments aimed at evaluating the interaction between the αGFP-His-Nanobody immobilized on the Ni-NTA chip surface and a GFP protein (without a histidine tag). Therefore, the Nb was used as ligand, while GFP was the analyte.
The appropriate nanobody immobilization level was determined by using the equation: $Rmax = \frac{analyte\,MW}{ligand\,MW} \times Rl \times Sm$, where $Rmax$ was 100 RU, as reporteded by previous studies. By solving this equation, one can find that the Rl, namely the nanobody (ligand) immobilization level to bearound 50 RU.
Therefore some experiments were performed in order to find the right concentration of αGFP-His-Nanobody necessary to achieve an immobilization level of 50 RU. As shown by the sensorgram in figure 3.10, 5 nM was the right nanobody concentration to be used to achieve this goal.

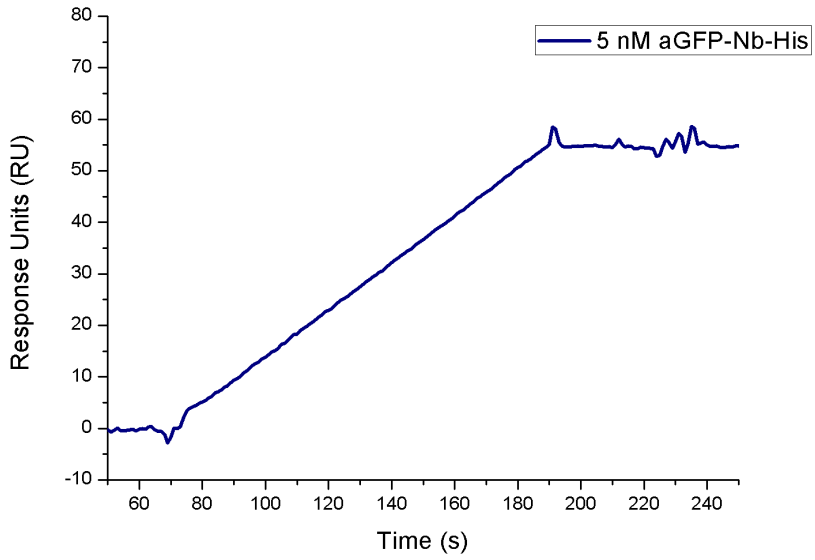

Figure 3.10 αGFP-Nb-His immobilization level on a Ni-NTA surface. The concentration of immobilized Nb used is 5 nM and the RU level reached is ~55 RU, as desired.

Once it was established that the concentration of αGFP-His-Nb to be used is 5 nM, a multi-cycle kinetics analysis was performed. This analysis started again with Nickel solution binding for NTA chip activation, where Nickel contact time was 60 seconds, Nickel dissociation time was 120 seconds, and flow rate 10 µl/min. For the nanobody immobilization, ligand contact time was 110 seconds, dissociation time was 220 seconds and flow rate 10 µl/min. GFP has been injected using several concentrations, similarly to the previous experiments: 1 nM, 5 nM, 10 nM, 50 nM, 100 nM,

500 nM, 1000 nM were the concentrations used. The conditions for the injection of the different GFP samples (analyte) were the following: contact time of 150 seconds, dissociation time of 400 seconds and flow rate of 30 µl/min.
In order to evaluate possible non-specific binding to the nanobody immobilized onto the Ni:NTA surface, another experiment was performed by injecting two different concentrations (10 nM and 100 nM) of bovine serum albumin (BSA), lysozyme (Lys) and streptavidin (SA). These were injected after the nanobody immobilization on the Ni:NTA surface.

3.2.2 Experiments on Anti-his-Ab immobilized on a CM5 chip

Buffers used in this set of experiments are listed in table 3.4 below.
For experiments on CM5 chip, composition of running and regeneration buffers varies from the ones used on the NTA chip, as illustrated by table 3.4. Also, instead of an activation buffer, here a pre-concentration buffer is needed for the correct immobilization of the Anti-his Ab. Choice of the right pH of the pre-concentration buffer will be discussed in the experiments.

Table 3.4 Buffers used in experiments on anti-his surface.

Buffer	Composition and pH
Running buffer	10 mM HEPES pH 7.4, 150 mM NaCl, 0.05% tween-20, 3 mM EDTA (HBS-EP+), pH 7.2
Pre-concentration buffer	10 mM sodium acetate or phosphate, pH in the range from 4.0 to 7.0
Regeneration buffer	10 mM glycine-HCl, pH 2.0

3.2.2.1 Immobilization of Penta-His-Ab on the CM5 chip via amine coupling: pH scouting

A monoclonal anti-his tag Ab (Qiagen), also called Penta-His Ab, has been selected and used for immobilization on a CM5 chip via amine coupling. A pre-concentration buffer for the correct immobilization of the Ab was prepared before the immobilization. An efficient pre-concentration necessitates that the pH is between the pka of the surface and the isoelectric point (pI) of the ligand, where pI is defined as the pH where there is no net charge on the protein. The operation aiming at finding the right pre-concentration or immobilization pH is called pH scouting; the immobilization buffer should be higher than 3.5, but lower than the isoelectric point of the ligand.
A series of experiment was performed by by Ph.D. Eduardo Antonio Della Pia in order to select the right pH for the immobilization buffer, and immobilize the anti-his-Ab on the surface, as shown in figure 3.11. This sensorgram shows the ligand (Penta-His-Ab) binding onto the chip surface, using different immobilization buffers: from pH 4.0 to pH 6.0.

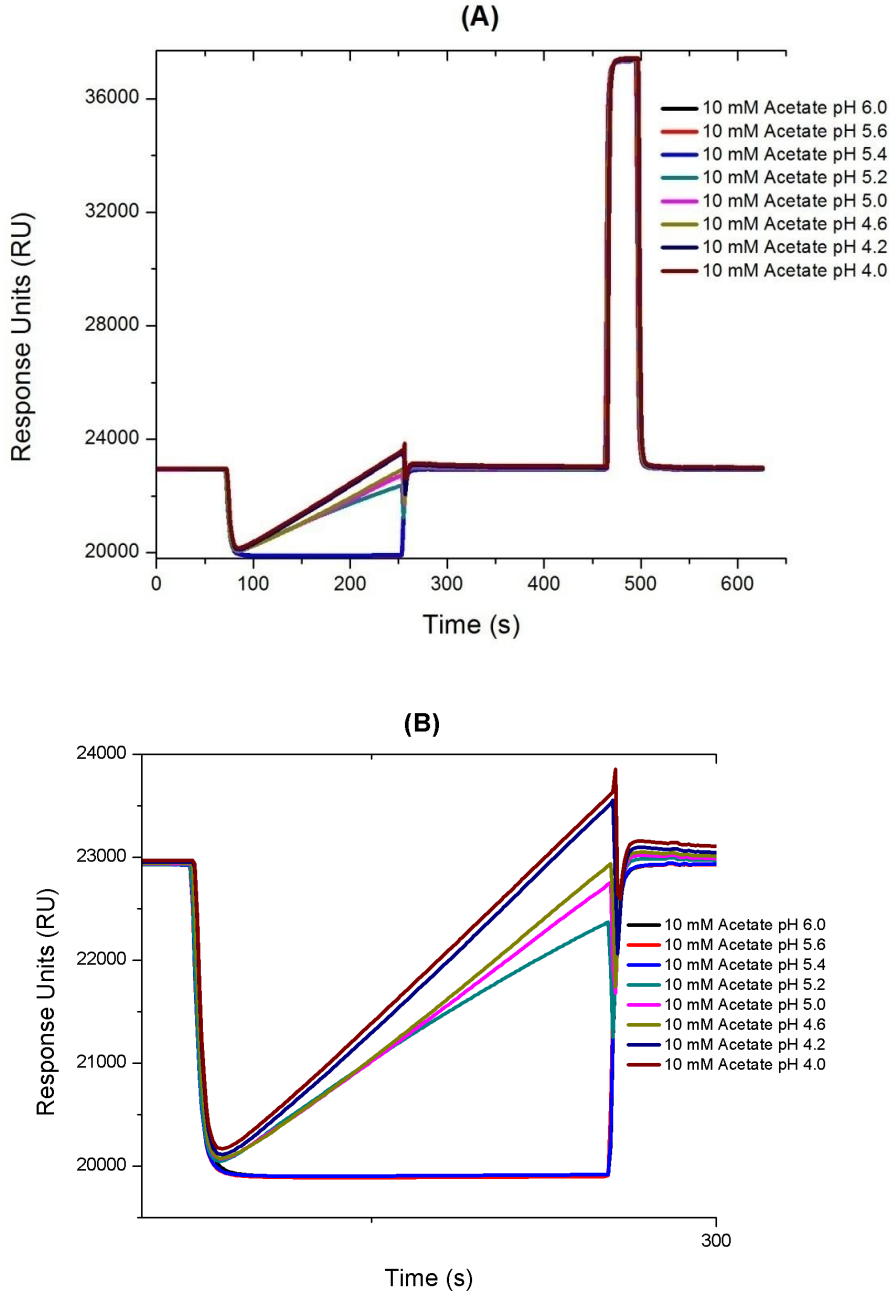

Figure 3.11.(a)Penta-His-Ab immobilization and pH scouting: eight 10 mM Acetate buffers at different pH ranging from 4.0 to 6.0 were used to immobilize the ligand (b) Zoom of ligand immobilization

Sensorgram in figure 3.11-a shows the complete pH scouting for the ligand immobilization ; it consists of an activation, following by ligand immobilization and blocking. Figure 3.11-b shows a zoom of the ligand contact; from this analysis, 10 mM Acetate buffer at pH 5.2 was chosen as the immobilization buffer, because the desired ligand response was reached at this immobilization buffer.

3.2.2.2 His-eGFP binding to the Anti-his-Ab

In this set of experiments the same protein concentrations and similar setup conditions of the experiment involving His-eGFP binding to the Ni:NTA chip surface were used, in order to obtain a comparable set of results.

Therefore, a multi-cycle kinetics analysis was performed using His-eGFP concentrations of 1 nM, 5 nM, 10 nM, 35 nM, 50 nM, 100 nM, 250 nM, 500 nM, 1000 nM and 1500 nM injected in the system in a random order. The ligand (His-eGFP) contact time was 120 seconds, dissociation time was 300 seconds and flow rate was 30 µl/min. Regeneration buffer was then injected for 60 seconds at a flow rate of 10 µl/min and finally running buffer for 300 seconds, to re-equilibrate the sensor surface.
Flow Cell 2 was the active surface, where the Anti-his-ab was covalently attached. Flow Cell 1 was the reference surface, lacking the Anti-his-ab, and therefore used to investigate any possible non-specific binding. The same surfaces have been used in the following two experiments described in paragraphs 3.2.2.3 and 3.2.2.4.

3.2.2.3 αGFP-Nb-His binding to the Anti-his-ab surface

This set of experiments involved a multi-cycle kinetics analysis using αGFP-Nb-His concentrations of 1 nM, 5 nM, 10 nM, 35 nM, 50 nM, 100 nM, 250 nM, 500 nM, 1000 nM injected in the system in a random order. The ligand (αGFP-Nb-His) contact time was 120 seconds, dissociation time was 300 seconds and flow rate was 30 µl/min. Regeneration buffer was later injected for 60 seconds at a flow rate of 10 µl/min and finally running buffer for 300 seconds.

3.2.2.4 GFP- αGFP-Nb-His binding to the Anti-his-ab surface

This set of experiments aimed at evaluating the interaction between the αGFP-His-Nb coupled to the Anti-his-Ab and a GFP protein (without a Histidine tag). Therefore, the Nb was used as ligand, while GFP was the analyte. This experiment is analogous to the experiment described in paragraph 3.2.1.3, therefore similar protein concentrations and setup conditions were used.

For the same reasons described in paragraph 3.2.1.3, a concentration of αGFP-His-Nb of 5 nM needed to be used to achieve a ligand binding level of around 50 RU. For the αGFP-His-Nb immobilization, ligand contact time was 110 seconds, dissociation time was 220 seconds and flow rate 10 µl/min. GFP has been injected using several concentrations, similarly to the previous experiments: 1 nM, 5 nM, 10 nM, 50 nM, 100 nM, 500 nM, 1000 nM were the concentrations used. The conditions for the injection of the different GFP samples (analyte) were the following: contact time of 150 seconds, dissociation time of 400 seconds and flow rate of 30 µl/min.

3.3 Results and discussion:

3.3.1 SPR experiments on Ni:NTA chip surface

The graphs below show the sensorgrams obtained after binding His-eGFP and αGFP-Nb-His at different concentrations onto the Ni:NTA surface.

3.3.1.1 His-eGFP binding to Ni:NTA:

His-eGFP binding to Ni:NTA multi-cycle was the first SPR set of experiments. Figure 3.12 shows the entire sensorgram of the experiment for one single concentration curve (500 nM), starting from Nickel binding and ending after surface regeneration. The sensorgram in figure 3.12 is the result of the subtraction between Flow cell 2, which is the active surface, and Flow cell 1, which is the reference surface.

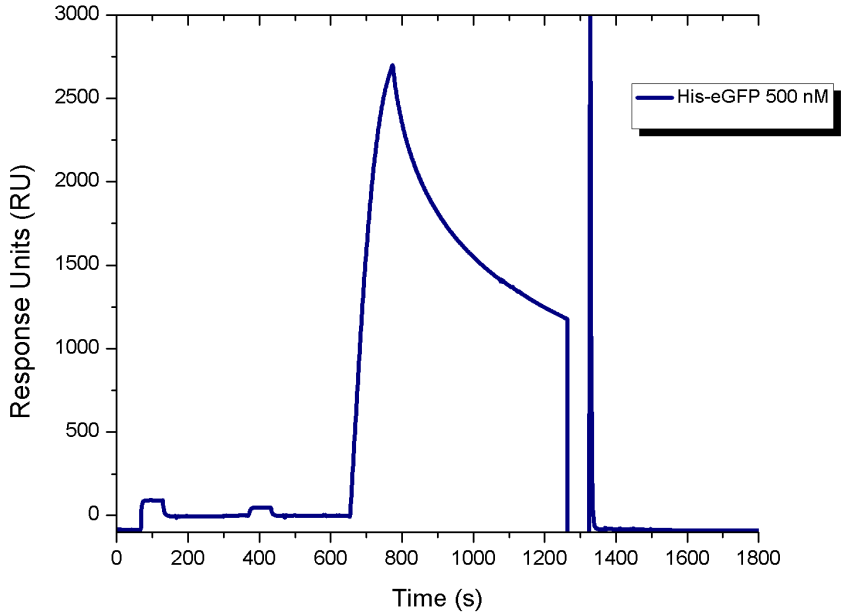

Figure 3.12. Subtracted sensorgram (active surface subtracted by reference surface) of His-eGFP at 500 nM immobilized on Ni:NTA surface, where His-eGFP concentration is 500 nM.

Figure 3.13 shows the corresponding reference surface (Flow cell 1) obtained from the same experiment and for the same concentration curve. The experiments demonstrated that the non-specific binding was less than 1% of the specific signal.
It is important to assess and evaluate some important aspects of the sensorgram. First of all, the Nickel binding must be evaluated. In figure 3.12, nickel binding for the curve at 500 nM can be observed after 60 seconds. As the whole set of experiments for His-eGFP binding to Ni:NTA is made up of several cycles, Nickel binding was performed at the beginning of each cycle to ensure proper activation of the NTA surface, with a possible variation of the Nickel level in each cycle, which is shown in figure 3.14 below. In this plot, it is possible to observe that nickel level does not vary significantly among the different cycles as it mostly lies between 79-82 RU, although in the last two cycles, corresponding to protein concentrations of 250 and 500 nM, the nickel level is a bit higher, as it is around 84-85 RU.

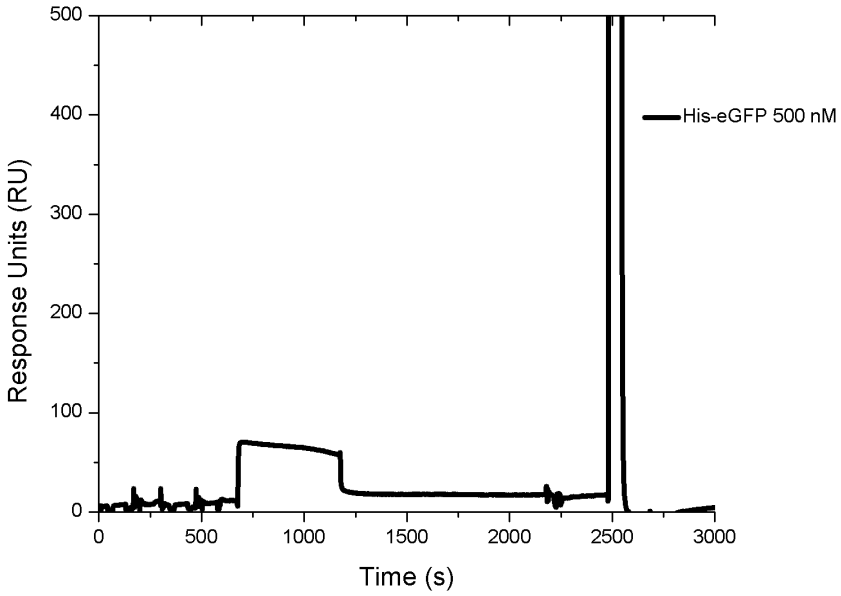

Figure 3.13. Sensorgram of the reference surface (Flow cell 1) of His-eGFP immobilized onto Ni:NTA chip, where His-eGFP concentration is 500 nM.

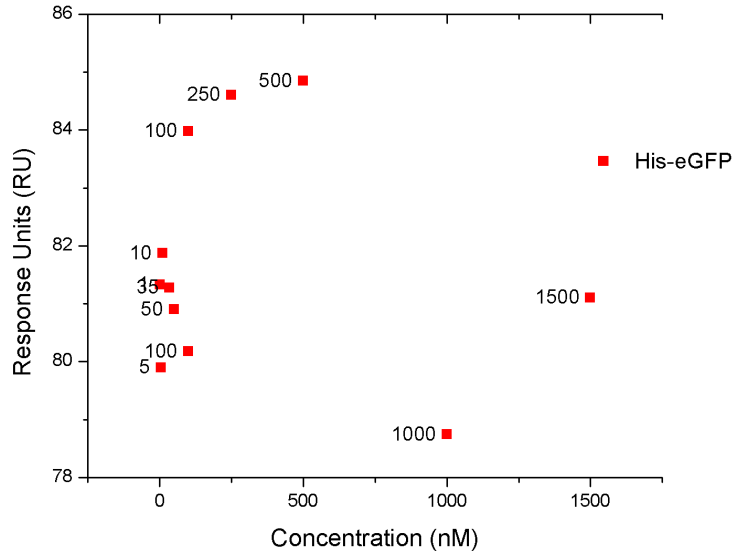

Figure 3.14 Plot of different nickel levels according to the sample concentration. On the X axis the sample concentration is shown in nM, on the Y axis the response units is shown, in RU.

Surface regeneration must also be assessed. Figure 3.15 shows a plot of different His-eGFP binding cycles showing the Response Units after surface regeneration in each cycle. It is possible to observe that high concentrations of proteins (1000 nM and 1500 nM) correspond to an incomplete surface regeneration, as the baseline response after regeneration is above zero, although still below 10 RU, which is within the instrument error. On the other hand, cycles related to lower protein concentrations show a complete surface regeneration, sometimes even too harsh, as one cycle reached a decreased baseline of around -20 RU; however, this negative value is probably due to a drift in the baseline. In order to obtain an ideal surface regeneration, the final baseline response should be around zero.

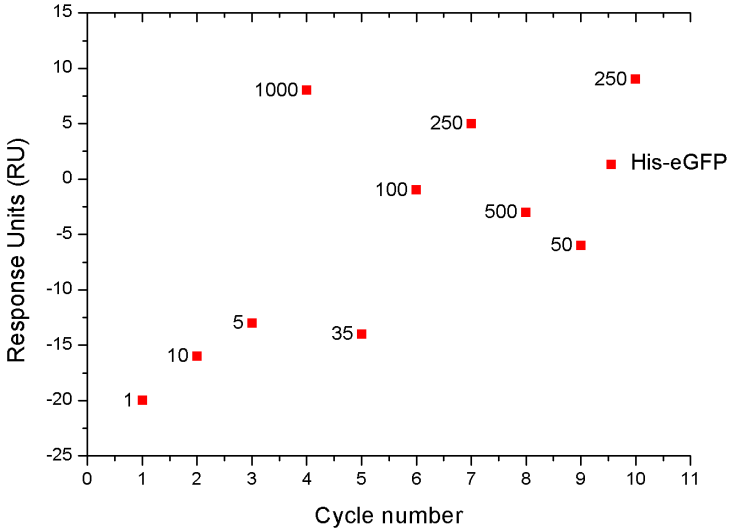

Figure 3.15. Plot showing the baseline response after regeneration of Ni:NTA among the different cycles. On the X axis there is the cycle number and on the Y axis the response units in RU.

Non-specific binding can be evaluated by examining both the reference surface (figure 3.13) and the GFP sample injection on the surface (figure 3.17). The reference surface in figure 3.13 shows that, for the curve corresponding to 500 nM and in the region corresponding to the His-eGFP injection (from 700 seconds onwards), there is a slight RU increase of around 80 RU, which rapidly decreases after 1200 seconds remaining to a constant response level of around 20 RU. Compared to the high response level of specific binding shown in figure 3.18, which is around 2500 R.U., this non-specific binding of 20 RU is still not very significant, as it accounts for only 1% of the total value. Plot in figure 3.16 investigates the non-specific binding level among the different cycles, showing that a higher non-specific binding correlates with a higher protein concentration but also with the latest cycles of the analysis; this non-specific binding is still very limited compared to the high level of specific binding.
Another way of assessing non-specific binding was to inject a sample of GFP and see if it binds to the Ni:NTA surface; the result shown in figure 3.17 indicates that the GFP protein does not remain bound to the surface after a short time, proving that Ni:NTA is a quite specific surface.

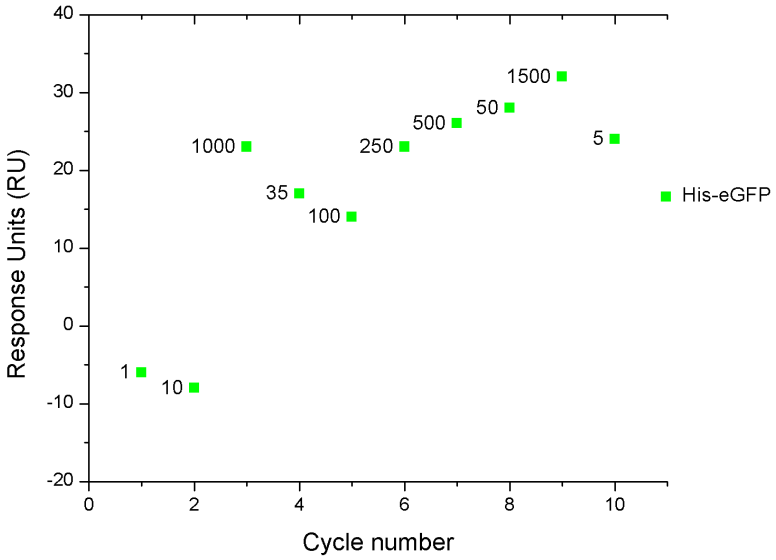

Figure 3.16 Non-specific binding level binding to the Ni:NTA chip plotted as cycle number (X axis) versus Response Units (Y axis). This analysis is based on the reference surfaces.

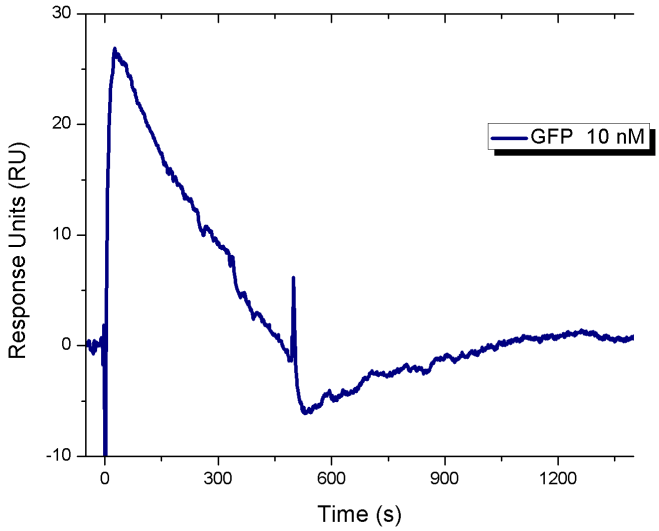

Figure 3.17 Specificity of Ni:NTA surface after injection of a GFP sample at 10 nM on the chip. This graph shows that after GFP injection the GFP does not remain bound to the surface.

Figure 3.18 shows the substracted sensorgram of His-eGFP binding to Ni:NTA, where only the region corresponding to the specific His-eGFP binding is shown for all the concentration curves of the multi-cycle experiment. The curves corresponding to the highest concentrations, 1000 nM and 1500 nM reach a response unit of around 3300 and 3500 RU respectively and they are characterized by a plateau state before dissociation begins. A steady state indicates that the amount of association is equal to the amount of dissociation, and this is referred as a state of equilibrium. The other curves do not reach this steady state yet, as a longer contact time would be needed to reach it. Concentrations of His-eGFP equal and below 10 nM do not bind to the surface, as binding starts above 35 nM. Curves corresponding to 1000 nM and 1500 have a good dissociation behavior. It is interesting to point out that the curve corresponding to 1500 nM dissociates faster than the one at 1000 nM: this phenomenon occurs because the curve at 1500

nM reaches steady-state before and therefore it dissociates faster. A good association curve should follow a single exponential and be characterized by at least some curvature, indicating a mass transport free interaction, as followed by the curves at 1000 nM and 1500 nM.

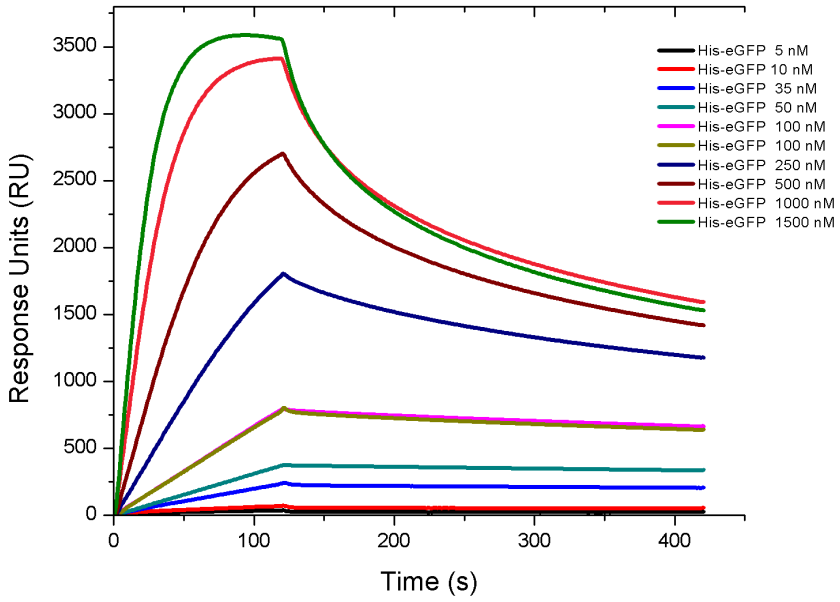

Figure 3.18. Subtracted sensorgram (active surface subtracted by reference surface) of specific His-eGFP binding on Ni:NTA. Binding is shown at concentrations of 5, 10 , 35, 50, 100, 250, 500, 1000, 1500 nM.

3.3.1.2 αGFP-Nb-His binding to Ni:NTA:

The substracted sensorgram of the binding of αGFP-Nb-His on the Ni:NTA surface shown in figure 3.19 indicates that there is no specific binding to the Ni:NTA surface below 5 nM of protein. Also, unlike the experiments with His-eGFP protein, it is possible to observe a specific binding starting from 10 nM of αGFP-Nb-His. Curves of this experiment show that the protein is binding to the Ni:NTA quite fast, as after only 50 seconds from the time of injection, protein concentrations of 500 nM, 1000 nM and 1500 nM already reached a steady state. Protein concentrations at 1000 nM and 1500 nM yield a high RU of around 3100 and 3200 respectively. This fast association indicates that these curves have an insufficient curvature, therefore suggesting that there might be some mass transport interaction involved. Also, at 1500 nM, the ligand almost saturates the surface. Proteins at concentrations starting from 250 nM and higher tend to dissociate quite fast after the dissociation phase begins, bringing the response level down to around 1600 RU after 400 seconds. This fast dissociation compared to a slower dissociation for curves below 250 nM was expected, as curves at higher concentrations reach steady state in a shorter time and they start to dissociate earlier at a higher rate.

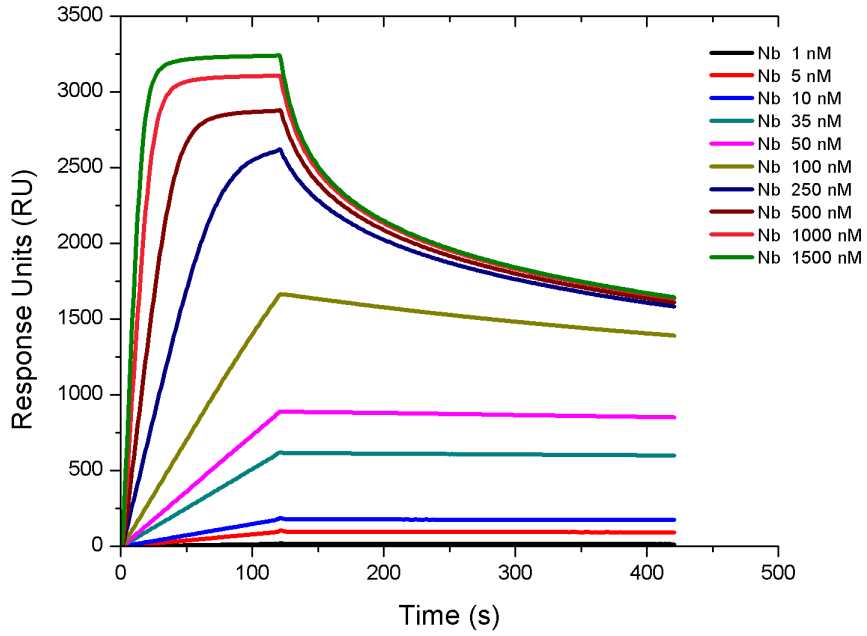

Figure 3.19. Sustracted sensorgram (active surface subtracted by reference surface) of specific αGFP-Nb-His binding on Ni:NTA. Binding is shown at ligand concentrations of 1, 5, 10 , 35, 50, 100, 250, 500, 1000, 1500 nM.

In this set of experiments, Nickel binding level has an average response of 83 RU, without a significant variation among cycles. Surface was regenerated quite efficiently at the end of each cycle, except the one with binding of high concentration of Nb (1500 nM), where a little amount of protein corresponding to around 20 RU remained bound to the surface after regeneration.
Non-specific binding was evaluated by assessing the reference surface, where an average level of 10 RU of non-specific binding was observed. This value is not very relevant as it accounts for only 2% of the total surface binding. These graphs are not shown here as they are very similar to plots in figure 3.14, 3.15 and 3.16, without any significantly different result.

3.3.1.3 GFP binding to αGFP-Nb-His on Ni:NTA

This section reports the experiments related to GFP interacting with αGFP-Nb-His on Ni:NTA immobilized on Ni:NTA.
In this set of experiments, nickel binding level gave an average response of 81 RU, without a signification variation among cycles. By examining the αGFP-Nb-His immobilization level on the surface, it was possible to see, as shown in figure 3.20, that the immobilized Nb gave an average response of 59.6 RU, without significant variation among the cycles, which is a positive result.

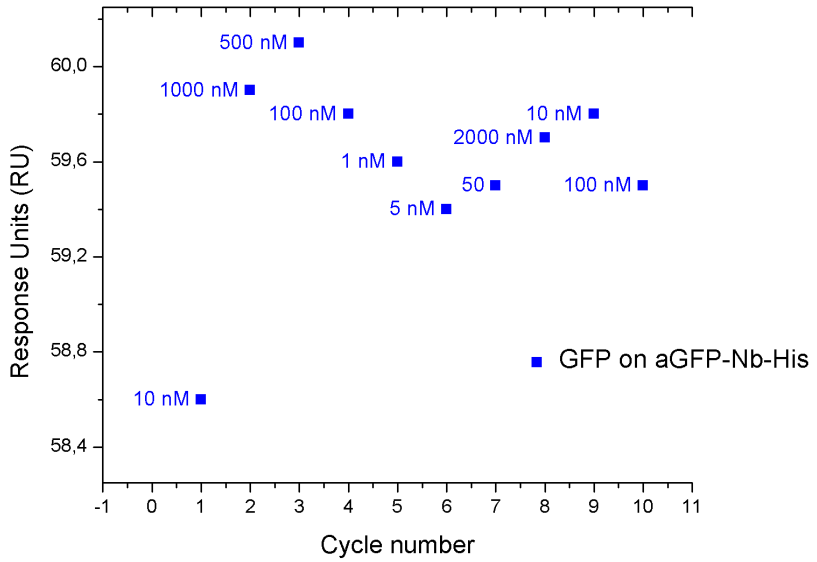

Figure 3.20. Plot showing αGFP-Nb-His immobilization level on Ni:NTA in all cycles. On the X axis, there is the cycle number, and on the Y axis the Response in RU.

Figure 3.21 shows the sensorgram of GFP binding at different concentrations binding to αGFP-Nb-His on Ni:NTA.
As it can be observed in this figure, the curves corresponding to 1000 nM and 1500 nM yielded a RU value of around 90 and 85 RU respectively, which is close enough to the desired value of 100 RU. Curve at 1 nM has a binding level of around 10 RU, while 5 nM of GFP already yielded around 35 RU. Curves at 100 nM and 1000 nM reach a steady state condition, while curve at 500 nM seems to start slightly dissociating before the actual dissociation begins. Curve at 2000 nM does not reach a steady state and continues binding to the surface before dissociation starts. In all curves of this experiment, it is possible to observe a RI (Refractive index) jump at 150 seconds, before the start of the dissociation phase, corresponding to a change in buffer.
Curves between 5 nM and 100 nM seem to have more curvature during association phase, while association curves for 500 nM and higher values are more characterized by a horizontal line. Dissociation looks very similar for all curves, with a more rapid dissociation rate characterizing curves at 500 nM and higher.

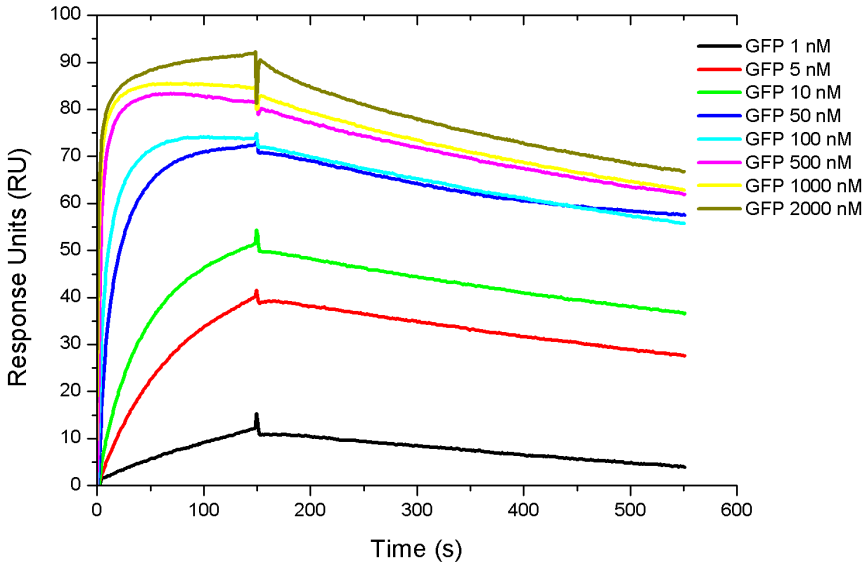

Figure 3.21. Subtracted sensorgram (active surface subtracted by reference surface) of GFP binding to αGFP-Nb-His on Ni:NTA (data from PostDoc Eduardo Della Pia). Binding is shown at analyte concentrations of 1, 5, 10 , 50, 100, 500, 1000, 2000 nM.

After investigation of the reference surface, it was also possible to observe that in cycle 9 (GFP 2000 nM), there was a non-specific binding of around 25 RU, while in cycle 6 (GFP 1000 nM), the non-specific binding was 18 nM. These values can be quite significant as the maximum specific binding level in the active surface is around 110 RU; therefore, for example for 1000 nM of GFP injected, non-specific binding accounted for around 16 % of all the total binding. Surface was well regenerated after each cycle.

In order to assess any possible non-specific binding to the αGFP-Nb-His immobilized onto the Ni:NTA surface, another experiment was performed by injecting two different concentrations of bovine serum albumin (BSA), lysozyme (Lys) and streptavidin (SA). These were injected after immobilization of 5 nM of αGFP-Nb-His on the Ni:NTA chip. The result in figure 3.22 illustrates that none of these proteins remained bound to the surface after the injection time. Only lysozyme at 100 nM was able to bind to the surface quite rapidly yielding a RU of around 120, but this binding level soon decreased close to zero after 200 seconds from the time of injection. This binding is due to the similarity between the lysozyme-Nb complex and the GFP-Nb complex. In the GFP-Nb complex, the CDR3 region of the Nb is shorter, therefore exposing the framework 2 region, which facilitates the binding with GFP. In the lysozyme-Nb complex on the other hand, this CDR3 loop is extended, allowing the binding to the lysozyme, although not as strong as in the GFP-Nb complex.[17]

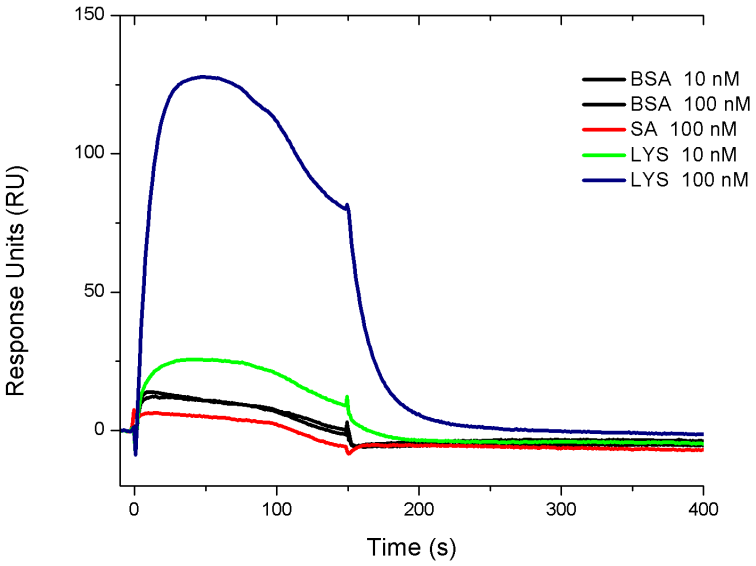

Figure 3.22. Binding of BSA, LYS and SA on a Ni:NTA surface after immobilization of 5 nM αGFP-Nb-His. These three proteins were injected at two concentrations: 10 nM and 100 nM.

3.3.2 Experiments on Anti-his CM5 chip surface

This section reports the experiments related to the sensorgrams obtained after binding His-eGFP and αGFP-Nb-His at different concentrations onto the Anti-his CM5 surface.

3.3.2.1 His-eGFP binding to Anti-his-ab:

Figure 3.23 shows the subtracted sensorgram (active surface subtracted by the reference surface) of His-eGFP binding to the Anti-his-ab bound to CM5, where the specific His-eGFP binding is shown for all the concentration curves of the multi-cycle experiment.
Surface was adequately regenerated at the end of almost all cycles, although in the cycle corresponding to 1500 nM of protein the surface was not fully regenerated, as the final response was slightly above the baseline (around 17 RU). In the cycles corresponding to 5 nM and 10 nM, the regeneration conditions were quite harsh, giving negative values of around -15 RU which are however probably due to a baseline drift. These results are comparable with the previous experiment of His-eGFP on Ni:NTA, which also showed similar surface regeneration results.
Non-specific binding was assessed by examining the reference surface, and it was shown that there was very little non-specific binding to the surface, around 4 RU, which is lower compared to the non-specific binding present on the Ni:NTA chip in the previous experiment.
Sensorgram in figure 3.23 shows that the strongest binding to the Anti-his surface with a His-eGFP concentration of 1500 nM reached a RU level of around 2500; for the same protein concentration, His-eGFP on Ni:NTA reached a RU of 3500. Unlike the experiment of His-eGFP on Ni:NTA, a steady state is not reached by these two concentration curves, and they seem to dissociation slower than the ones on Ni:NTA. Also, similarly as before, the lowest protein concentration that could bind to the anti-his surface was 35 nM.
Therefore, these curves are good but not optimal as a steady state is not reached by any of them. Curves at 1500 nM and 1000 nM present sufficient curvature during association but during dissociation they lack curvature, suggesting a strong interaction.

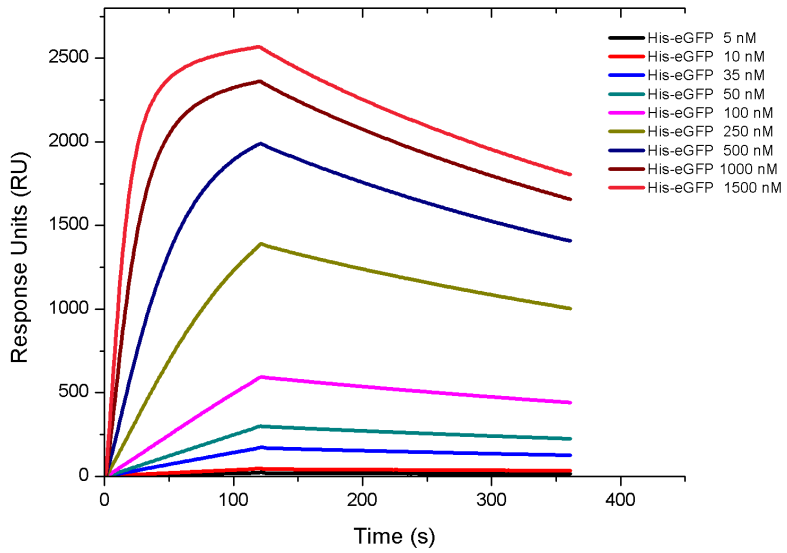

Figure 3.23.Subtracted sensorgram (active surface subtracted by reference surface) of specific His-eGFP binding to Anti-his-ab. Binding is shown at concentrations of 5, 10 , 35, 50, 100, 250, 500, 1000, 1500 nM.

3.3.2.2 GFP binding to αGFP-Nb-His on Anti-his-ab

Figure 3.24 shows the different concentration curves for the subtracted sensorgram (active surface subtracted by reference surface) of αGFP-Nb-His binding to the anti-his CM5. The curve at 1000 nM reached the highest response, at around 1300 RU, while protein at 500 nM yielded a similar response, reaching around 1200 RU. Similarly to the previous experiment for αGFP-Nb-His on Ni:NTA, for protein concentrations below 5 nM there was no binding to the surface.
Both the curves at 500 nM and 250 nM reached a steady state at 1200 nM and 1100 nM respectively. The curve corresponding to 1000 nM did not reach a plateau state, instead it seemed to continue binding to the surface; on the other hand, at lower concentrations, namely 250 nM and 500 nM, steady state was reached. The association curves at 1000 nM and 500 nM lack curvature, suggesting that some mass transport interaction is involved. The dissociation curves are almost horizontal; also, dissociation is slower compared to the experiment where the same protein was binding to Ni:NTA.
In conclusion, the curve at 250 nM seems to have the best quality, as the association curve has a little curvature and steady state is reached at around 1200 RU.

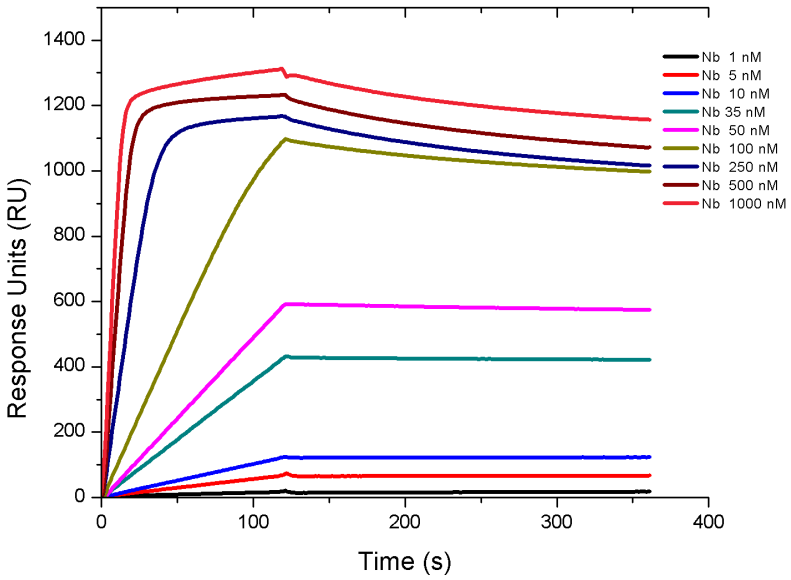

Figure 3.24 Subtracted sensorgram (active surface subtracted by reference surface) of specific αGFP-Nb-His binding to Anti-his-ab. Binding is shown at GFP concentrations of 1, 5, 10 , 35, 50, 100, 250, 500, 1000 nM.

Regarding surface regeneration, the surface was regenerated quite well in all cycles, although some harsh regeneration conditions were observed in the cycle corresponding to 10 nM. Additionally, no significant non-specific binding was observed in the different cycles. The average non-specific binding level was around 10 RU, which is 1% of the total binding to the surface, therefore this data is not relevant and will not be shown.

3.3.2.3 GFP binding to αGFP-Nb-His on Anti-his-ab

Figure 3.25 shows the substracted sensorgram (active surface subtracted by the reference surface) for GFP binding to αGFP-Nb-His on the anti-his surface. In this experiment, the aimed value of 100 RU was reached by GFP at 500 nM, while GFP at 250 nM reached a very close response. Binding was not achieved below GFP concentration of 5 nM, similarly to the previous experiment (figure 3.21). The average level of immobilized ligand (5 nM αGFP-Nb-His) was comparable to the previous experiment on Ni:NTA, giving an average response of 59.1 RU. Compared to the previous sensorgram of GFP-αGFP-Nb-His binding on Ni:NTA (figure 3.21), this experiment reached higher responses on the surface for the same GFP concentrations used. For example, as shown in figure 3.25, for the curve at 500 nM a yield of 100 RU was reached, while for the same GFP concentration the binding on Ni:NTA was around 80 RU.
The curve at 1000 nM did not reach steady state. The other curves are characterized by a good quality, with curves reaching steady state starting from 100 nM and higher. During association phase, curves from 10 nM until 250 nM are characterized by some curvature, which is lacking in the other curves.

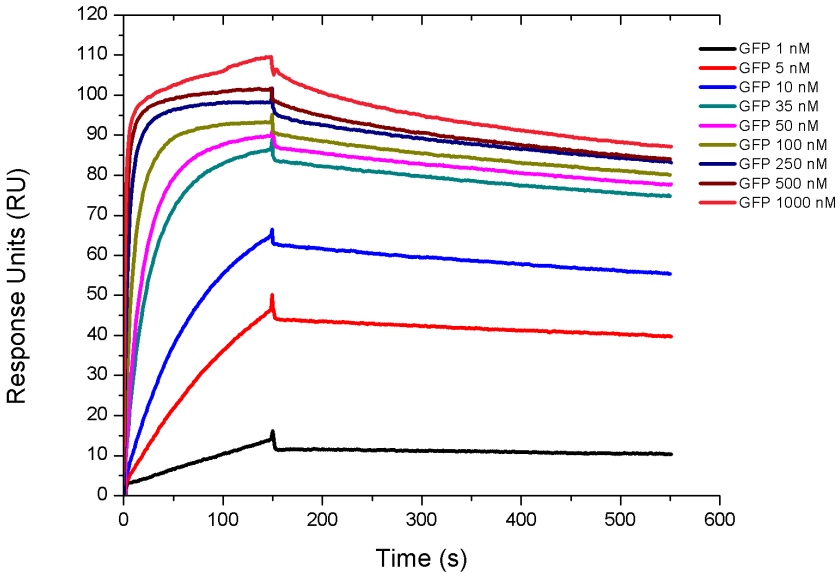

Figure 3.25 Subtracted sensorgram (active surface subtracted by reference surface) of GFP binding to αGFP-Nb-His on Anti-his-ab surface. Binding is shown at GFP concentrations of 1, 5, 10 , 35, 50, 100, 250, 500, 1000, nM.

3.3.3.1 Steady state affinity and fitted kinetics analysis of His-eGFP and αGFP-Nb-His experiments on Ni:NTA and anti-his-ab immobilized on CM5 surface.

In this section results obtained from the steady-state affinity analysis and the fitted kinetics analysis regarding all the experiments involving His-eGFP and αGFP-Nb-His binding to the two biosensor surfaces will be discussed.

Figure 3.26 shows the steady-state affinity for His-eGFP and αGFP-Nb-His proteins binding to the Ni:NTA surface. Figure 3.27 shows the steady-state affinity for His-eGFP and αGFP-Nb-His proteins binding to the anti-his surface.
For each set of data, the steady state affinity for all concentrations used in the experiments are plotted. The data are then fitted using a Hill equation.
The fitting performed in figure 3.26 shows that for His-eGFP the curve fitting the different K_D values does not reach a steady state, while the curve fitting the K_D values for αGFP-Nb-His reaches a more stable response level at high concentrations (1000 nM and 1500 nM). For concentrations below 500 nM, αGFP-Nb-His reaches a higher response on the Ni:NTA surface compared to His-eGFP, but at higher concentrations, His-eGFP reaches higher RU levels and this is expected as His-eGFP has a higher MW.
Figure 3.27 shows a similar behavior, where for concentrations below 100 nM, αGFP-Nb-His on Anti-his has a higher response, but for higher concentrations, His-eGFP reaches higher RU levels, reaching around 2750 RU for high analyte concentrations.
In each graph, K_D value is shown as a red vertical line for αGFP-Nb-His and as a black vertical line for His-eGFP.

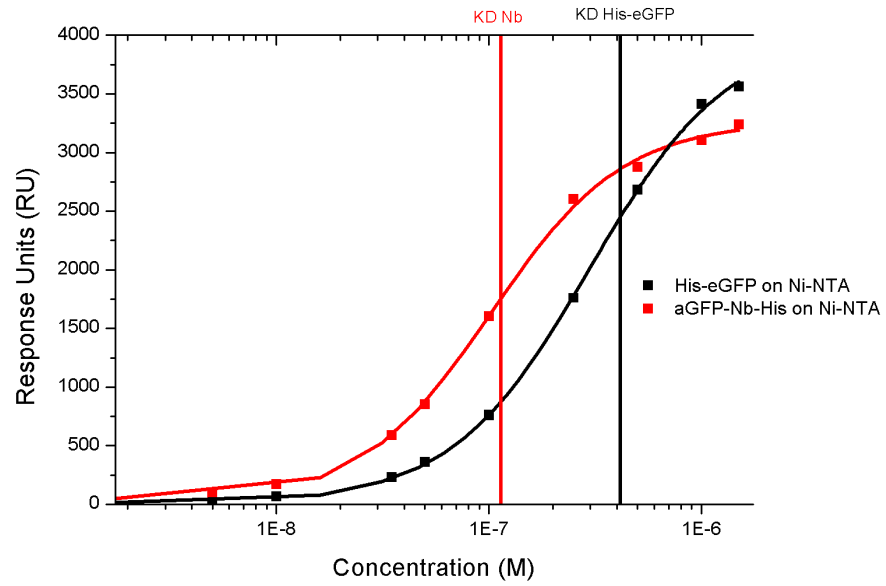

Figure 3.26. Steady-state affinity curves for His-eGFP and αGFP-Nb-His on Ni:NTA. All the K_D values are shown as dots and curves are fitted using a Hill equation.

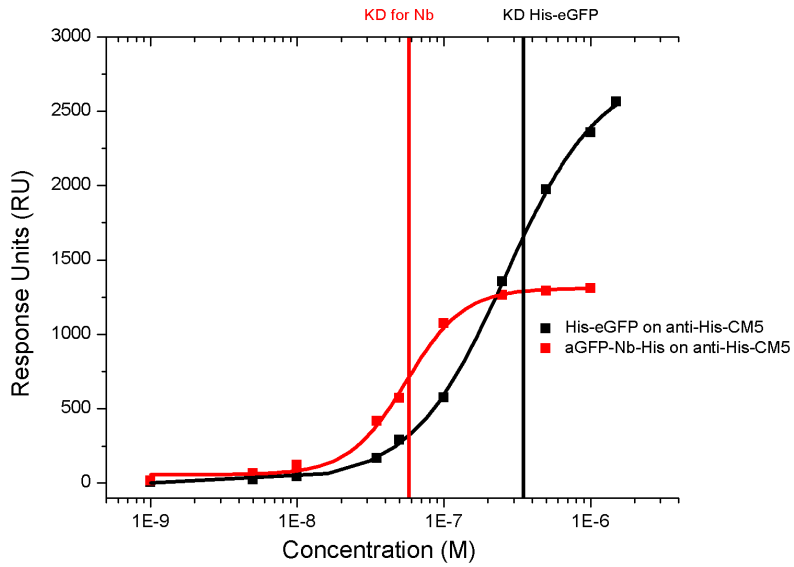

Figure 3.27. Steady-state affinity curves for His-eGFP and αGFP-Nb-His on Anti-his CM5. All the K_D values are shown as dots and curves are fitted using a Hill equation.

Table 3.5 shows the different K_D, R_{max}, Offset and Chi^2 values for both sets of experiments.
By examining the R_{max} values of these curves, it is possible to observe that for His-eGFP on Ni:NTA (figure 3.30, black curve the R_{max}, which is the total surface binding capacity, is 4829 RU, a very high value. The highest RU in this experiment was reached by 1500 nM of His-eGFP giving 3263 RU, which is only 67.6% of the total R_{max}.
K_D is lower for αGFP-Nb-His in both sets of experiments: for αGFP-Nb-His on Ni:NTA, K_D is 114 nM, while for αGFP-Nb-His on anti-his surface, K_D is 58 nM. On the other hand, for His-eGFP on Ni:NTA, K_D is 416 nM, while for His-eGFP on anti-his surface, K_D is 349 nM.

This means that αGFP-Nb-His, compared to His-eGFP, has a higher affinity to both surfaces. In particular, αGFP-Nb-His has the highest affinity for the anti-his-ab surface (K_D is 58 nM). His-eGFP also has a higher affinity for the anti-his-ab surface (K_D is 349 nM).
In conclusion, both proteins have a higher affinity for the anti-his-ab surface compared to the Ni:NTA chip.

Table 3.5. K_D, Rmax, Offset and Chi^2 values for each steady state affinity analysis

Protein immobilization	**K_D (M)**	**Rmax(RU)**	**Offset(RU)**	**Chi^2 (RU^2)**
His-eGFP on Ni:NTA	$4.16\ E^{-7}$	4829	-86.6	$9.84\ E^{+3}$
αGFP-Nb-His on Ni:NTA	$1.14\ E^{-7}$	3441	-74.3	$3.21\ E^{+3}$
His-eGFP on Anti-his CM5	$3.49\ E^{-7}$	3295	-66.63	$5.34\ E^{+3}$
αGFP-Nb-His on Anti-his CM5	$5.8\ E^{-8}$	1541	-65.83	$1.01\ E^{+4}$

Graph of figure 3.28 show the fitted kinetics analysis for His-eGFP binding to Ni:NTA chip surface, while figure 3.29 shows the fitted kinetics analysis for αGFP-Nb-His interacting with the anti-his-ab on CM5.
This kinetics analysis is based on the 1:1 Langmuir interaction model. In each graph, the original raw sensorgram is shown in black, while the fitting is shown in red. Firstly it is possible to evaluate the validity of the fitting by visual assessment. For graph 3.28, it is possible to observe that the fitting is optimal for curves from 5 nM to 250 nM, whereas for higher concentrations there is a slight deviation, especially for the curve at 1000 nM.
In order to assess if these deviations are significant, analysis of the residual plots was performed, where scatter values in these plots (not shown in this thesis) are a measure of the difference between the fitted curves and the raw data. It is possible to observe that for low concentrations the deviation is always in the range of ±2 RU, while for concentrations of 1000 nM an 1500 nM there is a systematic deviation which is not asymmetrical, suggesting that this error might be probably due to mass transport-limited kinetics and it is not due to heterogeneity in the system. However, these systematic deviations are not too pronounced and therefore they are not really significant.
Fitting shown in figure 3.29 also indicates some deviation from the raw data, especially during the association phase in the curves corresponding to the highest concentrations.
It is interesting to point out that in both graphs of figures 3.28 and 3.29, during dissociation phase at 1500 nM for His-eGFP and at 1000 and 1500 nM for αGFP-Nb-His the fitted curve dissociates faster than the actual raw curve, indicating an error due to mass transport-limited kinetics.

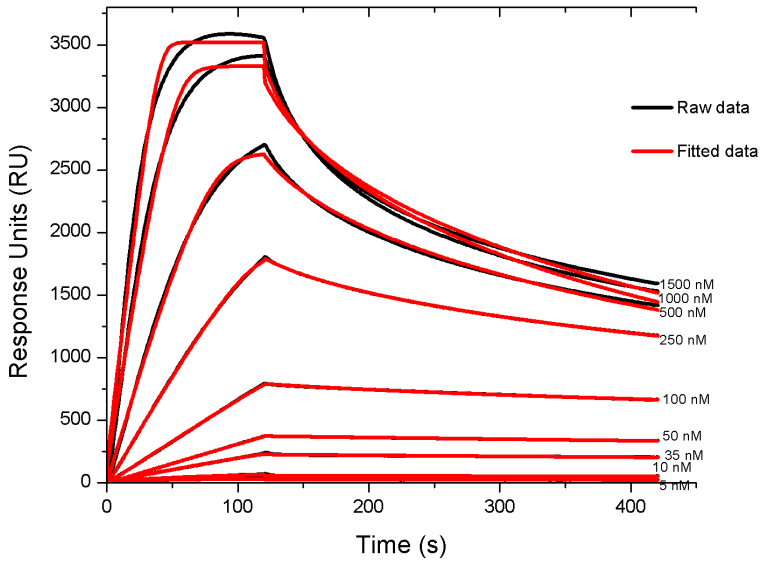

Figure 3.28 Fit kinetics analysis for His-eGFP on Ni:NTA surface: injected proteins concentrations were 5, 10, 35, 50, 100, 250, 500, 1000, 1500 nM.

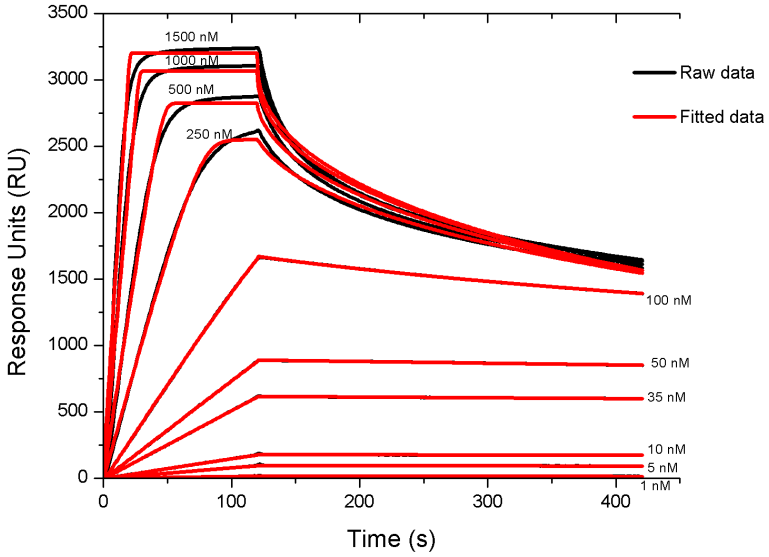

Figure 3.29. Fit kinetics analysis for αGFP-Nb-His on Ni:NTA surface: injected proteins concentrations were 5, 10, 35, 50, 100, 250, 500, 1000, 1500 nM.

Each fitted curve gives different parameters: K_{on}, K_{off}, K_D, R_{max}, RI, Chi². Chi^2 is a measure of the goodness of the fit. RI is the bulk signal determined by the refractive index deviation between the flow buffer and the buffer used with the analyte.
For my analysis two parameters will be mostly considered: K_{on}, which is the association rate constant measured in 1/Ms and K_{off}, which is the dissociation rate constant measured in 1/s. These values have been plotted in the scatter plot shown in figure 3.30.

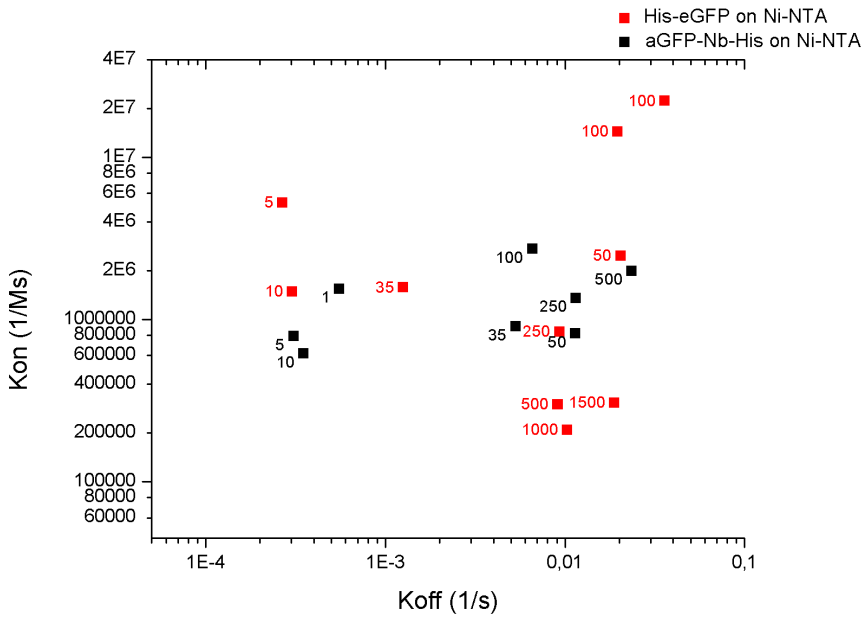

Figure 3.30. K_{on} and K_{off} plot for His-eGFP and αGFP-Nb-His on Ni:NTA.

K_{on} and K_{off} values define the kinetics of binding. A high affinity interaction between the analyte and the surface is characterized by a high K_{on}, or rapid "on rate", and a low K_{off}, or slow "off rate".
It is important to point out that in this experiment no actual ligand was used, and the aim was only to measure the kinetics of binding of the analyte (His-eGFP or αGFP-Nb-His) onto the surface. As it is illustrated in figure 3.30, higher His-eGFP concentrations correspond to a higher K_{off}, which means that higher concentrations have a higher dissociation rate constant: this was expected, as it possible to observe this phenomenon also in the sensorgram of figure 3.18, where a faster dissociation rate for higher His-eGFP concentrations is observed. For concentrations such as 5 nM, 10 nM, 35 nM (red squares) the dissociation rate is slower. For αGFP-Nb-His on Ni:NTA, higher concentrations also correspond to a higher K_{off}. By examining the association rate constant values, it is possible to observe that 100 nM in both groups have a relatively higher association rate constant, while high concentrations of His-eGFP have a relatively low K_{on}. On the contrary, for αGFP-Nb-His, high concentrations (100, 250 and 500 nM) correspond to a higher K_{on}.
In conclusion, His-eGFP and αGFP-Nb-His on Ni:NTA have comparable K_{on} and K_{off} constants on average, with αGFP-Nb-His having slightly higher K_{on} values than His-eGFP. This indicates that αGFP-Nb-His binds faster to the Ni:NTA compared to His-eGFP protein. All the K_{on} and K_{off} values are listed in tables e and f of the Appendix.

Figures 3.31 and 3.32 show the fitted kinetics analysis for His-eGFP and αGFP-Nb-His on the Anti-his-ab surface. Figure 3.31 shows that the fitting for His-eGFP is quite good and close to the original data. Compared to the fitting of His-eGFP on Ni:NTA (figure 3.28), in this case the deviations are minor and are less affected by mass transport-limited kinetics, showing only a minor buffer jump at the highest concentrations. The reason why the fitting for His-eGFP and αGFP-Nb-His interacting with the anti-his-ab is better than the one on the Ni:NTA chip is not only due to the minor mass transport limitations, but also because these two types of interactions are very different. The interaction between the Ni:NTA and the his-tagged proteins is much more labile, there are more binding sites on the same NTA molecule and, as explained before, the affinity

between Ni:NTA and the his-tagged proteins is lower compared to the affinity between the anti-his-ab and the his-tagged proteins.
Fitting in figure 3.32 is less optimal, as for high concentrations (500 nM and 1000 nm) some deviations can be observed, but only during association phase. This is a similar behavior which has been already encountered in fitting of αGFP-Nb-His on Ni:NTA (figure 3.29). In conclusions, fitting in figure 3.32 is still good, except for the curve at 1000 nM.

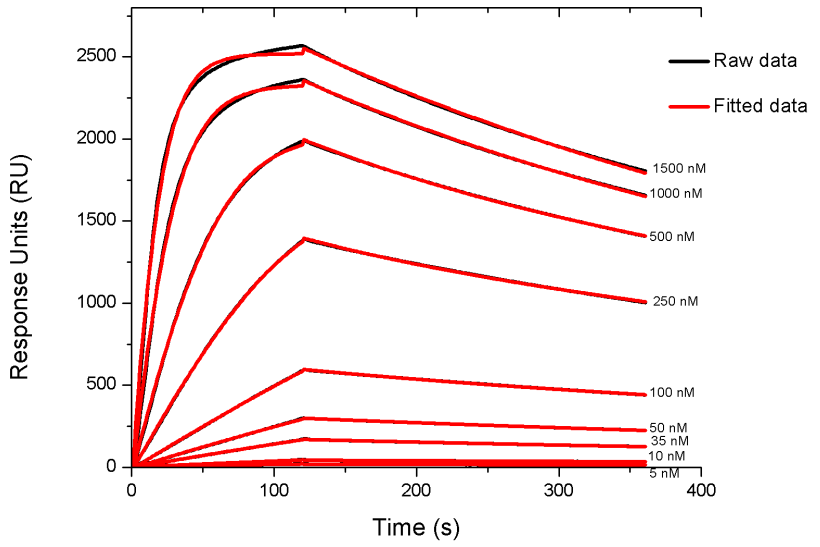

Figure 3.31. Fit kinetics for His-eGFP on Anti-his CM5: injected proteins concentrations were 5, 10, 35, 50, 100, 250, 500, 1000, 1500 nM.

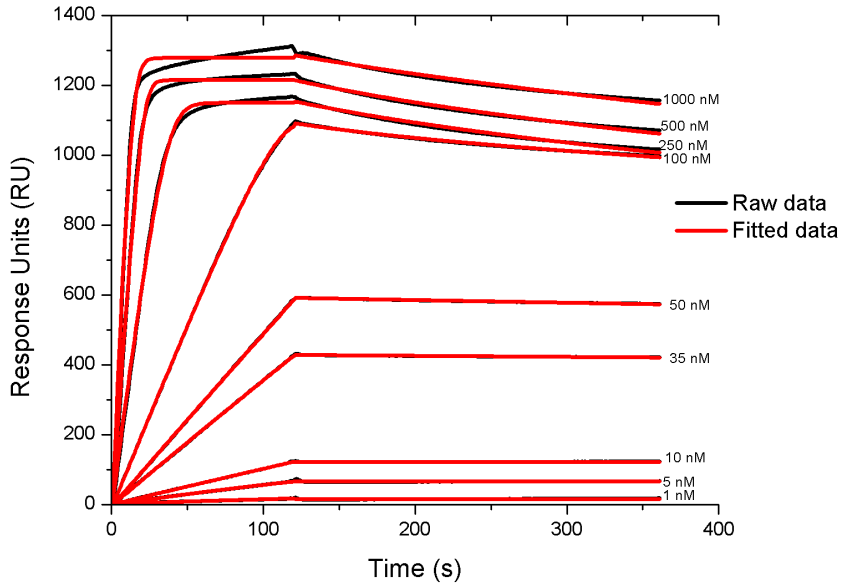

Figure 3.32. Fit kinetics for αGFP-Nb-His on Anti-his CM5: injected proteins concentrations were 1, 5, 10, 35, 50, 100, 250, 500, 1000 nM.

In plot of figure 3.33 it is possible to observe the K_{on} and K_{off} values for His-eGFP and αGFP-Nb-His on the Anti-his surface. All these values are listed in tables c and d of the Appendix. Values corresponding to 5 nM and 10 nM for αGFP-Nb-His are quite distant from the others, showing a very low K_{off}. All the others concentrations have a similar K_{off}, with His-eGFP having a slightly higher K_{off} compared to αGFP-Nb-His on Anti-his-Ab; also, 35 nM and 50 nM for His-eGFP have a very high K_{off}. This higher K_{off} for His-eGFP on Anti-his is expected if we compare the two previous sensorgrams in figures 3.31 and 3.32, showing a higher dissociation rate for His-eGFP.

Regarding the association rate constant K_{on}, αGFP-Nb-His on Anti-his CM5 seems to have higher values, especially for concentrations in the range between 5 nM and 250 nM. For example, for 250 nM, K_{on} for αGFP-Nb-His is 600000 $M^{-1}s^{-1}$, while Kon for His-eGFP is 156000 $M^{-1}s^{-1}$. This is a reasonable result if we also compare the sensorgrams in figures 3.31 and 3.32.

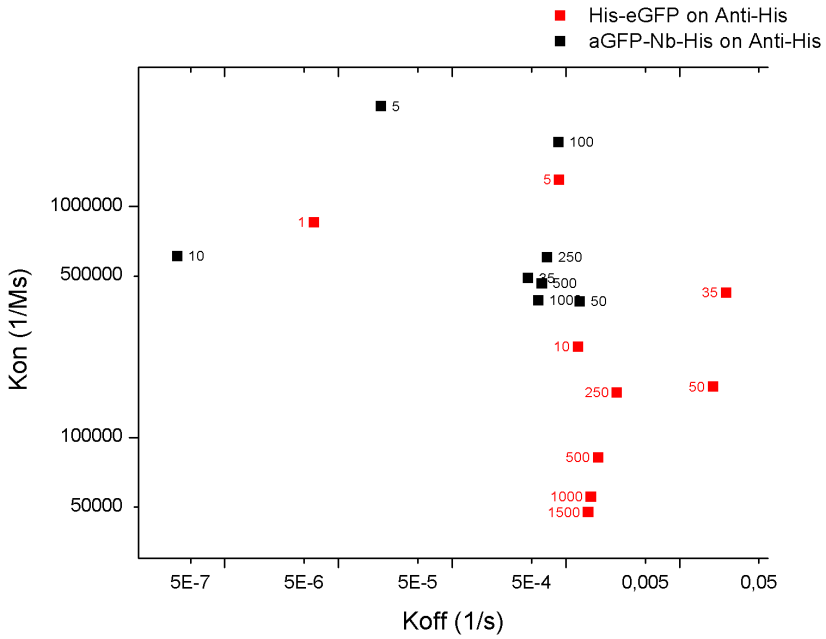

Figure 3.33. K_{on} and K_{off} plot for His-eGFP and αGFP-Nb-His on Anti-his CM5 surface.

Figure 3.34 presents all the K_{on} and K_{off} values in all four experiments, it is possible to observe that His-eGFP on Anti-his CM5 has relatively lower K_{on} values, which is expected if we compare this sensorgram (figure 3.31) to all the other ones, as the association rate in it is slower compared to the other sets of experiments.
Furthermore, for both experiments involving His-eGFP and αGFP-Nb-His on Ni:NTA, K_{off} values are relatively higher compared to the experiments on Anti-his CM5, indicating that both proteins have a faster dissociation rate on Ni:NTA. This is also reflected in the curves seen in the previous sensorgrams: in figures 3.31 and 3.32 (fitted sensorgram on Anti-his-ab) it is clear that the rate of dissociation is much slower compared to the sensorgrams in figure 3.28 and 3.29 (fitted sensorgrams on Ni:NTA).

In conclusion, these results indicate that αGFP-Nb-His binds to the anti-his surface more rapidly than the His-eGFP on the same surface, and it also dissociates slower than the His-eGFP. Therefore, αGFP-Nb-His has a higher affinity to the anti-his compared to His-eGFP.
Also, αGFP-Nb-His binds faster than His-eGFP also on the Ni:NTA surface, but it dissociates on average at the same rate.

Another important conclusion is that the Ni:NTA chip surface is clearly more labile than the anti-his surface, as both proteins dissociate faster from it.

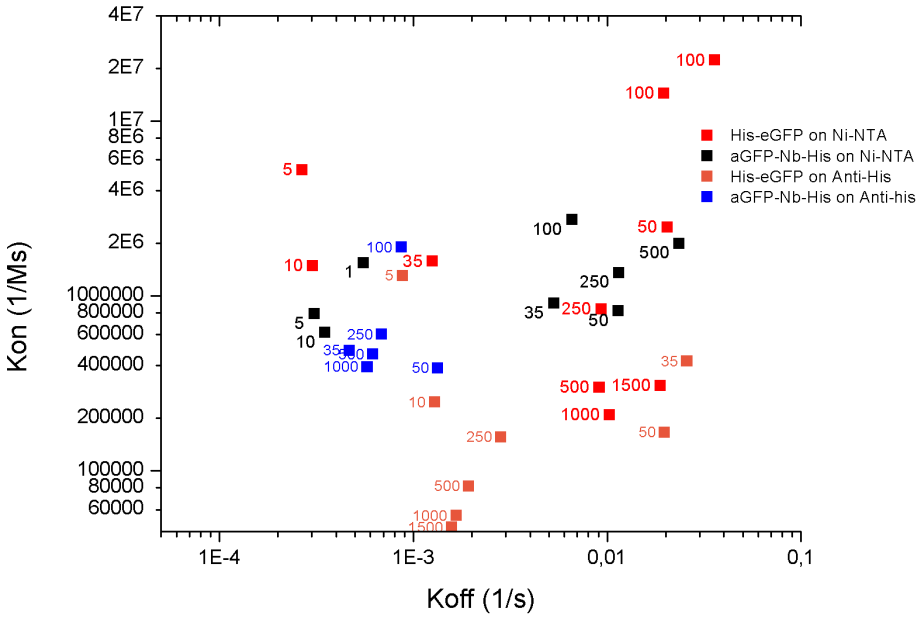

Figure 3.34 K_{on} and K_{off} plot for His-eGFP and αGFP-Nb-His on Ni:NTA and Anti-his CM5

3.3.3.2 Steady state affinity and fitted kinetics analysis of GFP interacting with αGFP-Nb-His on Ni:NTA and anti-his-ab immobilized on CM5

The steady-state affinity fitted curves for these experiments are shown in figure 3.35. Similarly as before, a scatter plot obtained by the steady-state affinity for all concentrations was prepared, followed by data fitting using the Hill function from Origin software. It is possible to see that the curves show a very similar behavior, where GFP-Nb reaches higher response values on the anti-his-CM5 surface, as it was expected if we compare this result to the corresponding sensorgrams in figures 3.21 and 3.25. K_D values are indicated by vertical lines in figure 3.35.

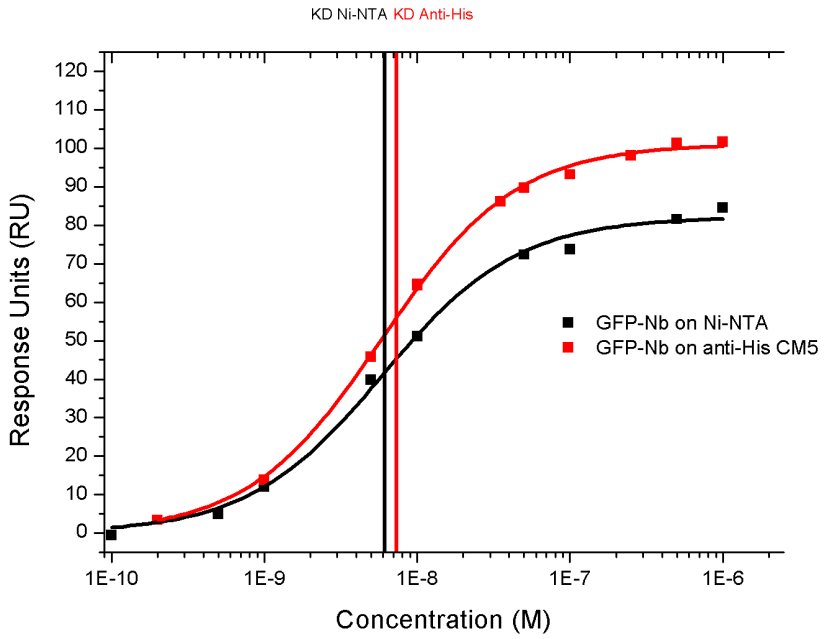

Figure 3.35. Steady-state affinity for GFP binding to αGFP-Nb-His on Ni:NTA (black) and Anti-his-CM5 (red). All the K_D values are shown as dots and curves are fitted using a Hill equation.

All K_D, Rmax, Offset and Chi^2 values are illustrated in table 3.6. The K_D values are very similar for the both curves, with K_D for GFP-Nb on Ni:NTA being slightly lower than the other one: K_D is 6.16 nM for GFP-Nb on Ni:NTA and it is 7.32 nM for GFP-Nb on anti-his. This would imply that GFP binding to αGFP-Nb-His has a slightly higher affinity for the Ni:NTA surface. However, this difference is very little, as it is only about 1 nM, and it could also be attributed to some errors. Therefore, it is possible to conclude that there is no significant difference in the affinity of GFP interacting with αGFP-Nb-His on the two biosensor surfaces.

Table 3.6. K_D, Rmax, Offset and Chi^2 values for each steady state affinity analysis

Protein immobilization	K_D(M)	Rmax(RU)	Offset(RU)	Chi^2 (RU^2)
GFP interacting with αGFP-Nb-His on Ni:NTA	6.16 E^{-9}	85.34	-0.95	16
GFP interacting with αGFP-Nb-His on Anti-his CM5	7.32 E^{-9}	103.7	2.6	23

Figures 3.36 and 3.37 show the fitted kinetics curves for both experiments described. In both cases, fitting was optimal for curves between 1 nM and 10 nM, while curves at the highest concentrations (2000 nM on Ni:NTA and 1000 on Anti-his CM5) show a poor fitting since the deviation from the raw curve is too high, especially for the latter.
For GFP-nanobody on Ni:NTA (figure 3.36), fitting of curves between 50 nM and 1000 nM presents a slight deviation from the original data; analysis of the residual plots showed that this error is a symmetrical systematic deviation probably due to mass transport kinetics. For GFP-nanobody on Anti-his CM5 (figure 3.37), curves between 50 nM and 500 nM also present a similar deviation from the raw data, where fitted curve at 500 nM is the one with the highest error. Fitting of the curve at 1500 nM has been removed because it was very poor.

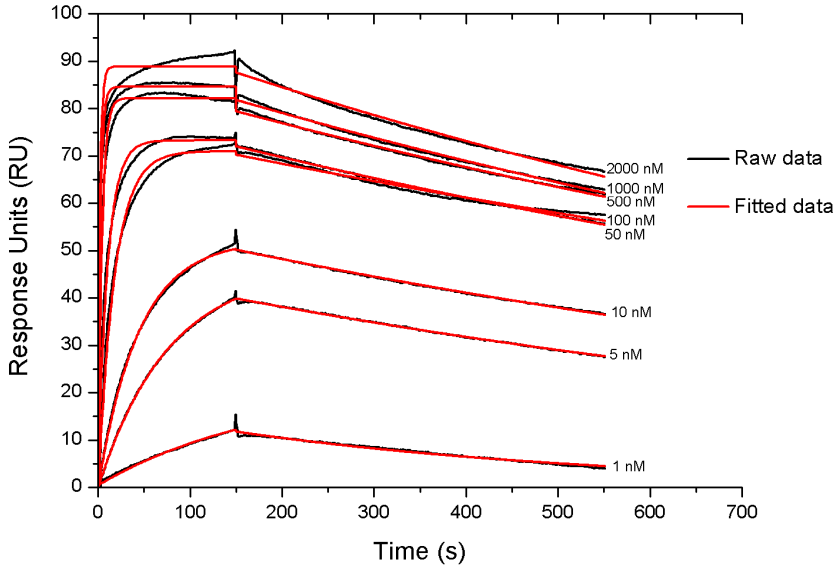

Figure 3.36 Fit Kinetics for GFP interacting with αGFP-Nb-His on Ni:NTA: injected proteins concentrations were 1, 5, 10, 35, 50, 100, 500, 1000, 2000 nM.

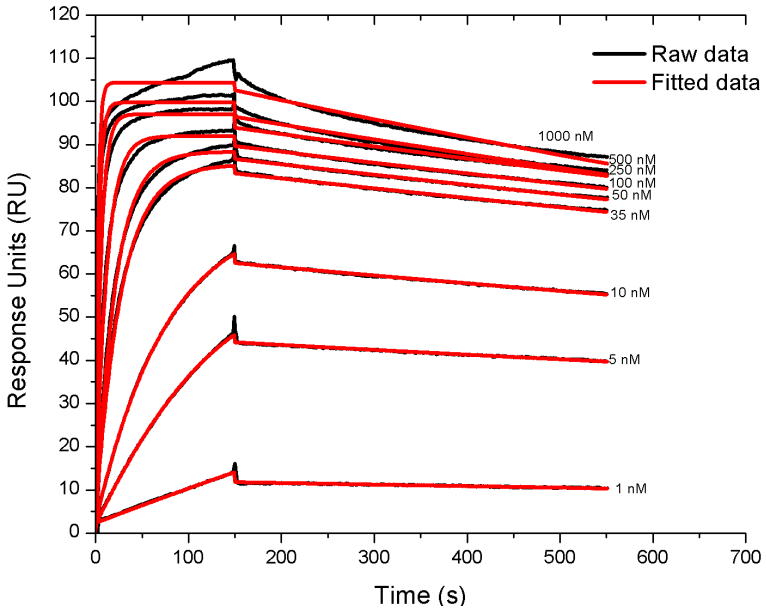

Figure 3.37 Fit Kinetics for GFP interacting with αGFP-Nb-His on anti-his-CM5: injected proteins concentrations were 1, 5, 10, 35, 50, 100, 250, 500, 1000 nM.

Plot in figure 3.38 shows K_{on} and K_{off} values for the experiment involving GFP interacting with αGFP-Nb-His on the two surfaces. These values are llisted in table a and b of the Appendix.
In both sets of experiments the association rate constant is higher as the concentration of injected GFP decreases. In the experiment on the anti-his-ab, higher concentrations of analyte also

correspond to a higher dissociation rate constant, which is an expected result because, as observed in the corresponding chromatogram of figure 3.37, curves at higher concentrations tend to dissociate slightly faster. The same trend is not followed by the experiment on Ni:NTA, where dissociation rate constants are only slightly differing from each other, except 5 nM and 10 nM which have a higher K_{off}.
While analyzing these data, it is important to point out that the analysis of the association rate will only give an apparent K_{on} value which is slower than the actual K_{on}.[61] This is because the analysis is performed under mass transport limited conditions, as already highlighted by the not so optimal fitting shown in figure 3.37, especially for higher GFP concentrations. Mass transport limited conditions mean that the rate at which the analyte is delivered to the surface is lower than the rate at which the analyte binds to the ligand, thus producing a slower K_{on} value. In my experiments, mass transport was already limited by increasing flow rate to the maximum, and choosing a relatively low immobilized ligand. K_{off} constant can also be affected by mass transport, as re-binding of the dissociated analyte to the ligand before getting off the sensor surface can happen.

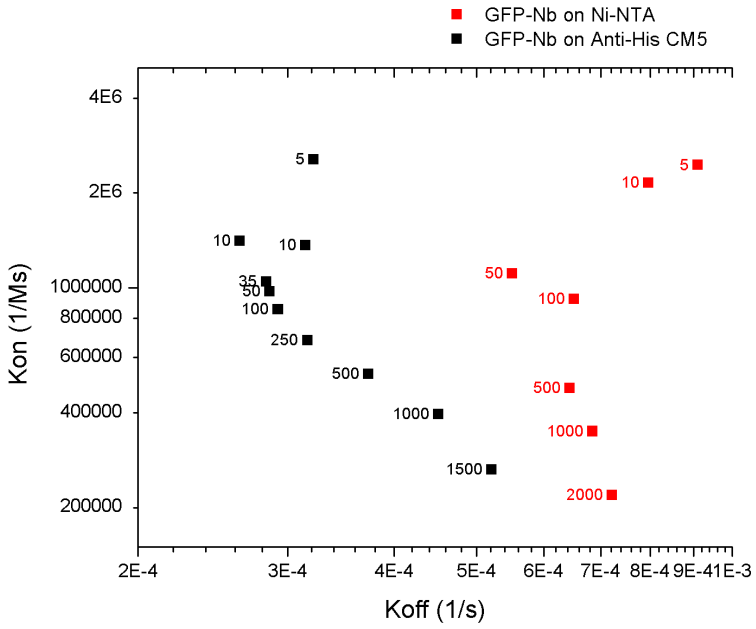

Figure 3.38. K_{on} and K_{off} plot for GFP interacting with αGFP-Nb-His on Ni:NTA (red) and anti-his-CM5 (black).

In conclusion, although setting in my experiments were carefully optimized, it was still hard to obtain data not affected by mass transport, especially for high concentrations of analyte. Therefore, K_{on} and K_{off} values corresponding to high concentrations are the most affected by mass transport limitations.

If we now compare the two sets of K_{on} and K_{off} values in figure 3.38, it is possible to observe that K_{on} values are quite comparable between the two groups, with GFP-Nb on anti-his-ab having slightly higher values for high concentrations. K_{off} values on the other hand are significantly higher for GFP binding to αGFP-Nb-His on Ni:NTA, meaning that the dissociation rate of GFP from αGFP-Nb-His immobilized on the Ni:NTA surface is faster. This is an expected result, as reflected by sensorgrams in figure 3.36 and 3.37: it is evident that the dissociation rate for GFP-Nb on Anti-his CM5 is slower for all dissociation curves.

Finally, it is possible to state that, for the same analyte concentrations used, GFP had a higher affinity for αGFP-Nb-His on the Anti-his-Ab-CM5 surface, as the results showed slower dissociation rate constants and slightly higher association rate values. Of course, this comparison must take into account the differences between the two different types of immobilization techniques, as well as the influence of mass transport limited kinetics, as already explained.

A way to assess the influence of mass transport in these measurements would be to compare the K_D affinity values between the steady affinity analysis and the kinetics analysis, where K_D values are calculated by the software from each pair of K_{on} and K_{off} values. By calculating the average K_D from kinetics measurements, I obtained a K_D of one order of magnitude less (around 4.3 E^{-10}) compared to the equilibrium measurements. This is another evidence showing that kinetics measurements are not reliable for calculating the K_D, whereas equilibrium binding analysis is in this case more accurate.

3.4 Summary

This chapter described a series of experiments aimed at first at evaluating the interaction of αGFP-Nb-His, a novel and promising tool used in nanoscience, with Ni:NTA and anti-his-Ab immobilized on CM5, and then to compare this interaction with His-eGFP interaction on both the surfaces. Results showed that αGFP-Nb-His has a higher affinity at equilibrium for both Ni:NTA and Anti-his-Ab-CM5 surfaces compared to His-eGFP. Kinetics measurements showed that αGFP-Nb-His on Anti-his-Ab has a clearly higher association rate constant compared to His-eGFP on the same surface, while His-eGFP has higher dissociation rates. Results on Ni:NTA were quite comparable for both proteins. In conclusion, as highlighted on figure 3.34, αGFP-Nb-His on Anti-his-Ab showed relatively high association rate constants and low dissociation rate constants compared to His-eGFP. Also, these results indicate the Ni:NTA chip surface is more labile than the anti-his surface, as both proteins dissociate faster from it.
The chapter then presented a set of experiments aimed at investigating the interaction between GFP and αGFP-Nb-His immobilized on Ni:NTA and on an anti-his-ab. The results showed that the affinity at equilibrium of GFP for the immobilized Nb was very similar in both cases (K_D is 6.16 nM for GFP-Nb on Ni:NTA and 7.32 nM for GFP-Nb on anti-his-Ab). Kinetics measurements on the other hand showed that dissociation rate was always lower for GFP interacting with αGFP-Nb-His captured on the Anti-his-Ab, and association rate constants were on average slightly higher compared to the experiment on Ni:NTA surface.
These experiments indicated that the interaction between Nbs and their partners can be investigated by SPR. However, care needs to be taken when choosing the experimental parameters (such as buffer, flow rate and density of immobilized ligand) in order to minimize mass transport problems, achieve good kinetics measurements and obtain reliable association rate constants.

Chapter 4.

Conclusion

This project was divided in two main parts: molecular biology and surface plasmon resonance. In the first part, GFP and His-eGFP proteins were succesfully overexpressed, purified and characterized, giving a final yield of around 1.6 mg/ml and 1.3 mg/ml respectively and a purity of around 90%, which is very satisfactory. Nanobody was overexpressed, but its purification through IMAC led to many challenges, even after repeating the whole experiment three times. This indicates that the protocol for nanobody overexpression and purification probably needs to be optimized in order to achieve better result. An alternative method to obtain and succesfully purify nanobodies could also be elaborated.

The investigation of the interaction between nanobody and its antigens was succesfully characterized and evaluated by SPR in the second part of this project. The results showed that nanobody has a higher affinity at equilibrium for both Ni:NTA and Anti-his-Ab-CM5 surfaces compared to His-eGFP. Furthermore, nanobody, compared to His-eGFP, proved to bind faster to the anti-his-Ab surface and its dissociation rate constants from this surface were significantly lower, therefore confirming the high affinity for the anti-his-Ab surface.

One of the major goals of this thesis was to investigate the interaction between a nanobody immobilized on Ni:NTA or anti-his-Ab surface and a GFP, used as analyte. The results of these experiments showed that GFP had a higher affinity for nanobody immobilized on the anti-his-Ab surface, as slower dissociation rate constants and slightly higher association rate values were obtained.

Appendix

Table a. Kon and Koff values for GFP binding to αGFP-Nb-His on Ni:NTA

Concentration (nM)	Kon (1/Ms)	Koff (1/s)
1	3417000	0.002535
5	2450000	$9.11\ E^{-4}$
10	2154000	$7.97\ E^{-4}$
50	1110000	$5.51\ E^{-4}$
100	$9.2\ E^{5}$	$6.52\ E^{-4}$
500	$4.8\ E^{5}$	$6.44\ E^{-4}$
1000	$3.49E^{5}$	$6.85\ E^{-4}$
2000	$2.19E^{5}$	$7.22\ E^{-4}$

Table b. Kon and Koff values for GFP binding to αGFP-Nb-His on anti-His CM5

Concentration (nM)	Kon (1/Ms)	Koff (1/s)
5	$2.554E^{6}$	$3.22E^{-4}$
10	$1.364E^{6}$	$3.149E^{-4}$
35	$1.043E^{6}$	$2.83E^{-4}$
50	971400	$2.859E^{-4}$
100	851700	$2.923E^{-4}$
500	531200	$3.734E^{-4}$
1000	395600	$4.514E^{-4}$
1500	264000	$5.21\ E^{-4}$

Table c. Kon and Koff values for His-eGFP on anti-His CM5

Concentration (nM)	Kon (1/Ms)	Koff (1/s)
1	849000	$6.14E^{-6}$
5	$1.3E^{6}$	$8.82E^{-4}$
10	246000	0.00129
35	422000	0.02587
50	165000	0.01984
250	156000	0.00284
500	81600	0.00194
1000	55200	0.00167
1500	47300	0.00158

Table d. Kon and Koff values for αGFP-Nb-His binding on anti-His CM5

Concentration (nM)	Kon (1/Ms)	Koff (1/s)
1	$4.86E^{6}$	$7.32E^{-7}$
5	$2.7E^{6}$	$2.38E^{-5}$
10	607000	$3.87E^{-7}$
35	487000	$4.68E^{-4}$
50	387000	0.00134
100	$1.89E^{6}$	$8.7E^{-4}$
250	600000	$6.89E^{-4}$
500	463000	$6.21E^{-4}$
1000	391000	$5.8E^{-4}$

Table e. Kon and Koff values for His-eGFP binding on Ni:NTA

Concentration	Kon (1/Ms)	Koff (1/s)
1	$9.375E^{7}$	0.0022
5	$5.248E^{6}$	$2.68E^{-4}$
10	$1.48E^{6}$	$3.035E^{-4}$
35	$1.571E^{6}$	0.00126
50	$2.461E^{6}$	0.02044
100	$2.222E^{7}$	0.03602
250	839100	0.00933
500	298900	0.00912
1000	208300	0.01033
1500	306700	0.01891

Table f. Kon and Koff values for αGFP-Nb-His binding on Ni:NTA.

Concentration(nM)	Kon (1/Ms)	Koff (1/s)
1	$1.543E^{6}$	$5.549E^{-4}$
5	787400	$3.091E^{-4}$
10	613800	$3.516E^{-4}$
35	903400	0.00532
50	818200	0.01142
100	$2.717E^{6}$	0.00659
250	$1.355E^{6}$	0.01154
500	$1.99E^{6}$	0.02352
1000	$1.782E^{10}$	281.4
1500	$2.135E^{9}$	39.55

References

[1] Gibbs, W. W. (2005). Nanobodies. *Scientific American Magazine* .

[2] Haard, M. M. (2007). Properties, production, and applications of camelid single-domain antibody fragments. *Applied Microbiology and Biotechnology* .

[3] Muyldermans, S. (2009). Camelid immunoglobulins and nanobody technology. *Veterinary Immunology and Immunopathology* .

[4] http://www.aimms.vu.nl/

[5] Zhu, X. (2009). Nanobodies - the new concept in antibody engineering. *African Journal of Biotechnology Vol. 8 (12).*

[6] Arbabi Ghahroudi, M. (1997). Selection and identification of single domain antibody fragments from camel heavy-chain antibodies. *FEsBS Letters 414.*

[7] Jespers, L. S. (2003). Domain antibodies: proteins for therapy. *Trends in Biotechnology 21.*

[8] Stanfield, R. (2004).Crystal structure of a shark single-domain antibody V region in complex with lysozyme. *Science 305 (5691).*

[9] Muyldermans, S. (2010). Nanobodies®: proficient tools in diagnostics. *Expert Rev. Mol. Diagn*.

[10] http://www.ablynx.com/en/research-development/nanobody-technology/nanobody-advantages [date of access: 10 April 2014]

[11] Baral T. (2013). Single domain antibodies and their utility. *Curr Protoc Immunol.*

[12] Stok, W. (1999). Comparison of physical chemical properties of llama VHH antibody fragments and mouse monoclonal antibodies.*Biochimica et Biophysica Acta 1431*.

[13] Rothbauer, U.(2006).Targeting and tracing antigens in live cells with fluorescent nanobodies. *Nature Method.*

[14] Rothbauer, U.(2007). A Versatile Nanotrap for Biochemical and Functional Studies with Fluorescent Fusion Proteins. *Molecular & Cellular Proteomics.*

[15] Ries, J. (2012). A simple, versatile method for GFP-based super-resolution microscopy via nanobodies. *Nature Methods.*

[16] Koide, S. (2009). Engineering of recombinant crystallization chaperones. *Current Opinion in Structural Biology.*

[17] Kubala M. (2010). Structural and thermodynamic analysis of the GFP:GFP-nanobody complex. *Protein science*.

[18] Harmsen M. (2006).Selection and optimization of proteolytically stable llama single-domain antibody fragments for oral immunotherapy. *Applied Microbiology and Biotechnology.*

[19] Muruganandam A. (2002). Selection of phage-displayed llama single-domain antibodies that transmigrate across human blood-brain barrier endothelium. *Faseb Journal.*

[20] Van De Broek, B. (2011). Specific Cell Targeting with Nanobody Conjugated Branched Gold Nanoparticles for Photothermal Therapy. *ACS Nano.*

[21] Ibanez, L. I. (2011). Nanobodies with in Vitro Neutralizing Activity Protect Mice Against H5N1 Influenza Virus Infection. *Journal of Infectious Diseases.*

[22] Rothbauer, U. (2006). Targeting and tracing antigens in live cells with fluorescent nanobodies. *Nature Methods*

[23] Ries, J. (2012). A simple, versatile method for GFP-based super-resolution microscopy via nanobodies. *Nature Methods*

[24] Muyldermans S. (2013). Nanobodies: Natural single-domains antibodies. *Annual Review of Biochemistr.*

[25] De Genst EJ. (2010). Structure and properties of a complex of α-synuclein and a single-domain camelid antibody. *J. Mol. Biol.*

[26] Kell AJ. (2009). Single-domain antibody-nanoparticles: promising architectures for increased *Staphylococcus aureus* detection specificity and sensitivity. *Bioconjug. Chem.*

[27] Saerens D. (2005). Engineering Camel Single-Domain Antibodies and Immobilization Chemistry for Human Prostate-Specific Antigen Sensing. *Analytical Chemistry*.

[28] Vaneycken I. (2011). Preclinical screening of anti-HER2 nanobodies for molecular imaging of breast cancer. *FASEB Journal.*

[29] Desmyter A. (2013). Viral infection modulation and neutralization by camelid nanobodies. *Biophysics and Computational Biolog.*

[30]Andersen J.T. (2012). Selection of Nanobodies that Target Human Neonatal Fc Receptor. *Scientific Reports 3.*

[31] Shimonura, O. (2008) Discovery of Green Fluorescent Protein, GFP. Nobel Lecture.

[32] Chalfie M. (2008) GFP: Lighting Up Life. Nobel Lecture.

[33] Chalfie M. (1994). Green fluorescent protein as a marker gene expression. *Science*, *26.*

[34] Heim, R. (1995). Improved Green Fluorescence. *Nature*, *373*, 663–664.

[35] Cormack, B. (1996). FACS-optimized mutants of the green fluorescent protein (GFP). *Gene*, *173*, 1 Spec No, 33–8.

[36] Ormö, M.(1996). Crystal structure of the Aequorea victoria green fluorescent protein. *Science*, *273*, 1392–1395.

[37] Cotlet, M (2001). Excited-State Dynamics in the Enhanced Green Fluorescent Protein Mutant Probed by Picosecond Time-Resolved Single Photon Counting Spectroscopy. *The Journal of Physical Chemistry B*, *105*.

[38] Phillips GJ (2001). Green fluorescent protein--a bright idea for the study of bacterial protein localization". *FEMS Microbiol Lett.*

[39] Yuste R (2005). Fluorescence microscopy today. *Nat Methods*.

[40] Charlton A (2008). Immobilized metal ion affinity chromatography of histidine-tagged fusion proteins. *Methods Mol Biol. 2008;421:137-49.*

[41] www.gelifesciences.com [date of access: 10 March 2014].

[42] www.bio-rad.com [date of access: 14 March 2014].

[43] Herold A. (2007). Probing Size Exclusion Mechanisms of Complex Hydrocarbon Mixtures: The Effect of Altering Eluent Compositions. *Energy Fuels.*

[44] Hagel L. (2010). Size Exclusion Chromatography. *GE Healthcare Bio-Sciences AB.*

[45] S. Yamamoto (1988). Ion exchange chromatography of proteins.

[46] S. Furusaki (1987). Separation of proteins by ion-exchange chromatography using gradient elution. *Bioprocess Engineering*

[47] www.addgene.org [date of access: 12 February 2014]

[48] P. Englebienne (2003). Surface plasmon resonance: principles, methods and applications in biomedical sciences. *Journal of Spectroscopy.*

[49] Cooper M. (2002). Optical biosensore in drug discovery. *Nature Reviews Drug Discovery* 1, 515-528.

[50] Mirabella F.M. (1985). Internal Reflection Spectroscopy: Review andSupplement, *Harrick Scientific Corporation*

[51] Biacore (2001). Surface Plasmon Resonance, *Technology Note 1*

[52] www.sprpages.nl [date of access: 2 April 2014].

[53] Zeder-Lutz J. (1997). Thermodynamic analysis of antigen-antibody binding using biosensor measurements at different temperatures. *Analytical Biochemistry.*

[54] Malmqvist M. (1993). Surface plasmon resonance for detection and measurement of antibody-antigen affinity and kinetics. *Current Opinion in immunology.*

[55] Quinn J. (2000). Development and Application of Surface Plasmon Resonance-Based Biosensors for the Detection of Cell–Ligand Interactions. *Analytical biochemistry*

[56] Stenberg, E. (1991). Quantitative determination of surface concentration of protein with surface plasmon resonance by using radiolabelled proteins.*J.Colloid Interface*

[57] Improving Protein Interaction Analysis. (2006). *Genetic engineering and biotechnology news*

[58] Helmerhorst E. (2012). Real-time and Label-free Bio-sensing of Molecular Interactions by Surface Plasmon Resonance: A Laboratory Medicine Perspective. *Clinical Biochemistry Review*.

[59] www.biacore.com [date of access: 2 April 2014]

[60] Fischer MJ. (2010). Amine coupling through EDC/NHS: a practical approach. *Molecular Biology*

[61] http://www.bioch.ox.ac.uk/aspsite/services/equipmentbooking/biophysics/spr.pdf [date of access: 8 July 2014]